

Deciphering molecular and tissue mechanisms of
Catecholaminergic Polymorphic Ventricular Tachycardia (CPVT)

By

Matthew James Wleklinski

Dissertation

Submitted to the Faculty of the
Graduate School of Vanderbilt University
in partial fulfillment of the requirements
for the degree of

DOCTOR OF PHILOSOPHY

in

Pharmacology

May 31st, 2022
Nashville, Tennessee

Approved:

Dan M. Roden, M.D. (Chair)

Katherine T. Murray, M.D.

Eric J. Delpire, Ph.D.

C. David Weaver, Ph.D.

Bjorn C. Knollmann, M.D, Ph.D (Advisor)

Copyright © 2022 by Matthew James Wleklinski

All Rights Reserved

I want to dedicate this work to my friends and family.
They have always supported me and motivated me to be the best person I can be.

ACKNOWLEDGEMENTS

I would like to first start by thanking the Vanderbilt Medical Scientist Training Program (MSTP) and the leadership team for accepting me into the program and for all their support throughout my time in graduate school. This thesis work was supported by a grant from the National Institutes of Health (NIH) Heart, Lung, and Blood Institute (HLBI) number: F30-HL145917 and grant NHLBI R35 HL144980 from Dr. Bjorn Knollmann.

At Vanderbilt I would like to thank the Pharmacology department for their graduate school curriculum and dedication to training students. I want to thank Dr. Christine Konradi who is the director of graduate studies for the department and Dr.'s Sean Davies and Claus Schneider for involvement in the program. Throughout the project there were many resources used that were provided by Vanderbilt University (VU) and the Vanderbilt University Medical Center (VUMC). I would like to thank the Molecular Cell Biology Resource (MCBR), the Cell Imaging Shared Resource (CISR), and the Materials Durability and Environmental Research Facilities Hub (MDERFH) for providing their services and assistance on various parts of the each of the projects.

I would like to thank the collaborators that were involved in my thesis work and provided their help and guidance in multiple areas of the project. Dr. Prince Kannankeril, Dr. Clara Franzini-Armstrong, Dr. Ramesh Iyer, Dr. Michela Faggioni, Dr. Erron Titus, and Dr. Shan Parikh were pivotal to the success of each project.

I want to thank my thesis committee for their involvement in my training and for their advice throughout my time in graduate school. Dr. Dan Roden, Dr. Katherine Murray, Dr. Eric Delpire, and Dr. David Weaver were instrumental in my growth as a scientist. They challenged me to be better but were always supportive. I felt that I could always talk to them about any issues I was having or look to them for guidance when it felt like I was out of options. Each one of them was involved in improving my skills as a scientist and as a student. I want to thank Dr. Roden for chairing my committee and Dr. Murray, Dr. Delpire, and Dr. Weaver again for their help.

I want to thank the members of the Knollmann Lab for everything throughout my graduate years. Words cannot express how grateful I am for how wonderful they were to work with and how willing they were to help me throughout my time in the lab. Dan Blackwell, Lili Wang, Christian Egly, Dima Kryshtal, Kyungsoo Kim, and Jeff Schmeckpeper all have contributed to my growth as a researcher, and I was very lucky to have them in the lab. I also want to give a big thank you to Kaylen Woodall. As our lab manager she always made sure everything was running smoothly and was always willing to help. She managed the mouse colonies for me and provided the project with numerous mouse isolations and reagents.

I also want to thank Dr. Bjorn Knollmann. He took a chance on letting me join the lab and was supportive of me from the beginning. He made an effort to learn what I needed to help grow as an independent scientist and was always open to meeting with me. He helped me learn more about my strengths and weaknesses and gave me many opportunities to improve on all my skills. I appreciated the community he helped establish in the lab and I knew I could go to him with any issues I was having. Thank you again Dr. Knollmann, I couldn't have asked for a better mentor.

I want to thank all of my friends who helped keep me grounded and motivated during my graduate school training. This includes the new friends I have made since joining the program, and the ones that have stuck with me since high school. They provided me a much-needed outlet when times were hard and were always there to celebrate when things went well.

I finally want to thank my family. My mom has always been my number one supporter and is the reason I was able to accomplish what I have today. She taught us to never let anything keep you down and the importance of working hard. My dad was consistently one of the first people to read anything that I was working on. He helped make my work feel like it was reaching more people than just the research community and he helped me grow a lot during my time in graduate school. My brothers, Nick, Mike, and John are one the best support systems I could ask for. We have gone through a tremendous amount of life experiences together, and I can't wait to see where life takes us. Thank you all so much, I love you, and I am lucky to have you in life.

Table of Contents

	Page
ACKNOWLEDGEMENTS	iv
LIST OF TABLES	viii
LIST OF FIGURES	ix
LIST OF ABBREVIATIONS	xi
INTRODUCTION	1
Calsequestrin-2	1
Catecholaminergic Polymorphic Ventricular Tachycardia (CPVT).....	6
Molecular mechanisms of CPVT.....	7
Tissue mechanisms underlying CPVT.....	16
Treatment of CPVT patients.....	23
Summary and Motivation	29
CHAPTER I.....	31
Uncovering a mechanism for autosomal dominant CPVT2	31
Introduction	31
Methods.....	34
Results	43
Conclusion.....	68
CHAPTER II.....	73
Targeting Casq2 to discover the tissue mechanism of CPVT	73
Introduction	73
Methods.....	75

Results	83
Conclusion.....	108
CHAPTER III	113
Generation and characterization of the <i>CASQ2</i> knockout human induced pluripotent stem cell-derived cardiomyocytes.....	113
Introduction	113
Methods.....	115
Results	124
Conclusion.....	135
CHAPTER IV	138
Conclusion, Limitations, and Future Directions.....	138
Motivation	138
A novel mechanism for autosomal dominant CPVT2.....	141
The Purkinje-myocardial junction is the anatomical origin of CPVT.....	144
Generation of a Casq2KO CPVT human induced pluripotent stem cell (hiPSC) model.....	147
Limitations	151
Future directions.....	154
Final Thoughts	158
REFERENCES	162

List of Tables

Table	Page
Table 1. Calcium handling parameters of WT and K180R cardiomyocytes	52
Table 2. Analysis of cytosolic and intra-SR calcium handling in K180R cardiomyocytes.....	66
Table 3. Summary of calsequestrin-2 (Casq2) tissue specific mouse models	97
Table 4. Colocalization data of cardiac-specific proteins	100
Table 5. Antibody concentrations used during Western blotting of CASQ2 hiPSC lines.....	122
Table 6. Calcium transient properties in <i>CASQ2</i> ^{-/-} hiPSC cardiomyocytes.....	133

List of Figures

Figure	Page
Figure 1. The SR calcium release complex in cardiac muscle	5
Figure 2. Cellular pathogenesis of catecholaminergic polymorphic ventricular tachycardia (CPVT).....	8
Figure 3. Summary of current hypotheses for how RyR2 mutations could lead to CPVT.....	11
Figure 4. Cardiac conduction system (CSS) targeted <i>CASQ2</i> gene deletion or rescue	21
Figure 5. Generation of K180R founder mice	44
Figure 6. K180R mice display a CPVT phenotype.....	45
Figure 7. K180R increases spontaneous SR calcium release in single cardiomyocytes.	48
Figure 8. Characteristics of calcium sparks from isolated cardiomyocytes.....	49
Figure 9. Characteristics of calcium waves from isolated cardiomyocytes.....	50
Figure 10. K180R increases rates of spontaneous calcium release events	51
Figure 11. Levels of junctional SR proteins are normal in K180R mice.....	55
Figure 12. K180R does not change intra-SR localization of Casq2.	56
Figure 13. Electron microscopy of WT and K180R cardiomyocytes.....	57
Figure 14. K180R does not change total SR calcium content.	60
Figure 15. SR calcium release refractoriness is impaired in K180R cardiomyocytes.....	61
Figure 16. Cytosolic calcium transient and SR calcium content handling in intact K180R cells	62
Figure 17. K180R decreases dynamic SR calcium buffering.	65
Figure 18. SR calcium buffering in intact K180R cardiomyocytes paced at 1 Hz.....	67
Figure 19. Generation and characterization of Casq2 tissue-specific mouse models part 1.....	86
Figure 20. Generation and characterization of Casq2 tissue-specific mouse models part 2.....	87
Figure 21. Representative immunostaining images in tissue-specific <i>CASQ2</i> ^{-/-} mouse lines	88

Figure 22. Optical mapping and ECG recording in Casq2 null mouse hearts	91
Figure 23. Endocardial ablation reduces arrhythmia burden in Casq2 null hearts	92
Figure 24. Casq2 expression in subendocardial ventricular myocytes juxtaposed to Purkinje cells reduces PVC burden and prevents arrhythmia.....	95
Figure 25. Nearest neighbor distance distributions for each heart shown in Figure 24.....	96
Figure 26. Contactin-2 negative cells staining for Connexin-43, Connexin-40, and Copine 5..	101
Figure 27. Juxta-Purkinje cells staining for Connexin-43, Connexin-40, and Contactin-2.....	102
Figure 28. Juxta-Purkinje ventricular myocytes morphological analysis.....	103
Figure 29. Schematic representation of the computational model.....	106
Figure 30. Subthreshold delayed afterdepolarization (DAD)-like activity in ventricular cells of the Purkinje-myocardial junction cause retrograde excitation of Purkinje fibers.....	107
Figure 31. Generation of hiPSC Casq2 lines	125
Figure 32. RNA sequencing data of <i>CASQ2</i> ^{-/-} hiPSC lines	126
Figure 33. Casq2 protein levels are decreased in <i>CASQ2</i> ^{-/-} hiPSC cardiomyocytes	127
Figure 34. Impedance-based contractility measurements.....	130
Figure 35. Calcium handling is altered in <i>CASQ2</i> ^{-/-} hiPSC cardiomyocytes.....	131
Figure 36. <i>CASQ2</i> ^{+/-} and <i>CASQ2</i> ^{-/-} have increased calcium leak and spontaneous/fractional calcium release compared to isogenic control	132
Figure 37. The effect of magnesium concentration on spark frequency in K180R cardiomyocytes.....	159
Figure 38. The effect of magnesium concentration on wave frequency in K180R cardiomyocytes	160

List of Abbreviations

AAV - adeno-associated virus

Ca - calcium

CaM - calmodulin

CaMKII - calmodulin kinase II

Casq - calsequestrin

Casq1 - skeletal muscle calsequestrin

Casq2- cardiac calsequestrin

CCS - cardiac conduction system

CDI - calcium dependent inactivation

ChR2 – channelrhodopsin-2

CICR - calcium induced calcium release

CM - cardiomyocyte

Cpne5 – copine-5

CPVT- catecholaminergic polymorphic ventricular tachycardia

CRISPR - clustered regularly interspaced short palindromic repeats

CRU – calcium release unit

Cx40 – connexin 40

Cx43 – connexin 43

DAD - delayed afterdepolarizations

EAD - early afterdepolarization

EC - excitation-contraction

EKG/ECG - electrocardiogram

FDHM – full duration at half maximum

FKBP - FK506 binding protein

FWHM - full width at half maximum

HET – heterozygous

hiPSC - human induced pluripotent stem cell

HOM – homozygous

HRC - histidine-rich calcium binding protein

HRP - horseradish peroxidase

ICD - implantable cardiac defibrillator

iPSC - induced pluripotent stem cell

jSR – junctional SR

kD - kilodalton

KO – knockout

LQTS - long QT syndrome

LTCC - L-type calcium channels

LV – left ventricle

NCX - sodium-calcium exchanger

NND – nearest neighbor distance

NT – normal Tyrode

PC – Purkinje cell

PCR – polymerase chain reaction

PF – Purkinje fiber

PKA - protein kinase A

PTM – post-translational modifications

PVC – premature ventricular contraction

RV – right ventricle

RyR2 - cardiac ryanodine receptor

SCR - spontaneous calcium release events

SD – standard deviation

SOICR - store-overload-induced calcium release

SR - sarcoplasmic reticulum

TA - triggered arrhythmia

TAM - tubular aggregate myopathy

VEB - ventricular ectopic beat

VM – ventricular myocardium

VT - ventricular tachycardia

WT – wild-type

INTRODUCTION*

Calsequestrin-2

Calsequestrin (Casq) is the most abundant calcium binding protein within the sarcoplasmic reticulum (SR) of skeletal and cardiac muscle (Rossi *et al.*, 2021). Discovered in 1971, Casq was described as a unique protein within the SR that was found to bind up to 970 nM calcium per milligram of protein (MacLennan & Wong, 1971). It was hypothesized to play a role in sequestering calcium within the SR and was given the name Calsequestrin. Since then, more work has been done to understand the properties of Casq, its function within the SR, the isoforms that exist, and its role in human disease. Currently, two isoforms of Casq exist. In skeletal muscle *CASQ1* is expressed at a higher level, and in cardiac muscle *CASQ2* has higher expression. While there are small differences between them, both proteins perform the same role within the SR.

Casq is a 399 amino acid, high capacity, low affinity calcium binding protein that binds 40-50 calcium ions through its 60-70 negatively charged amino acid residues (Yano & Zarain-Herzberg, 1994). The Kd of Casq for calcium has been estimated to be about 1.1 mM (Volpe & Simon, 1991). Together, Casq's calcium binding properties make it the perfect protein to manage the large amounts of calcium that are necessary for muscle contraction. Due to the large calcium binding capacity of Casq, it has been estimated that the amount of calcium released by Casq is about twenty times higher than the amount of free calcium within in the SR at the start of each excitation-contraction (EC) coupling cycle (Pape *et al.*, 2007). The ability of Casq to bind such a

* This chapter is adapted from "Molecular tissue and mechanisms of catecholaminergic polymorphic tachycardia" published in *The Journal of Physiology* and has been reproduced with the permission of the publisher and my co-authors: Prince Kannankeril and Bjorn C. Knollmann. Wleklinski MJ, Kannankeril PJ & Knollmann BC. (2020). Molecular and tissue mechanisms of catecholaminergic polymorphic ventricular tachycardia. *J Physiol* **598**, 2817-2834.

large amount of calcium comes from the complex quaternary structure that the protein assumes in the SR lumen. It was first discovered that high calcium binding occurs when levels of Casq and calcium are high. It was found that two-thirds of the total amount of calcium bound was due to the Casq aggregates that formed (Tanaka *et al.*, 1986). Several reports based on biochemical data confirm that Casq exists in a wide range of high-molecular-mass clusters (Maguire *et al.*, 1997; Maguire *et al.*, 1998). The first crystals of Casq were obtained from canine cardiac muscle in 1994 and from rabbit skeletal muscle in 1998 (Hayakawa *et al.*, 1994; Wang *et al.*, 1998). Using crystallization, equilibrium dialysis, and multiangle light scattering, Casq polymers were found to form in a calcium dependent matter (Park *et al.*, 2003; Park *et al.*, 2004). The proposed mechanism for polymer formation was that calcium binding would induce the formation of front-to-front contact between two monomers. This dimerization would be followed by another calcium-induced formation of a second contact, where two dimers would polymerize through back-to-back interactions (Park *et al.*, 2003).

The proposed mechanism of polymerization was confirmed when the polymer itself was crystallized in 2020. The study utilized very low-pH (3.5) conditions to crystallize a novel structure for the Casq polymer filament (Titus *et al.*, 2020). The filaments are an assembly of Casq dimers that interact with one another to form three different thioredoxin helices that come together to form the filament. Two of the three domains form a double helix at the core of the filament, while the final domain creates an outer “collar” and winds around the inner double helix. The new structure was used to identify novel potential calcium binding sites. The analysis found calcium binding sites that bridged both intra and inter-dimer interfaces of Casq, suggesting that calcium is involved

in the ability for Casq to form dimers and those dimers to form subsequent filaments (Titus *et al.*, 2020).

Functionally, Casq regulates the amount of calcium released from the SR during the EC coupling cycle by buffering intra-SR calcium (Zhang *et al.*, 1997; Bers, 2002). In the heart, electrical activation couples to mechanical force via the secondary messenger calcium (Bers, 2002). Membrane depolarization during the cardiac action potential opens L-type calcium channels (Figure 1), which bring calcium into the cell. Calcium binds to and opens the cardiac ryanodine receptor (RyR2) located in the terminal cisternae of the SR, the junctional SR (Figure 1), through a process known as calcium-induced calcium-release (CICR) (Fabiato, 1985). During systole, cytosolic calcium initiates myofilament contraction before being taken back up into the SR or pumped out into extracellular space during diastole. Proteins regulating SR calcium release can be categorized based on function and location. Proteins that are located within the SR lumen (e.g. Casq2, histidine-rich calcium (HRC) binding protein) affect the levels of free calcium present in the SR during the EC cycle. Proteins located within the junctional membrane of the SR (e.g. triadin, junctin) facilitate the interaction between calcium handling proteins (e.g. Casq2 and RyR2). Finally, there are a group of proteins that bind to the cytoplasmic surface of RyR2 (e.g. calmodulin, FK506 binding proteins) and regulate RyR2 sensitivity to cytoplasmic and SR luminal calcium levels.

To regulate calcium release in the heart, cardiac Casq2 localizes to the terminal cisternae that form the junctional SR (Figure 1). There, Casq2 is anchored to RyR2 by two proteins, triadin and junctin. It has been suggested that the interaction between calsequestrin and RyR2 may contribute to the refractory period of calcium release that occurs after each physiological CICR, but the mechanism is still not well understood (Györke *et al.*, 2009; Katz *et al.*, 2009; Liu *et al.*,

2009). Studies using skeletal calsequestrin (Casq1) showed changes in diffusional mobility of Casq1 after depletion of SR calcium (Manno *et al.*, 2017). If Casq2 acts in a similar manner in the heart, the findings from Casq1 would provide a plausible mechanism for how Casq2 is regulating calcium release and termination.

Alterations in Casq's structure or function disrupt calcium handling in both skeletal and cardiac muscle. Mutations in *CASQ1* and *CASQ2* are found in diseases such as tubular aggregate myopathy (TAM) and catecholaminergic polymorphic ventricular tachycardia (CPVT).

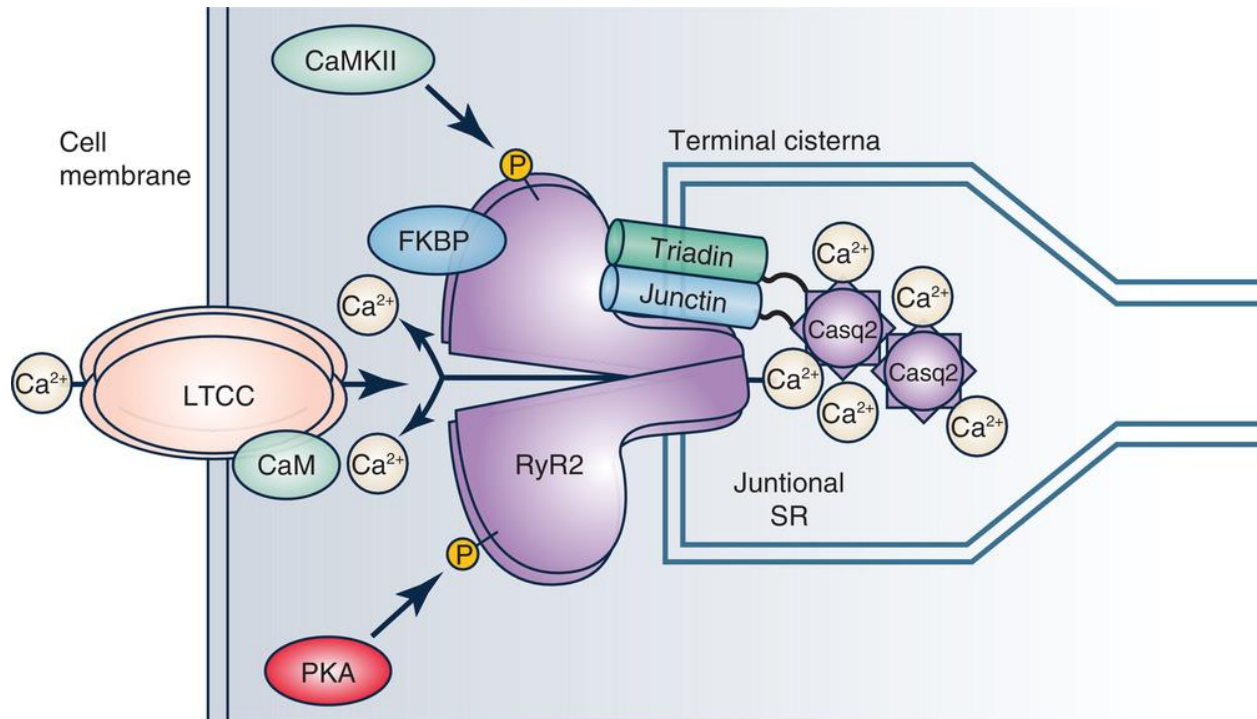


Figure 1. The SR calcium release complex in cardiac muscle. Pictured above are the proteins that are involved in the regulation of calcium release from the sarcoplasmic reticulum (SR) during excitation-contraction coupling. The ryanodine receptor type 2 (RyR2) is a large conductance calcium channel located in the junctional SR membrane that is gated by calcium influx via the L-type calcium channels (LTCC) in the cell membrane. RyR2 open probability is regulated by post-translational modifications (e.g. phosphorylation by Calcium-calmodulin kinase II, CaMKII, protein kinase A, PKA), by cytosolic RyR2 binding proteins (calmodulin [CaM], immunophilins such as FK506 binding protein [FKBP]) and SR luminal proteins (calsequestrin [Casq2], triadin, junctin). Casq2 forms polymers that are anchored to RyR2 and the junctional SR by triadin and junctin. CaM bound to LTCC mediates calcium dependent inactivation of LTCC. Figure from (Wleklinski *et al.*, 2020).

Catecholaminergic Polymorphic Ventricular Tachycardia (CPVT)

Catecholaminergic polymorphic ventricular tachycardia (CPVT) is a lethal, stress-induced cardiac channelopathy. First described in 1995, CPVT is characterized by polymorphic ventricular arrhythmias that are triggered by catecholamines released during exercise, stress, or sudden emotion in individuals with structurally normal hearts (Leenhardt *et al.*, 1995). Symptoms range from palpitations to cardiac arrest, with mortality rates between 30-50% in untreated individuals (Pérez-Riera *et al.*, 2018). Patients are normally diagnosed during early childhood but initial symptoms can occur in patients as old as 40 years of age (Pérez-Riera *et al.*, 2018). CPVT is rare, with an estimated prevalence of 1:5000 to 1:10000 depending on the population studied (Modell *et al.*, 2012; Pérez-Riera *et al.*, 2018). The true prevalence of CPVT is likely higher, since CPVT cases are frequently missed as most patients present with a normal resting electrocardiogram and structurally normal heart on cardiac workup (Imberti *et al.*, 2016).

Human genetic studies have established that CPVT is caused by mutations in genes that encode proteins of the SR calcium release complex (Swan *et al.*, 1999b; Lahat *et al.*, 2001a; Lahat *et al.*, 2001b). Supported mostly by experimental studies in mouse CPVT models (Cerrone *et al.*, 2005; Knollmann *et al.*, 2006; Rizzi *et al.*, 2008; Uchinoumi *et al.*, 2010), the current understanding of cellular CPVT pathophysiology is that catecholamines released during stress or exercise activate β -adrenergic receptor signaling, leading to a cellular chain reaction that culminates into pathological calcium release during diastole and calcium-triggered action potentials (Figure 2).

Open questions remain as to how exactly mutations in CPVT genes cause functional alterations in the SR calcium release machinery that leads to pathological calcium release during diastole (*molecular mechanisms*). Even less well understood is how the altered cellular function

causes CPVT at the whole heart and *in vivo* level. It remains to be determined if and to what extent the dysfunction of the sinus node, the cardiac conduction system and the ventricular working myocardium contribute mechanistically to CPVT (*tissue mechanisms*). Next, I will discuss the current understanding of the molecular and tissue mechanisms of CPVT to help consolidate the information and shed light on the areas where more work is needed before talking about the treatments for CPVT.

Molecular mechanisms of CPVT

Six different CPVT disease genes have been identified, which account for 60-75% of CPVT cases. The genetic cause of the remaining clinical CPVT cases is not yet known (Pérez-Riera *et al.*, 2018; Roston *et al.*, 2018b). All six CPVT genes (*RYR2*, *CASQ2*, *TRDN*, *CALM1*, *CALM2*, *CALM3*) encode proteins that are directly involved in regulating SR calcium release during excitation-contraction coupling (Figure 1). The following section reviews proteins of interest in CPVT, their physiological role and how mutations lead to CPVT.

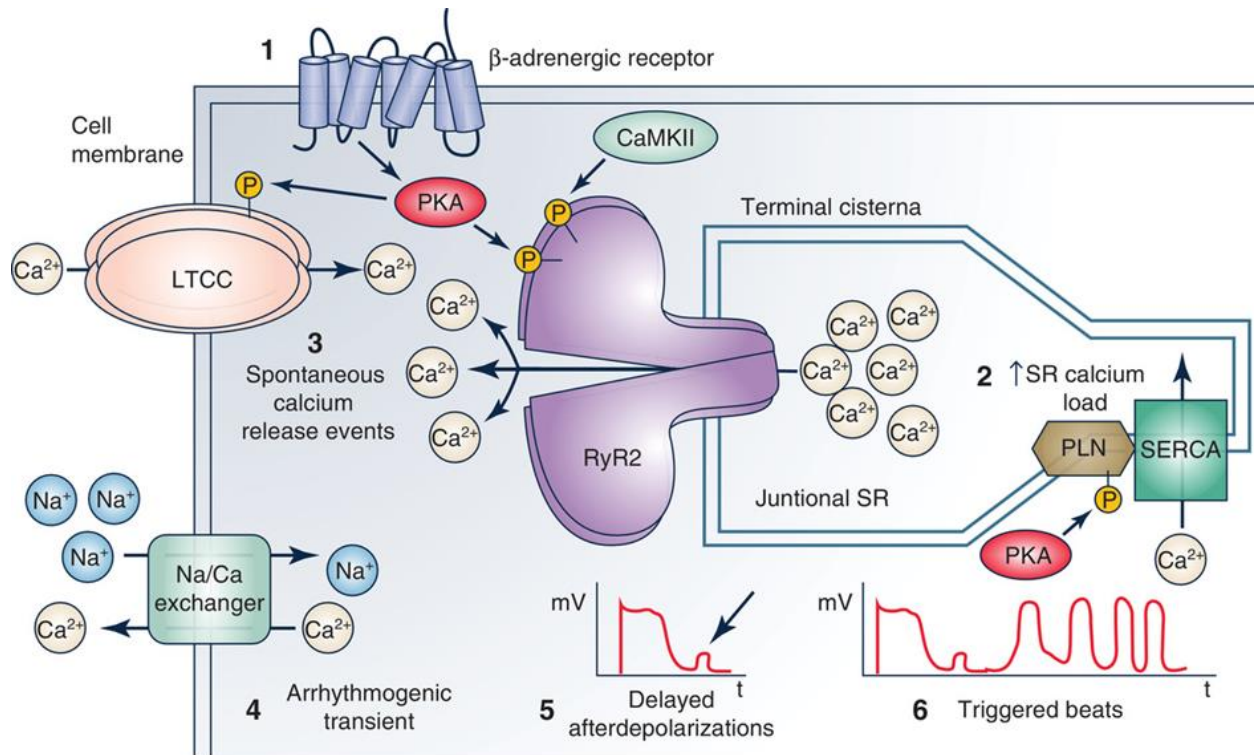


Figure 2. Cellular pathogenesis of catecholaminergic polymorphic ventricular tachycardia (CPVT). **1)** Catecholamines released during stress or exercise activates β -adrenergic receptor signaling, leading to cardiomyocyte calcium loading and enhanced SR calcium uptake. **2)** The increased SR calcium load is a physiological response necessary for increasing cardiac output during the physiological fight or flight response (Bers, 2001). Normally, ventricular myocytes can handle the increased SR calcium load. **3)** If a CPVT mutation is present, RyR2 SR calcium release channels open spontaneously during late diastole, causing unregulated “pathological” SR calcium release termed spontaneous calcium release events (SCR). **4)** The rise in cytosolic calcium during the SCR activates the electrogenic sodium calcium exchanger, which generates an arrhythmogenic transient inward current. **5)** This induces a cell membrane depolarization termed delayed afterdepolarizations (DADs). **6)** DADs are a well-established cellular mechanism that can then cause triggered beats that lead to ventricular arrhythmias (Priori & Corr, 1990). Figure from (Wleklinski *et al.*, 2020).

Ryanodine Receptor type 2 (RyR2)

Gain-of-function mutations in the *RYR2* gene are found in about 95% of patients with a genetically-confirmed diagnosis of CPVT (Pérez-Riera *et al.*, 2018) and are designated as CPVT type 1 (CPVT1). CPVT1 is autosomal-dominant and was first described in 1999 (Swan *et al.*, 1999b) before being mapped to *RYR2* in 2001 (Priori *et al.*, 2001). Since then, more than 200 gain-of-function variants in *RYR2* have been discovered. Loss-of-function *RYR2* variants also exist but are less common and associated with ventricular arrhythmia syndromes distinct from CPVT (Roston *et al.*, 2017). *RYR2* encodes a 565 kD protein, which forms a homotetrameric, high-conductance, cation-selective channel that releases calcium from the SR (Figure 1) (Seidel *et al.*, 2015). RyR2 interacts with many other proteins including Casq2 (Costello *et al.*, 1986; Franzini-Armstrong *et al.*, 1987), triadin (Guo *et al.*, 1996), junctin (Zhang *et al.*, 1997), calmodulin (Yamaguchi *et al.*, 2003; Yamaguchi *et al.*, 2007), junctophilin, and the immunophilins FKBP 12 and FKBP 12.6 (Jayaraman *et al.*, 1992; Yano *et al.*, 2009). FKBP12s are thought to stabilize the closed conformation of RyR2 and prevent diastolic release of calcium from the SR (Wehrens *et al.*, 2003). Currently, there are several hypotheses as to why mutations in RyR2 lead to CPVT, see Figure 3 (Ikemoto & Yamamoto, 2002; Wehrens *et al.*, 2003; Jiang *et al.*, 2004; Liu *et al.*, 2009). One theory is that mutations in RyR2 affect the ability for FKBP 12.6 to interact with RyR2, leading to dissociation of FKBP 12.6 and the opening of RyR2 during diastole (Wehrens *et al.*, 2003). However, others have challenged this hypothesis (Xiao *et al.*, 2007), and at present time it seems unlikely that loss of FKBP 12.6 is responsible for CPVT. Rather, FKBP12s still bind to mutant RyR2 but fail to inhibit them (Zhang *et al.*, 2016). The most-widely held hypothesis states that CPVT mutations sensitize RyR2 channels to SR luminal calcium, causing them to open at a lower intra-SR calcium concentration, termed store-overload-induced calcium release (SOICR) (Jiang *et*

al., 2004). According to the SOICR hypothesis, mutations in RyR2 decrease the threshold of SR calcium that is required to activate RYR2, leading to increased probability of calcium leak and diastolic SR calcium release. A third hypothesis focuses on the interactions within the structure of RyR2. Normally, intramolecular interactions occur between the N-terminal and central domain of RyR2 monomers, termed “zipping”, which are critical to stabilizing the protein. When RyR2 is activated during the EC coupling cycle, the intramolecular interactions are weakened “unzipping” the domains, opening the channel, and causing the release of calcium. Mutations in RyR2 that occur within the interaction domains have been shown to cause a similar “unzipping”, which results in calcium leak (Ikemoto & Yamamoto, 2002; George *et al.*, 2006; Sumitomo, 2016). While it is still debated which hypothesis is correct, common to all of them is that CPVT-linked RyR2 mutations increase the likelihood of spontaneous RyR2 openings and pathological calcium release during diastole.

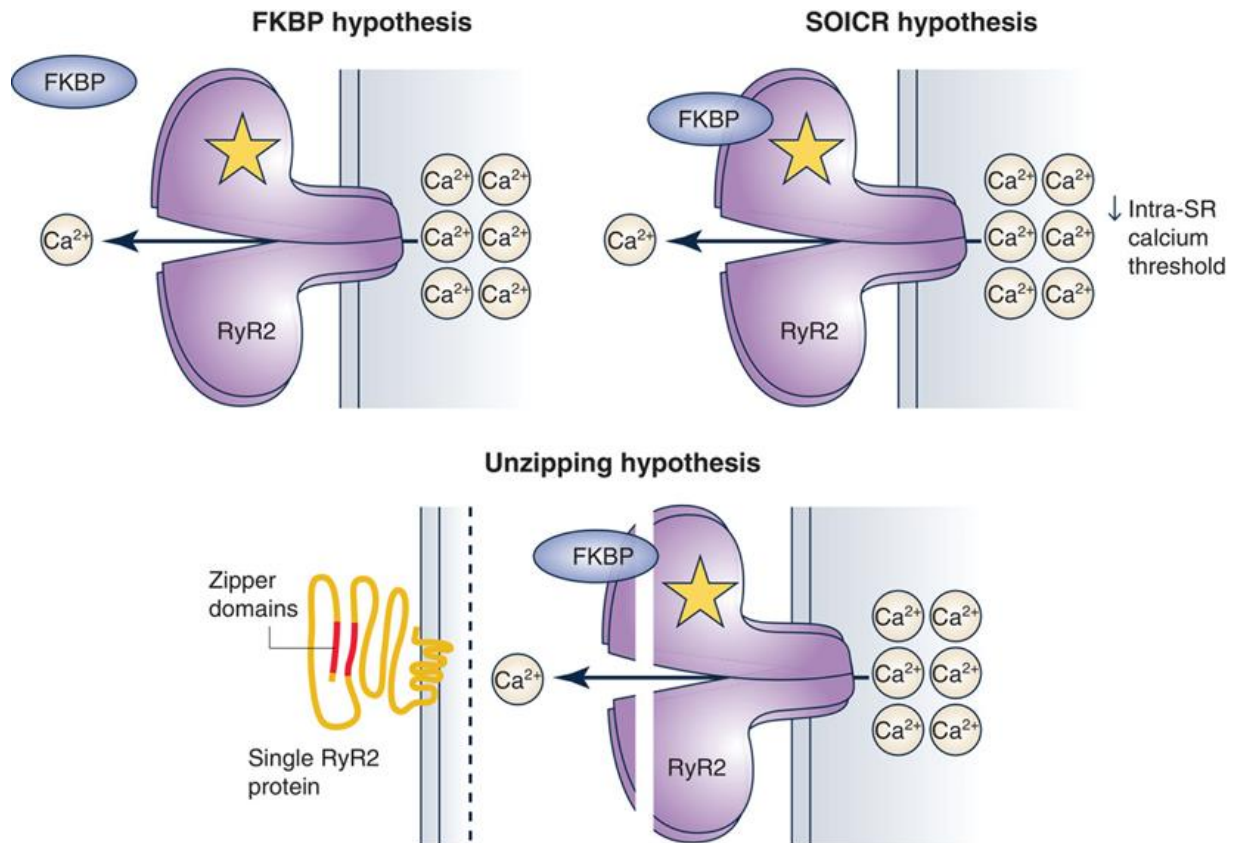


Figure 3. Summary of current hypotheses for how RyR2 mutations could lead to CPVT. The first theory states that mutations prevent FKBP binding to RyR2. The second theory states that a mutation can lower the intra-SR calcium threshold needed RyR2 to open during diastole termed store-overload-induced calcium release (SOICR). Finally, the “unzipping” theory stems from the observation that the N-terminal and central domain of RyR2 interact with one another forming a tight seal. Mutations in RyR2 can affect the interaction and lead to an unzipping of the protein, making RyR2 more prone to open spontaneously. Figure from (Wleklinski *et al.*, 2020).

Calsequestrin 2 (Casq2)

The second most common cause of CPVT are mutations in the *CASQ2* gene, termed CPVT2 (Lahat *et al.*, 2001a; Lahat *et al.*, 2001b). Casq2 was first associated with CPVT when missense mutations were discovered in a family with autosomal recessive CPVT in 2001 and nonsense mutations in a similar family in 2002 (Postma *et al.*, 2002). Casq2-linked CPVT was thought to be an autosomal recessive disease only (Postma *et al.*, 2002; de la Fuente *et al.*, 2008; Kirchhefer *et al.*, 2010b), but in 2016 a report of a novel *CASQ2* mutation (K180R) in a family with autosomal dominant inheritance of CPVT was published (Gray *et al.*, 2016). The simplest explanation why mutations in Casq2 cause CPVT is that they impair Casq2's ability to buffer calcium in the SR, resulting in a much faster rise of intra-SR free calcium concentration close to RyR2 release channels. Although intra-SR calcium kinetics have not yet been measured experimentally in Casq2 CPVT models, there is extensive evidence that absence of Casq2 in mice leads to hyperactive RyR2 channels, impaired calcium-release termination, shortened calcium release refractory period, and enhanced spontaneous release of calcium (Knollmann *et al.*, 2006; Chopra *et al.*, 2007; Kryshnal *et al.*, 2015). While impaired calcium buffering is the generally accepted mechanism for Casq2 nonsense mutations that result in loss of Casq2, missense mutations (e.g. R33Q) may alter Casq2 interaction with RyR2 in addition to reducing calcium buffering (Terentyev *et al.*, 2006). For autosomal-dominant CPVT2, the current hypothesis is that Casq2 mutations affect the ability for polymerization to occur. Two autosomal-dominant mutations (K180R, and S173I) were unable to form polymers in a turbidity assay. Interestingly, the defect for the K180R mutation only occurred in the presence of magnesium. While the exact mechanism

is unknown, magnesium may affect the ability of Casq2 to form filaments and could be involved in the pathogenesis of the K180R mutation (Titus *et al.*, 2020).

Calmodulin (CaM)

Three different genes – *CALM1*, *CALM2*, *CALM3* – encode identical CaM proteins and are located on chromosome 14q32, 2p21, and 19q13 respectively. Mutations in each of the three CaM genes have been linked to three distinct genetic arrhythmia disorders: CPVT (Nyegaard *et al.*, 2012; Yin *et al.*, 2014; Gomez-Hurtado *et al.*, 2016), idiopathic ventricular fibrillation (Marsman *et al.*, 2014), and long-QT syndrome (Jiménez-Jáimez *et al.*, 2016). Structurally, CaM has an alpha-helical structure and contains four classical calcium-binding EF hand motifs, two on each N- and C-terminal lobe. The motifs can bind to one calcium ion each with the N-terminal lobe having a lower affinity for calcium (Linse *et al.*, 1991; VanScyoc *et al.*, 2002). When calcium binds to CaM, the protein undergoes a conformational change that exposes the hydrophobic patches in each lobe. The patches contain a large amount of methionine residues that utilize a central linker between the two lobes to interact with a large number of protein targets (Yamniuk & Vogel, 2004). Within the EC coupling machinery, CaM binds to RyR2 and the L-type calcium channel (LTCC) (Figure 1). The binding of calmodulin to RyR2 inhibits calcium release from the SR during diastole (Yamaguchi *et al.*, 2003; Yamaguchi *et al.*, 2007) and the binding to LTCC inactivates the channel (Peterson *et al.*, 1999; Zühlke *et al.*, 1999), a process termed calcium-dependent inactivation (CDI). In addition to RyR2 and LTCC, CaM regulates other membrane ion channels important for the cardiac action potential (e.g., Nav 1.5, K_v7.1). Mutations in the three *CALM* genes have a wide range of effects, which may explain the diverse arrhythmia phenotypes associated with CaM mutations. For example, CaM mutants linked to CPVT either fail to inhibit

or even activate RyR2 (Hwang *et al.*, 2014; Gomez-Hurtado *et al.*, 2016). CPVT calmodulin mutants tend to bind to RyR2 with higher affinity than wild-type CaM (Hwang *et al.*, 2014; Gomez-Hurtado *et al.*, 2016), which can explain their autosomal-dominant mode of action. On the other hand, CaM mutants associated with LQTS do not affect RyR2, but rather impair LTCC inactivation, leading to a profound action potential lengthening and QT prolongation (Limpitikul *et al.*, 2014). Due to the many CaM targets within the cell, CaM mutations may also cause ventricular arrhythmias by other mechanisms, but so far none have been definitively confirmed.

Triadin

Triadin is a trans SR membrane protein that forms a complex with RyR2, calsequestrin, and junctin to create the SR calcium release unit (Jones *et al.*, 1995; Kobayashi & Jones, 1999). Triadin localizes to the junctional SR membrane in both cardiac and skeletal muscle (Figure 1). Triadin has a single membrane spanning domain, a short N-terminal segment located in the cytoplasm, a long C-terminal tail that projects intraluminally and is highly basic and charged, and a long run of charged amino acid residues called “KEKE” association motifs that promote protein-protein interactions (Knudson *et al.*, 1993; Jones *et al.*, 1995; Guo *et al.*, 1996; Zhang *et al.*, 1997). Triadin is thought to act mainly as a scaffolding protein to help anchor Casq2 to RyR2 near the junctional SR membrane. The anchoring properties of triadin are important for maintaining the ultrastructure of the terminal cisterna. When triadin is knocked out in mice (Chopra *et al.*, 2009), protein levels of RyR2, Casq2 and junctin were all reduced despite normal RNA expression. Consistent with a role of triadin as the primary anchoring protein that retains Casq2 in the terminal cisterna, Casq2 can be detected in the free SR of triadin knockout myocytes (Chopra *et al.*, 2009). Loss of triadin also resulted in profound structural remodeling of the terminal cisterna, with an

approximately 50% reduction of the junctional SR – t-tubule interface. As a result of the structural remodeling, coupling efficiency between LTCC and RyR2 was impaired and LTCC calcium dependent inactivation reduced. Due to the impaired LTCC inactivation, triadin loss results in a gain of function effect on LTCC, increased calcium current and prolonged cardiac action potential. The ensuing cellular and SR calcium overload causes an increase in spontaneous calcium release events especially during catecholaminergic stimulation (Chopra *et al.*, 2009). Other roles of triadin have been proposed, such as the ability of overexpressed triadin to enhance SR calcium release by directly affecting the RyR2 channel, but the work was conducted in cultured myocytes and needs to be confirmed at the single channel level (Terentyev *et al.*, 2005). The first triadin mutation linked to CPVT was discovered in 2012 and another was found in 2015 (Roux-Buisson *et al.*, 2012; Rooryck *et al.*, 2015). Triadin mutations are thought to result in decreased levels of the protein. For example, the triadin-T59R mutations renders the triadin protein unstable and leads to enhanced degradation (Roux-Buisson *et al.*, 2012). More recently, triadin mutations were also found in patients suffering from long-QT. The mutations caused a frameshift in the *TRDN* gene leading to a syndrome termed “triadin knockout syndrome” (Altmann *et al.*, 2015). Patients suffered from multiple episodes of exertion-induced syncope and cardiac arrest in early childhood. Other symptoms include mild to moderate muscle weakness. Further electrocardiographic workup demonstrated extensive T-wave inversion and QT prolongation. Normally, patients with similar findings would be classified as having long-QT syndrome. It has been proposed that patients with triadin mutations that decrease the levels of triadin should be diagnosed with “triadin knockout syndrome” (Altmann *et al.*, 2015), which is essentially an overlap syndrome with features of both CPVT and long QT.

Other candidate genes for CPVT

Although not yet identified, mutations in other genes that are integral to SR calcium handling could potentially cause CPVT and should be screened for in patients carrying a clinical diagnosis of CPVT. Junctin, encoded by the gene aspartyl-beta-hydroxylase (*ASPH*), is a junctional SR protein (Figure 1) that interacts with triadin and RyR2 (Jones *et al.*, 1995; Kobayashi & Jones, 1999). Like triadin, junctin functions as a scaffold for Casq2 and is involved in the polymerization of Casq2 as calcium increases in the SR (Lee *et al.*, 2012). Other CPVT candidates are proteins that regulate RyR2 calcium sensitivity such as FKBP 12 and FKBP 12.6 (Figure 1). Both proteins are expressed in cardiac myocytes and are thought to promote the closed state of the channel. FKBP 12 and 12.6 bind to the same region of RyR2 which suggests that the competition between them is important for the functional outcome of RyR2 (Gonano & Jones, 2017). Another candidate is histidine-rich calcium (HRC) binding protein, a SR luminal calcium binding buffering that is upregulated when Casq2 is knocked out (Murphy *et al.*, 2011). Increased HRC may activate RyR2 calcium release channels and contribute to CPVT (Liu *et al.*, 2015).

Tissue mechanisms underlying CPVT

It is generally agreed that CPVT mutations render the RyR2 calcium release channels hyperactive, generating pathological calcium release during diastole. What remains unclear are the tissue mechanisms of CPVT. For example, a key question is the mechanistic contribution of low sinus heart rates, since sinus node dysfunction is a hallmark of CPVT in patients and animal models (Faggioni *et al.*, 2014b; Miyata *et al.*, 2018). Another key question is whether the arrhythmic trigger that causes the ventricular arrhythmias originates from ventricular cardiomyocytes in the working myocardium or from specialized cells of the cardiac conduction system, the Purkinje cells.

Theoretical considerations and modeling studies favor the ventricular Purkinje network as the primary cellular source of CPVT (Xie *et al.*, 2010) but conclusive experimental evidence is lacking.

Pathophysiological role of sinus node dysfunction in CPVT

Sinus node dysfunction and bradycardia are well-documented phenotypes of CPVT in humans and in mouse models of CPVT (Faggioni *et al.*, 2014b; Miyata *et al.*, 2018). The mechanisms of how CPVT mutations cause sinus node dysfunction is thought to be multifactorial. For example, one theory is that the loss of Casq2 causes a regional microfibrosis in the sinus node, which would alter the generation and propagation of an electrical impulse through the node (Glukhov *et al.*, 2015). It is hypothesized that the microfibrosis could form from apoptosis and fibrogenesis due to an overload of diastolic calcium (Swaminathan *et al.*, 2011). The increase in calcium levels could also trigger the activation of CaMKII, which has been shown to be involved in the upregulation of genes that could promote structural remodeling (Huke & Knollmann, 2011). Understanding how sinus node dysfunction originates is important as sinus node chronotropic incompetence has been shown to be a risk predictor for ventricular arrhythmia in children and young adults with CPVT (Franciosi *et al.*, 2019). A likely explanation is that low sinus rates prolong the diastolic interval, allowing the spontaneous SR calcium release to occur before CICR during the next action potential can empty the SR and resets the SR calcium clock. Our group tested this hypothesis experimentally at the cellular level and *in vivo* using the Casq2 KO mouse CPVT model (Faggioni *et al.*, 2013). We found that increasing the pacing rate reduced the likelihood of spontaneous calcium release and triggered beats in isolated cardiomyocytes. *In vivo*, artificially raising resting heart rates with atropine or by overdrive pacing prevented CPVT (Faggioni *et al.*, 2013). To study the role of the cardiac conduction system in CPVT in more detail,

our group recently developed two novel mouse models where the *CASQ2* gene can be either inactivated (i.e., conditional KO) or activated (i.e., conditional rescue) by Cre-mediated recombination (Flores *et al.*, 2018). Thus, we were able to modulate *CASQ2* gene expression in a tissue and temporal manner by crossing our new mouse models with mice that carry Cre controlled by tissue selective and/or inducible promoters. For example, using the HCN4KiT-Cre system (Hoesl *et al.*, 2008), we were able to re-express *Casq2* in the SA node of adult *Casq2* KO mice, which accelerated sinus heart rates and prevented CPVT (Flores *et al.*, 2018), as illustrated in Figure 4. Hence, dysfunction of the sinoatrial node and the ensuing slow sinus heart rates may independently contribute to arrhythmia risk in CPVT.

Purkinje cells as the cellular source of CPVT

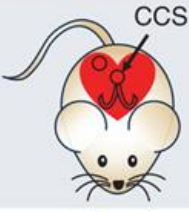



Theoretical considerations and modeling studies favor the ventricular Purkinje network as the primary cellular source of CPVT because of a favorable source-sink relationship (Xie *et al.*, 2010). There are also key differences between Purkinje cells and ventricular myocytes that could explain why Purkinje cells are more likely to generate arrhythmias. Purkinje cells have a much lower number of T-tubules compared to ventricular cardiomyocytes and hence more corbular SR (Sommer & Johnson, 1968). The differences in organelle structure results in a calcium activation process that is unique to Purkinje cells termed reverse mode-excitation-contraction coupling. The calcium release units within the center of Purkinje fibers do not respond to voltage but instead are activated by calcium waves (Stuyvers *et al.*, 2005). Experimental evidence to support that CPVT originates from the Purkinje system stems from a mouse model with a heterozygous mutation in *RyR2* (*RyR2/RyR2^{R4496C}*) (Cerrone *et al.*, 2005). Optical mapping of whole mouse hearts demonstrated that breakthrough patterns from ventricular tachycardias may originate from the His-

Purkinje network in both ventricles (Cerrone *et al.*, 2007). To confirm the arrhythmias were generated from the Purkinje fibers, chemical ablation (Lugol's solution) of the right ventricular endocardial cavity was performed. Mice treated with Lugol's had conversion of bidirectional VT into monomorphic VT, suggesting endocardial Purkinje fiber ablation prevented the development of arrhythmias from the right ventricle (Cerrone *et al.*, 2007). Follow up studies in single cells found that RyR2/RyR2^{R4496C} Purkinje cells developed spontaneous calcium release events and triggered beats at a significantly higher rate compared to ventricular myocytes (Herron *et al.*, 2010; Kang *et al.*, 2010).

The experimental studies in the RyR2/RyR2^{R4496C} mice had suggested that alternating beats of bi-directional VT originated from the right and left bundle branches, but the mechanism by which the triggered activity generated an alternating pattern was not addressed (Cerrone *et al.*, 2007). Using a simulated two-dimensional anatomic model of rabbit ventricles with a simplified His-Purkinje system, a computer modeling study attempted to gain a better understanding of the mechanism underlying bidirectional ventricular tachycardia, which is a hallmark of CPVT (Leenhardt *et al.*, 1995). Based on the results of the modeling, the authors proposed that a “ping-pong” mechanism, called reciprocating bigeminy, could account for the bi-directional VT pattern that was seen in CPVT (Baher *et al.*, 2011). The “ping-pong” mechanism is based on the findings that above a certain threshold heart rate, a DAD triggers an action potential that initiates ventricular bigeminy, and that the threshold heart rate for bigeminy varies at different locations in the heart (Baher *et al.*, 2011). The findings from the model suggested that DAD-triggered arrhythmias could cause ventricular bigeminy when a single site in the His-Purkinje system or the ventricular myocardium developed a DAD-triggered beat following a sinus beat. Bi-directional VT occurred when a second site developed ventricular bigeminy and reciprocally activated the first site by the

“ping-pong” mechanism. Bi-directional VT could degenerate into polymorphic VT when the increase in heart rate recruited additional sites in the His-Purkinje to develop bigeminy (Baher *et al.*, 2011). The data from the RyR2^{R4496C} model suggests that the His-Purkinje system could serve as both the source of initiation and the propagation of ventricular arrhythmias.

While the above evidence suggests Purkinje cells in the conduction system as the source for CPVT, direct experimental evidence was lacking until recently, when (Flores *et al.*, 2018) tried to establish causation by knocking out Casq2 only in the conduction system using the HCN4Kit-Cre recombinase system. Cre expression is driven by the promoter of the *HCN4* gene, which is expressed in the sinus node and the cardiac conduction system but not in the ventricular working myocardium. Surprisingly, the deletion of Casq2 in the Purkinje network did not produce a CPVT phenotype (Figure 4) (Flores *et al.*, 2018). Since deletion of Casq2 is an established molecular mechanism of CPVT, the results of the study suggest that Purkinje cells in the conduction system may not be capable to generate CPVT on their own. Rather, ventricular myocytes may be the cellular culprit responsible for CPVT, which is discussed next.

		Heart rate	Arrhythmia phenotype
Wild type		Normal	None
Casq2 knockout		Sinus bradycardia	Ventricular tachycardia
Casq2 CCS deletion		Normal	None
Casq2 CCS rescue		Sinus tachycardia	None

The Journal of
Physiology

Figure 4. Cardiac conduction system (CCS) targeted *CASQ2* gene deletion or rescue. Cartoon showing the heart rate and ventricular arrhythmia phenotype of mice with conditional deletion or rescue of *Casq2* in the CCS. Red/yellow color indicates functional *CASQ2*. Figure from (Wleklinski *et al.*, 2020).

Ventricular cardiomyocytes as the cellular source of CPVT

Based on experimental studies of cells isolated from the ventricular myocardium of CPVT mouse models, ventricular cardiomyocytes are clearly capable of generating spontaneous calcium release, DADs, and spontaneous action potentials in response to catecholaminergic stimulation, making them candidates to be the origin of ventricular arrhythmias in CPVT (Knollmann *et al.*, 2006; Liu *et al.*, 2006; Cerrone *et al.*, 2007). Other studies also support these findings. For example, human cardiomyocyte models of CPVT generated from patient-specific induced pluripotent stem cells (iPSCs) also exhibit DADs and action potentials triggered by spontaneous calcium release (Novak *et al.*, 2012; Novak *et al.*, 2015). Drug efficacy in isolated ventricular cardiomyocytes can predict antiarrhythmic efficacy in mouse models and in humans with CPVT (Knollmann, 2011; Batiste *et al.*, 2019). Furthermore, CPVT patients frequently present with atrial tachycardia or atrial fibrillation that can occur prior or during their ventricular tachycardia (Leenhardt *et al.*, 1995). Up to 74% of patients with CPVT experience supraventricular tachycardias at slower heart rates than the ventricular arrhythmias (Sumitomo *et al.*, 2007; Cerrone *et al.*, 2009; Sy *et al.*, 2011). Based on optical mapping data from a Casq2 null mouse model, the atrial tachyarrhythmias are driven by spontaneous calcium release events in atrial myocardium that cause DADs and atrial triggered beats (Faggioni *et al.*, 2014a), supporting that calcium-triggered tachyarrhythmias can originate outside the specialized conduction system. Finally, in clinical studies of CPVT patients, 60-70% of ventricular ectopy originated from the right and left ventricular outflow tracts (Sumitomo *et al.*, 2003; Sy *et al.*, 2011). Although there is not universal agreement on where to find Purkinje fibers in the human ventricle, researchers have suggested that the outflow tract has little or no Purkinje fibers present (Shimizu, 2009). However, a recent anatomical study of the human heart identified what appear to be specialized conducting cells in

the right ventricular outflow tract. The specialized cells are thought to be the ramifications of the right bundle branch that do not extend past the pulmonary valves, but more studies are needed to understand the nature of these cells. Of note, some of the arrhythmia foci identified within the right ventricular outflow tract were at anatomical locations distinct from that of the specialized conduction cells (De Almeida *et al.*, 2020). Together, the human data could indicate that ventricular cardiomyocytes are capable of triggering CPVT, at least in portions of the left or right outflow tract. More research with tissue-targeted genetic models such as in Figure 4 is needed to determine the tissue origin of CPVT, and to help understand how ventricular cardiomyocytes can overcome the sink-source mismatch to trigger CPVT.

Treatment of CPVT patients

For CPVT patients, there are several therapeutic options recommended by consensus guidelines (Priori *et al.* 2013): First line therapy are beta-adrenergic receptor blockers (Class I recommendation). If patients on maximally tolerated beta-blocker therapy continue to have syncope or recurrent sustained VT, treatment should be intensified with combination medical therapy (e.g. adding flecainide, Class IIA) or left cardiac sympathetic denervation (Class IIB). There is no role for an ICD as standalone therapy, nor programmed electrical stimulation in CPVT (Class III).

Beta-adrenergic receptor inhibitors (beta-blockers)

Beta-blockers are first line drug therapy to treat CPVT since CPVT is triggered by beta-adrenergic stimulation. Based on clinical studies (Hayashi *et al.*, 2009; Leren *et al.*, 2016), the most effective beta-blocker is nadolol, although it is not known why nadolol is superior to other

beta-blockers. Although beta-blockers are recommended as first line therapy, they are not completely protective: Over 30% of patients experienced events during a 8-year follow-up period (van der Werf *et al.*, 2012).

Flecainide and Propafenone

The class 1C antiarrhythmic drugs flecainide and propafenone both prevent exercise-induced VT in mice and humans with CPVT (Watanabe *et al.*, 2009; Hwang *et al.*, 2011). At the cellular level, their efficacy can be attributed to their dual inhibition of sodium and RyR2 calcium release channels, resulting in a profound suppression of spontaneous calcium release and triggered beats. Since the initial report in 2009, five clinical studies including a randomized placebo-controlled trial (Kannankeril *et al.*, 2017) have investigated flecainide therapy in CPVT patients that were experiencing exercise-induced ventricular arrhythmia despite therapy with beta-blockers. After the initiation of flecainide, approximately 80% of patients had either a partial or a complete suppression of exercise-induced VT (van der Werf *et al.*, 2011; Khoury *et al.*, 2013; Watanabe *et al.*, 2013; Kannankeril *et al.*, 2017; Wangüemert Pérez *et al.*, 2018). Propafenone, another class 1C antiarrhythmic drug, has also been used to treat CPVT (Marx *et al.*, 2019). Similar to flecainide, propafenone inhibits RyR2 single channels (Hwang *et al.*, 2011) and inhibits arrhythmogenic calcium waves in CPVT cardiomyocytes (Savio-Galimberti & Knollmann, 2015). While both antiarrhythmic drugs are effective clinically, additional studies are still needed to gain a better understanding of the role of sodium channel versus RyR2 inhibition, and the potential as a first-line therapy (Behere & Weindling, 2016).

Calcium channel blockers

Although effective in cell and animal models of CPVT (Katz *et al.*, 2010; Alcalai *et al.*, 2011), clinically L-type calcium channel blockers by and large provide only transient or partial benefit in CPVT patients already treated with beta-blockers (Swan *et al.*, 2005; Rosso *et al.*, 2007; Katz *et al.*, 2010). Both beta-blockers and flecainide are superior at preventing VT. Calcium channel blockers could be considered in patients that are unable to take flecainide or in refractory cases of CPVT.

Cardiac sympathetic denervation

Left or bilateral cardiac sympathetic denervation reduces catecholamine signaling in the heart by preventing the release of norepinephrine from sympathetic nerve terminals. It was first reported to be successful for CPVT in 2008 when 3 patients that were refractory to their medications became symptom free after the procedure (Wilde *et al.*, 2008). A larger follow-up study found a reduction of major cardiac events from 86% to 21% (De Ferrari *et al.*, 2015). The most recent guidelines recommend sympathetic denervation as an option for patients that are still experiencing symptoms on maximum beta-blocker therapy (Class IIB).

Implantable cardiac defibrillator (ICD)

The 2013 guidelines recommended (Class I) that a patient with CPVT have an ICD implanted if the patient has survived a cardiac arrest or if a patient has syncope/documentated sustained VT despite optimal medical management and/or LCSD (Al-Khatib *et al.*, 2018). A recent meta-analysis reviewed 53 studies containing 1429 CPVT patients, 35% of whom had an ICD implanted (Roston *et al.*, 2018a). During follow-up, 40% of patients received at least 1 appropriate

shock, 21% of patients received at least 1 inappropriate shock, and electrical storm (3 or more sustained episodes of ventricular tachycardia, ventricular fibrillation, or appropriate shocks from an ICD within 24 hours) occurred in 20% of patients. 7 patients died despite ICD placement, with 4 deaths associated with electrical storm. The effectiveness of the shocks was also assessed. 99% of shocks for ventricular tachycardia failed despite being appropriate whereas 94% of shocks for ventricular fibrillation were successful (Roston *et al.*, 2018a). Thus, the efficacy of ICD shocks in CPVT appears dependent on the arrhythmia mechanism - effective for ventricular fibrillation but ineffective for VT. (Miyake *et al.*, 2013) A recent multicenter study of 136 CPVT patients who presented with cardiac arrest showed no survival benefit associated with ICD implant (van der Werf *et al.*, 2019). These data indicate that ICD therapy can be both ineffective and proarrhythmic, and can cause serious medical complications and psychological burden, especially in pediatric populations. Hence, ICD implantation is controversial and of questionable utility in CPVT patients.

Possible future CPVT therapies

One promising approach is to target the sinus node dysfunction that is characteristic of CPVT. As proof of concept, artificially raising heart rates with atropine, by atrial overdrive pacing or by re-expressing Casq2 in the sinoatrial node prevented catecholamine-induced ventricular arrhythmia in the Casq2 KO mouse CPVT model (Faggioni *et al.*, 2013) (Flores *et al.*, 2018). Observational patient data also suggests efficacy of raising sinus heart rates as a novel therapeutic approach that can prevent exercise-induced VT (Faggioni *et al.*, 2013), which we recently confirmed in a small open-label clinical trial, where raising sinus heart rates with atropine

prevented or reduced exercise-induced ventricular ectopy in 6 CPVT patients (Kannankeril *et al.*, 2020).

Another approach that has been tested successfully in CPVT mouse models is gene therapy via adeno-associated viral (AAV) vectors. Multiple studies have seen beneficial effects from delivering various calcium handling proteins such as Casq2 (Denegri *et al.*, 2014; Kurtzswald-Josefson *et al.*, 2017; Cacheux *et al.*, 2019) and an engineered CaM that inhibits RyR2 calcium release (Liu *et al.*, 2018). AAV was also successfully used for *in vivo* CRISPR/Cas9-mediated gene editing of an RyR2 CPVT mutation in mice (Pan *et al.*, 2018). As gene therapy continues to improve, the above studies demonstrate the power that a targeted approach could have on arrhythmic diseases, and potentially prevent patients from needing any pharmacologic or surgical interventions.

More selective small molecule inhibitors of RyR2 mediated calcium release could provide a better tolerated and effective CPVT therapy. Dantrolene, a drug used clinically to treat hyperactive skeletal muscle calcium release, decreased exercise-induced ventricular ectopy in some but not all CPVT patients (Penttinen *et al.*, 2015). Our group recently reported the discovery of ent-verticilide, a cyclic depsipeptide that has nanomolar potency, is selective for RyR2 over RyR1, and exhibits antiarrhythmic efficacy *in vivo* (Batiste *et al.*, 2019). Another promising drug target is the calmodulin-dependent serine-threonine protein kinase II (CaMKII) (Figure 1). RyR2 phosphorylation by CaMKII increases RyR2 calcium leak. CaMKII inhibition with KN-93 (Liu *et al.*, 2011) or with AAV-mediated delivery of a CaMKII peptide inhibitor (Bezzarides *et al.*, 2019) was effective in suppressing arrhythmias in a murine model of CPVT. Finally, Kifuensine, an inhibitor of mannosidase-I, was used to successfully rescue expression of Casq2 and reduce CPVT

occurrence in triadin-KO mice by preventing proteasomal degradation of misfolded proteins (Cacheux *et al.*, 2019).

Uncovering new therapies

A majority of drug treatments for CPVT were investigated in animal models but with the recent development of more mature cardiomyocytes being generated from human induced-pluripotent stem cells (hiPSC) (Parikh *et al.*, 2017), researchers have begun utilizing stem cell models to identify potential compounds that could treat CPVT. Mouse models have well-known limitations in trying to reproduce human physiology (Sallam *et al.*, 2014; Sallam *et al.*, 2015; Liang *et al.*, 2016). iPSCs, first generated in 2001, overcome some of these limitations and provide a more patient-specific model. One of the biggest areas iPSCs have proven to be useful is in disease modeling (Kim, 2014). Reports have demonstrated that patch clamp analysis can be used to investigate cellular triggers of CPVT phenotypes, such as delayed after depolarizations (DADs), early afterdepolarizations (EADs), and triggered arrhythmias (TAs) (Novak *et al.*, 2015). These hiPSC-CM also had abnormal calcium handling such as multiple peaks, oscillations, varying amplitude, and local calcium release events within beats (Novak *et al.*, 2015). One of the most promising aspects of modeling CPVT in iPSC cardiomyocytes is the ability to screen different pharmacological treatments. Studies have shown the ability for standard medications (e.g. flecainide) to prevent arrhythmias in an iPSC-CM model, and subsequently reduce the symptoms experienced by patients (Preininger *et al.*, 2016). This shows that iPSC cardiomyocytes can serve as a model to investigate arrhythmias and screen for potential therapeutic targets that may help patients suffering from these diseases.

Summary and Motivation

The goal of the following work has been to gain a better understanding of Casq2 and CPVT by studying CPVT2 in various models. Casq2 is vital for calcium homeostasis in the heart, and the results found here have implications in all areas of the body (e.g. skeletal muscle) where calcium handling is vital for normal physiology. Autosomal recessive *CASQ2* mutations are the second most common cause of CPVT, but recent reports suggest that autosomal dominant mutations occur more frequently than previously thought (Ng *et al.*, 2020). How the autosomal dominant mutations cause CPVT is currently unclear. While the pathophysiology of CPVT has been investigated extensively, there are still questions surrounding how mutations in less common calcium handling proteins can cause CPVT and where in the heart the disease originates from.

At a molecular level, six genes that affect calcium handling have been found to cause CPVT: *RYR2*, *CASQ2*, *TRDN*, *CALM1*, *CALM2*, and *CALM3*. More work is needed to understand how exactly mutations disrupt protein function and cause pathological calcium release at the cellular level. At a tissue level, current research suggests that sinus node dysfunction contributes mechanistically to the development of exercise-induced ventricular ectopy and could be targeted therapeutically by increasing the sinus heart rate. With current research, it is still unclear whether the ectopic beats originate in the ventricular conduction system (i.e., Purkinje cells) or in the ventricular working myocardium.

Insights gathered from studying the molecular and tissue mechanisms would extend beyond CPVT. RyR2 hyperactivity and abnormal calcium handling is also common feature of structural heart diseases such as ischemic cardiomyopathy or non-ischemic heart failure, which are the leading cause of sudden death in the developed world. Hence, CPVT can serve as an important paradigm for studying calcium-related arrhythmia mechanisms and developing novel therapeutics

that prevent ventricular arrhythmia and sudden death. The following work expands our knowledge of Casq2 and CPVT by uncovering a novel mechanism for autosomal dominant CPVT2, using Casq2 to understand the anatomic origin of CPVT, and generating a human stem cell model to investigate potential therapies for diseases caused by abnormal calcium handling.

CHAPTER I

Uncovering a mechanism for autosomal dominant CPVT2

Introduction

As discussed before, catecholaminergic polymorphic ventricular tachycardia (CPVT) is a lethal, stress-induced cardiac channelopathy characterized by polymorphic ventricular arrhythmias that are triggered by catecholamines released during exercise, stress, or sudden emotion in individuals with structurally normal hearts (Leenhardt *et al.*, 1995). There are six different CPVT disease genes that account for 60-75% of CPVT cases (Pérez-Riera *et al.*, 2018; Roston *et al.*, 2018b). All six CPVT genes (*RYR2*, *CASQ2*, *TRDN*, *CALM1*, *CALM2*, *CALM3*) encode proteins that are directly involved in regulating SR calcium release during excitation-contraction (EC) coupling. In the heart, electrical activation couples to mechanical force via the secondary messenger calcium (Bers, 2002). Membrane depolarization during the cardiac action potential opens L-type calcium channels, which bring calcium into the cell. calcium binds to and opens cardiac ryanodine receptors (RyR2) located in the terminal cisternae of the SR, which form the junctional SR, a process known as calcium-induced calcium -release (CICR) (Fabiato, 1985). During systole, cytosolic calcium initiates myofilament contraction before being taken back up into the SR or pumped out into extracellular space during diastole. Supported mostly by experimental studies in mouse CPVT models (Cerrone *et al.*, 2005; Knollmann *et al.*, 2006; Rizzi *et al.*, 2008; Uchinoumi *et al.*, 2010), the current understanding of cellular CPVT pathophysiology is that catecholamines released during stress or exercise activate β -adrenergic receptor signaling, leading to a cellular chain reaction that culminates into pathological calcium release during diastole and calcium-triggered action potentials.

Cardiac calsequestrin (Casq2), encoded by the *CASQ2* gene, is the most abundant calcium binding protein located in the junctional SR. Casq2 is a high capacity, low affinity calcium binding protein that binds 40-50 calcium ions through its 60-70 negatively charged amino acid residues (Yano & Zarain-Herzberg, 1994). Functionally, Casq2 regulates the amount of calcium released from the SR through RyR2 during E-C coupling by buffering intra-SR calcium (Zhang *et al.*, 1997; Bers, 2002). Casq2 is known to form homo-polymers in a calcium-dependent manner (Park *et al.*, 2003). The polymerization and depolymerization of Casq2 is thought to have an important role in the regulation of RyR2 during the E-C coupling cycle by affecting the termination of calcium release from the SR during the EC coupling cycle through the binding of Casq2 monomers to RyR2 or calcium release channels (Györke *et al.*, 2009), but it is still not well understood how important polymerization is for the function of Casq2.

Variants in *CASQ2* are the second most common cause of CPVT, termed CPVT2 (Lahat *et al.*, 2001a; Lahat *et al.*, 2001b). Casq2 was first associated with CPVT when missense variants were discovered in a family with autosomal recessive CPVT in 2001 and nonsense variants in a similar family in 2002 (Postma *et al.*, 2002). The simplest explanation why variants in Casq2 cause CPVT is that they impair Casq2's ability to buffer calcium in the SR, resulting in a much faster rise of intra-SR free calcium concentration close to RyR2 release channels. Although intra-SR calcium kinetics have not yet been measured experimentally in Casq2 CPVT models, there is extensive evidence that absence of Casq2 in mice leads to hyperactive RyR2 channels, impaired calcium-release termination, shortened calcium release refractory period, and enhanced spontaneous release of calcium (Knollmann *et al.*, 2006; Chopra *et al.*, 2007; Kryshtal *et al.*, 2015). While impaired calcium buffering is the generally accepted mechanism for Casq2 nonsense

variants that result in loss of Casq2, missense variants (e.g. R33Q) may alter Casq2 interaction with RyR2 in addition to reducing calcium buffering (Terentyev *et al.*, 2006).

CPVT2 was thought to be an autosomal recessive disease only (Postma *et al.*, 2002; de la Fuente *et al.*, 2008; Kirchhefer *et al.*, 2010a), until in 2016 investigators reported a novel *CASQ2* variant in a family with autosomal dominant inheritance of CPVT (Gray *et al.*, 2016). Whole exome sequencing led to the discovery of a conservative amino acid change from a lysine to an arginine at amino acid 180 (K180R). This amino acid is conserved across species and in silico analysis of the protein structure predicted the variant to have a deleterious effect on the protein's function. Given that all previously reported *CASQ2* variants cause either a complete loss or a severe reduction of Casq2 protein, it was proposed that the variant could have a dominant negative effect that would lead to a reduction in Casq2 levels and thus cause CPVT (Gray *et al.*, 2016). The current hypothesis is that autosomal-dominant Casq2 variants lead to CPVT by affecting the ability of Casq2 to polymerize. The hypothesis is supported by recent data from a novel crystal structure of a polymer filament of Casq2 (Titus *et al.*, 2020). Using the new filament, the authors mapped two autosomal dominant variants (K180R, and S173I) to understand how they would affect Casq2 function. The analysis also utilized the filament to identify novel calcium binding sites that bridged both intra and inter-dimer interfaces of Casq2, suggesting that calcium is involved in the ability for Casq2 to form dimers and those dimers to form subsequent filaments (Titus *et al.*, 2020). Both autosomal dominant variants were unable to form polymers in an *in vitro* turbidity assay and were found to be a part of the novel calcium binding sites. Yet, the exact mechanism of how autosomal dominant variants cause CPVT is unknown. To answer this question, we generated and studied a K180R knockin mouse model. We find that unlike previously reported *CASQ2* variants associated with autosomal-recessive CPVT2, K180R causes CPVT2 via a heretofore unknown mechanism:

K180R impairs the rate of calcium binding to the Casq2 polymer within the SR without altering total SR calcium buffering or SR calcium content.

Methods

Generation of K180R mice

To generate the K180R heterozygous mouse, mouse zygotes underwent genetic editing using CRISPR/Cas9. The zygotes were microinjected with Cas9 mRNA, a single strand repair template (sequence 5' to 3' = CAAGTGAGCAGTTTGCCTCTTGCAAACATTTCTCTCTTTTCTCCTAGATTACAGAGCATTCCAGGAAGCAGCTGAACACTTCCAGCCTTACATCAAGTTCTTTGCCACCTTTGACAAGGC), and a guide RNA (sequence 5' to 3' = AGAT TACAAAGCATTCCAAGAGG). The repair template was used to create a missense variant (lysine to arginine), a silent variant to induce a BstNI restriction enzyme site, and a silent variant to remove the PAM site needed for Cas9. Following injection, the zygotes were transferred to into C57Bl/6 pseudo-pregnant females. The resulting litters were then sequenced using primers that flanked the 180th amino acid in Casq2. The positive mice were then crossed with C57Bl/6 mice to generate heterozygous K180R mice. The K180R mice continued to be backcrossed with C57Bl/6 mice to minimize any off-target variants that occurred during the genetic editing. Pairs of K180R heterozygous mice were used to breed wild-type, heterozygous, and homozygous mice for experiments.

Telemetry

Mice were anesthetized with 3% (v/v) isoflurane inhalation before receiving 10 mg/kg of ketoprofen subcutaneously. A small incision was made on the dorsal side of the neck, and a subcutaneous pocket was formed by blunt dissection. A radiofrequency transmitter (ETA-F10; Data Science International, St. Paul, MN, USA) containing two ECG leads was placed in the pocket. Two small incisions were then made on the ventral side just caudal and medial of each forelimb. The negative and positive leads were attached to the underlying muscle in an effort to mimic a lead 1 configuration. Animals were allowed to recover for at least 48 hours after surgery before participating in an exercise stress test or pharmacologic stress test.

As described previously (Hernandez *et al.*, 2005), mice undergoing the exercise stress test were placed individually into a special chamber of the motorized rodent treadmill (Exer-6M; Columbus Instruments) and exercised until they exhibited signs of exhaustion. Exhaustion was defined as the mouse spending more than 50% of the time or more than 15 seconds consecutively on the shock grid (Desai *et al.*, 1997). Immediately after the shock grid was turned off, high-quality ECGs could be recorded. An analysis program (LabChart 8) was used to review the records. Arrhythmia susceptibility was quantified as ventricular ectopic beats (VEB) per minute per mouse and as the number of mice with ventricular tachyarrhythmias (VT; >2 consecutive VEB) in each group.

Mice undergoing the pharmacologic stress test would have a baseline heart recorded (1 minute) before receiving an intraperitoneal (i.p.) injection of 3 mg/kg isoproterenol + 60 mg/kg caffeine. ECG traces were recorded for 15 minutes. Arrhythmia susceptibility was quantified as ventricular ectopic beats (VEB) per minute per mouse and as the number of mice with ventricular tachyarrhythmias (VT; >2 consecutive VEB) in each group.

Isolation of ventricular myocytes

Ventricular myocytes from K180R wild-type, K180R heterozygous, or K180R homozygous mice were isolated from the heart by collagenase digestion as previously described (Knollmann *et al.*, 2006). Cells were then washed twice by gravity sedimentation for 20 minutes at room temperature in standard Tyrode solution with 0.2 mM CaCl₂. The final suspension contained 0.6 mM calcium and the cells were immediately used.

Spark measurements in permeabilized cardiomyocytes

Isolated ventricular myocytes were plated onto laminin-coated glass cover slips and allowed to attach for 10 minutes at room temperature (22 - 24 °C). The attached cells were first exposed to a calcium free relaxing solution for 30 seconds and then were permeabilized with saponin (40 µg/mL) for 35 seconds and then bathed in a freshly-made internal solution (pH = 7.2) containing (mM): K-aspartate (120), KCl (15), K₂HPO₄ (5), MgCl₂ (5.6), HEPES (10), dextran (4% w/v), MgATP (5), Phosphocreatine-Na₂ (10), creatine phosphokinase (10 U/mL), reduced L-glutathione (10), EGTA (0.5), CaCl₂ (0.12), and Fluo-4 (0.03). Confocal imaging was performed on a Zeiss LSM 510 inverted laser scanning confocal microscope equipped with a 40X / 1.30 NA planar oil immersion objective. Fluo-4 was excited by an argon laser at 488 nm and the fluorescence emission was passed through a 505 nm long pass filter to photomultiplier tube detectors. Cell sparks were imaged in linescan mode in those cells that had characteristic brick-shape morphology. Lines were positioned longitudinally near the center of the cell, avoiding nuclei. SR calcium load was measured as the calcium transient amplitude induced by application of 10 mM caffeine. Image analysis was performed in ImageJ with the SparkMaster plugin (Picht *et al.*, 2007) using a background setting of 5 and criteria of 3.8. Spark mass was calculated from

the equation: spark mass = 1.206 * Amplitude *FWHM³. FWHM stands for full width at half maximum. Leak was calculated from the equation: leak = spark frequency * spark mass.

Wave measurements in permeabilized cardiomyocytes

Isolated ventricular myocytes were plated onto laminin-coated glass cover slips and allowed to attach for 10 minutes at room temperature (22 - 24 °C). The attached cells were first exposed to a calcium free relaxing solution for 30 seconds and then permeabilized with saponin (40 µg/mL) for 35 seconds and bathed in a freshly-made internal solution (pH = 7.2) containing (mM): K-aspartate (120), KCl (15), K₂HPO₄ (5), MgCl₂ (5.6), HEPES (10), dextran (4% w/v), MgATP (5), Phosphocreatine-Na₂ (10), creatine phosphokinase (10 U/mL), reduced L-glutathione (10), EGTA (0.5), CaCl₂ (0.056), and Fluo-4 (0.03). Confocal imaging was performed on a Zeiss LSM 510 inverted laser scanning confocal microscope equipped with a 40X / 1.30 NA planar oil immersion objective. Fluo-4 was excited by an argon laser at 488 nm and the fluorescence emission was passed through a 505 nm long pass filter to photomultiplier tube detectors. Cell waves were imaged in linescan mode in those cells that had characteristic brick-shape morphology. Lines were positioned longitudinally near the center of the cell, avoiding nuclei. SR calcium load was measured as the calcium transient amplitude induced by application of 10 mM caffeine. Calcium wave analysis was performed as described (Galimberti & Knollmann, 2011).

Sarcoplasmic reticulum and cytosolic calcium buffering measurements in permeabilized cardiomyocytes

Isolated ventricular myocytes were incubated in a 0.6 mM calcium solution (11g MEM, 2.60 Na-HEPES, 0.40 g Na-bicarbonate, 0.47 g MgCl₂ (anhydrous), 0.22 g sodium pyruvate, 0.4

g Taurine, 0.2 cc insulin, pH 7.3) with 6.25 μ M of Calbryte-520L, AM, 0.025% Pluronic-127, and 10 μ M of MYK-461 for 30 minutes at 37 °C to allow for dye to cross into the SR. The cells were then washed 3 times with 0.6 mM calcium solution for 10 minutes each. The cells were resuspended in 0.6 mM calcium solution, 1 mM probenecid and 10 μ M MYK-461 for 15 minutes to wash out cytosolic dye. The cells were plated onto laminin-coated glass cover slips and allowed to attach for 10 minutes at room temperature (22 - 24 °C). The attached cells were first exposed to a calcium free relaxing solution for 30 seconds and then permeabilized with saponin (40 μ g/mL) for 35 seconds and bathed in a freshly-made internal solution (pH = 7.2) containing (mM): K-aspartate (120), KCl (15), K₂HPO₄ (5), MgCl₂ (5.6), HEPES (10), dextran (4% w/v), MgATP (5), Phosphocreatine-Na₂ (10), creatine phosphokinase (10 U/mL), reduced L-glutathione (10), EGTA (0.1), CaCl₂ (0.12), and Calbryte-590, potassium salt (5 mM). Confocal imaging was performed on a Zeiss LSM 510 inverted laser scanning confocal microscope equipped with a 40X / 1.30 NA planar oil immersion objective. Calbryte-520L, AM was excited by an argon laser at 488 nm and the fluorescence emission was passed through a 505 nm long pass filter to photomultiplier tube detectors. Calbryte-590, potassium salt was excited by an argon laser at 535 nm and the fluorescence emission was passed through a 585 nm long pass filter to photomultiplier tube detectors. Cell waves were imaged in linescan mode in those cells that had characteristic brick-shape morphology. Lines were positioned longitudinally near the center of the cell, avoiding nuclei. To analyze calcium buffering, intra-SR and cytosolic transients were used to measure amplitude, relaxation time constant (τ), time to peak, width 70, width 50, and width 10. Transients were collected and analyzed using ImageJ and LabChart8.

Western blotting

Cell lysates were prepared from hearts in homogenization buffer (50 mM TRIS, 320 mM sucrose, 1 mM Dithiothreitol (DTT), 0.1% IGEPAL CA-630, pH = 7.0) containing 1% protease inhibitor cocktail (Sigma P8340) and phosphatase inhibitor (Sigma P0044). Hearts from congenital *CASQ2*^{-/-} mice (Knollmann *et al.*, 2006), triadin knockout mice, and wild-type littermates were included as controls. Lysate used for analyzing RyR2, triadin, and junctin were boiled at 65°C for 10 mins. Samples were separated on a 4 – 20% polyacrylamide gel (Bio-Rad Mini-PROTEAN), transferred to a polyvinylidene difluoride membrane, blocked in TBST + 5% milk for 1 hour at room temperature, and incubated overnight at 4 °C with primary antibody. Blots were washed 3X in TBST and incubated with secondary antibody for 1 hour at room temperature, washed 3X in TBST, and then developed with ECL reagent (GE Healthcare) and imaged using a ChemiDoc MP (Bio-Rad). Casq2 immunolabeling, blots were incubated with 1:2,000 anti-Casq2 (Abcam ab108289) and 1:5,000 anti-rabbit HRP conjugate (Promega W401B). For RyR2 immunolabeling, blots were incubated with 1:1,000 anti-RyR2 (Thermo Fisher MA3-916) and 1:2,500 anti-mouse HRP conjugate (Invitrogen 31430). For triadin immunolabeling, blots were incubated with 1:1,000 anti-T32 (provided by Dr. Isabelle Marty, Univ Grenoble Alpes, Grenoble, France) and 1:2,500 anti-rabbit HRP conjugate (Promega W401B). For junctin immunolabeling, blots were incubated with 1:2,000 anti-junctin (provided by Dr. Karl Pfeifer, National Institutes of Health, Bethesda, Maryland) and 1:5,000 anti-rabbit HRP conjugate (Promega W401B). For GAPDH, blots were incubated with 1:10,000 anti-GAPDH (ThermoFisher AM4300) and 1:5000 anti-mouse HRP conjugate (Invitrogen 31430).

Immunostaining

Isolated ventricular myocytes were plated onto laminin-coated glass cover slips and allowed to attach for 3 hours at room temperature (22 - 24 °C). Cells were fixed in 2% paraformaldehyde for 20 minutes, blocked with 5% goat serum in DPBS + 0.4% triton for 1 hour at room temperature, and incubated with primary antibodies overnight. The Casq2 (Pierce PA1-913), RyR2 (Thermo Fisher MA3-916), and Triadin (anti-T32-mouse, provided by Dr. Isabelle Marty) antibodies were diluted in DPBS+triton at 1:500. Blocking solution was used as a negative control. Secondary antibodies were diluted in DPBS + triton at 1:400. Slides were incubated with an Alexa Fluor 488 secondary antibody for 1 hour at room temperature. Cover slides were mounted using ProLong Gold antifade with DAPI (Invitrogen P36941) and left to dry overnight. Imaging was carried out at 40x magnification on an Olympus confocal microscope (IXplore SpinSR). Excitation was elicited using a LS 100 mw diode laser at either 488 nm or 561 nm (Coherent Obis laser lines). Images were acquired using Olympus cellSens Dimension 2.3 software and were analyzed in ImageJ. The images were reviewed and scored by an individual blinded to the genotype and phenotype.

Intra-sarcoplasmic reticulum calcium measurements

For the intra-SR calcium measurements, freshly isolated murine ventricular myocytes from K180R (HET), Casq2 KO and WT mice were voltage-clamped at -70 mV, then pre-stimulated with a short, 4-pulse train (0.2 s depolarizing steps to +10 mV applied with 1 Hz frequency), and then a rapid caffeine (10 mM) spritz was applied few seconds after the last pulse to release calcium from the SR. The integral of the resulting NCX current represented total SR calcium, and the amplitude of corresponding fluorescent signal represented free calcium during the SR calcium

release. The pipette solution contained (in mM): CsCl (110), MgATP (5), MgCl₂ (1), EGTA (1), cAMP (0.2), HEPES (20), adjusted to pH 7.25 with CsOH. The external K-free solution contained (in mM): NaCl (134), CsCl (5), MgCl₂ (1), CaCl₂ (2), glucose (10), HEPES (10), adjusted to pH 7.4 with NaOH. Experiments were performed at room temperature (22-25 °C). All chemicals, unless otherwise specified, were obtained from Sigma (St. Louis, MO).

SR calcium release restitution assay

To determine the refractoriness and restitution characteristics of SR calcium release, we used an A1-A2 stimulation protocol in voltage-clamp mode as described previously (Kornyeyev *et al.*, 2012). Cells were loaded with fluo-4 pentapotassium salt (final concentration 100 μM), added into pipette solution from stock. The pipette solution contained (in mM): CsCl (125), MgATP (5), MgCl₂ (1), glutathione (GSH) (5), cAMP (0.05), HEPES (20), adjusted to pH 7.25 with CsOH. The external K-free solution, used in both experiments, contained (in mM): NaCl (134), CsCl (5), MgCl₂ (1), CaCl₂ (2), glucose (10), HEPES (10), adjusted to pH 7.4 with NaOH. At the end of the experiment each cell was exposed to a rapid spritz of 10 mM caffeine to estimate total SR calcium content. Experiments were performed at room temperature (22-25 °C). All chemicals, unless otherwise specified, were obtained from Sigma (St. Louis, MO).

Electron microscopy

Hearts from 18–20-week-old K180R mice were harvested, the aorta cannulated, and hearts fixed by retrograde reperfusion with 5% glutaraldehyde and 2% paraformaldehyde in 0.1 M sodium cacodylate buffer, pH 7.2. Hearts were teased apart and placed in 2.5% glutaraldehyde in 0.1 M sodium cacodylate buffer for 1 hour at room temperature before being stored in 4°C fridge

overnight. Samples were processed and imaged by the Vanderbilt Cell Imaging Share Resource (CISR) core. Images were analyzed by Dr. V. Ramesh Iyer.

Intracellular calcium measurements in intact myocytes

Isolated ventricular myocytes were loaded with Fura-2 acetoxymethyl ester (Fura-2, AM; Invitrogen) as described previously (Hwang *et al.*, 2011). Briefly, isolated single ventricular myocytes were incubated with 2 μ M Fura-2 AM for 6 minutes, washed twice for 10 minutes with normal Tyrode (NT) solution containing 250 μ M probenecid to retain the indicator in the cytosol. A minimum of 30 minutes was allowed for de-esterification of the indicator before the cells were imaged. The composition of NT used for Fura-2 loading and washing was (in mM): (134) NaCl, (5.4) KCl, (1.2) CaCl₂, (1) MgCl₂, (10) glucose, and (10) HEPES, pH adjusted to 7.4 with NaOH. After Fura-2 loading, all following experiments were conducted in NT solution containing 2 mM CaCl₂ and 1 μ M isoproterenol. Calcium transients from Fura2-loaded myocytes were paced and recorded at 1 Hz and 3 Hz field stimulation for 10 seconds each, followed by no electrical stimulation for 30 seconds for quantification of spontaneous calcium release events. Myocytes were then exposed to NT solution containing 10 mM caffeine for 5 seconds to estimate total SR calcium contents. Intracellular calcium transients were measured using a dual-beam excitation fluorescence photometry setup (IonOptix Corp.). All experiments were conducted at room temperature. 1 Hz paced calcium transients were analyzed for calcium parameters using commercially available data analysis software (IonWizard, IonOptix, Milton, MA).

Statistics

Statistical analyses were performed using Prism v9.0.2 (GraphPad Software, Inc.). Statistical tests were used as reported in the figure legends. To account for day-to-day variation in cardiomyocyte isolation and quality, experiments that utilized isolated cardiomyocytes were compared using a hierarchical statistical model with Bonferroni correction in R, following the procedures outlined by (Sikkel *et al.*, 2017). A P value of 0.05 was used as the threshold to reject the null hypothesis.

Study approval

The use of animals was approved by the Animal Care and Use Committee of Vanderbilt University, USA (animal protocol #'s M1600090-00 and M1600259-00) and performed in accordance with NIH guidelines.

Results

Generation of K180R mice

The K180R variant results in a relatively conservative amino acid change from lysine to arginine. However, the lysine residue at position 180 within *CASQ2* is conserved across species (Figure 6A) suggesting that K180 could be important to the structural properties of Casq2. To determine if K180R could produce a phenotype, we generated a genetic mouse model using CRISPR/Cas9. The gRNA was designed to target K180 on exon 11. C57BL/6 mouse zygotes were injected with the Cas9 enzyme, the gRNA, and a repair template to replace the lysine with an arginine. Sequencing the offspring of the mice (Figure 6B) identified three founders carrying the K180R mutation. Heterozygous offspring from all three founder lines displayed a CPVT phenotype *in vivo* (Figure 5). Two founder lines were backcrossed into C57BL/6 mice for 10 generations and both founder lines were used in all subsequent experiments.

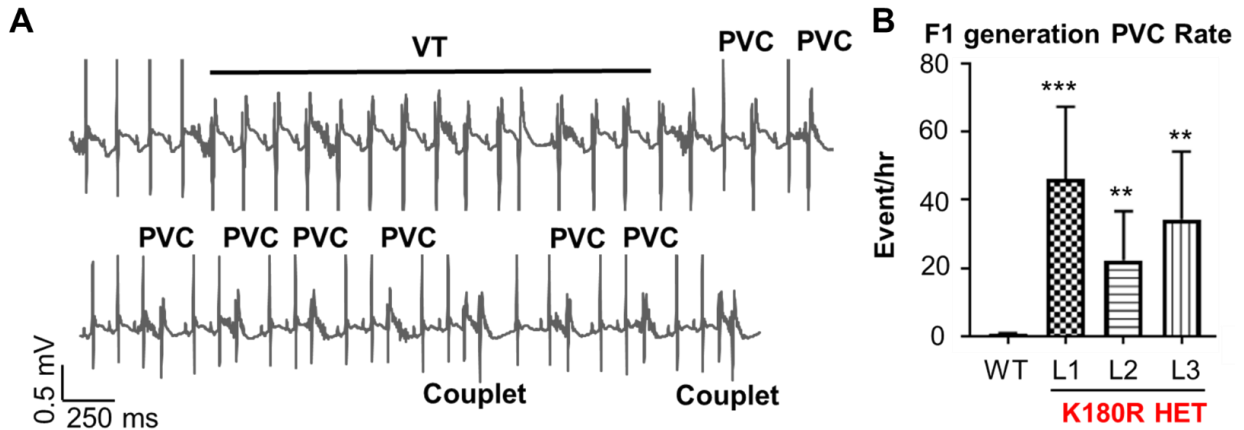


Figure 5. Generation of K180R founder mice. **A)** Representative ECG trace showing that heterozygous (HET) K180R founder mice display episodes of ventricular tachycardia (VT) and have multiple premature ventricular contractions (PVC). **B)** PVC rate per hour for three different founder lines of K180R mice. Data displayed as mean \pm SD. All data were compared using one-way ANOVA and Tukey's multiple comparison test.

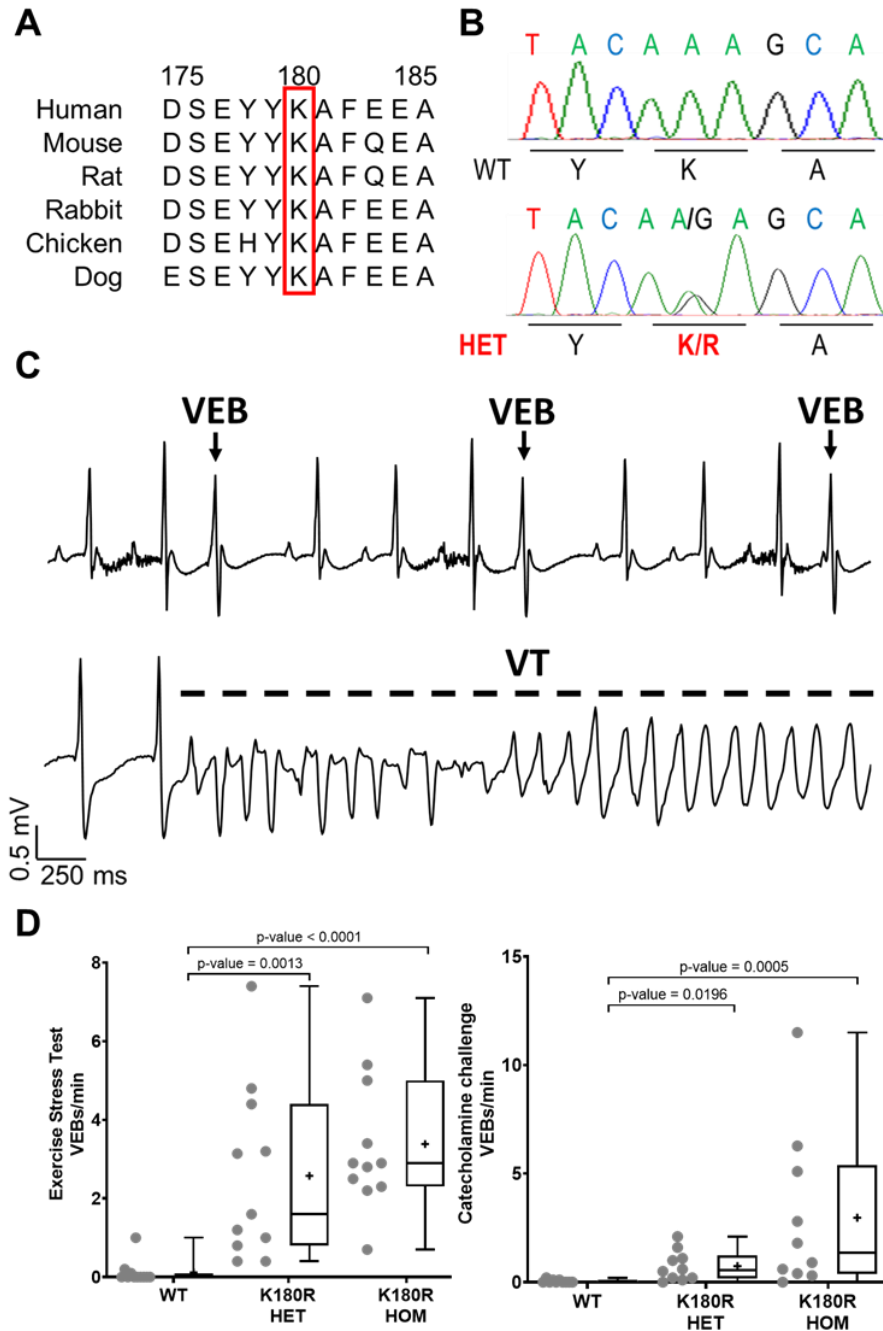


Figure 6. K180R mice display a CPVT phenotype. **A)** Amino acid 180 is conserved across species in *CASQ2*. **B)** Mice are heterozygous for AGG mutation. **C)** Example traces from a K180R HET mouse displaying characteristics of CPVT including ventricular ectopic beats (VEBs) and an episode of ventricular tachycardia (VT) **D)** K180R mice underwent two different stress tests. Following implantation of a telemeter, mice were either stressed with a 3 mg/kg isoproterenol/60 mg/kg caffeine injection or exercise treadmill running. (n = 11 mice for each group). Data displayed as a box and whisker plot. Median is displayed as a line within the box and whisker plot. Mean is displayed as a plus sign within the box and whisker plot. Data analyzed using Kruskal-Wallis test with Dunn's multiple comparisons.

K180R mice display a CPVT phenotype

Arrhythmia susceptibility was investigated by two different stress tests. Mice between the ages of 12-18 weeks had telemeters implanted before undergoing an exercise stress test or a catecholamine stress test with isoproterenol and caffeine. Both heterozygous (HET) and homozygous (HOM) K180R mice displayed characteristics of CPVT, including ventricular ectopic beats (VEBs) and episodes of ventricular tachycardia (VT) (Figure 6C). For each stress test, the number of VEBs was counted during a 10-minute recording period. K180R HET and HOM mice that underwent the stress test, displayed a significant increase in VEBs per minute compared to WT K180R mice (Figure 6D). Similar results were seen when K180R mice were given a catecholamine challenge. K180R HET and HOM mice had significantly more VEBs when compared to WT mice (Figure 6D). K180R HET and HOM mice had a VT incidence of around 20% in both tests, which was not significantly different between K180R mice. VT usually was non-sustained, lasting for less than 1 second. One mouse had sustained VT that lasted 100 seconds. There was no significant difference between the K180R HET and HOM mice in VEBs per minute or VT incidence in either test, consistent with the autosomal-dominant disease caused by the K180R variant in humans.

K180R increases the rate of spontaneous SR calcium release

It is generally accepted that genetic variants associated with CPVT render RyR2 channels hyperactive, resulting in increased likelihood of spontaneous SR calcium release (Cerrone *et al.*, 2005; Knollmann *et al.*, 2006), which will cause delayed afterdepolarizations that can trigger ectopic beats. Given that the K180R variant produces a CPVT phenotype *in vivo* (Figure 6), we next examined calcium handling in isolated K180R cardiomyocytes. In the first set of experiments,

the rate of spontaneous RyR2 openings was quantified by measuring calcium sparks and calcium waves after membrane permeabilization with saponin. This experimental design allows complete control of cytosolic free calcium concentration, thereby directly examining the rate of RyR2 opening for a given cytosolic free calcium concentration. Compared to WT cardiomyocytes, HET and HOM K180R cardiomyocytes exhibited a significant increase in spark frequency (Figure 7A-7B). Spark characteristics, including spark amplitude, spark mass, and full duration half max (FDHM) were not significantly different between groups (Figure 8). Calcium leak, calculated using spark frequency and spark mass, was significantly higher in K180R HET and HOM cardiomyocytes. Consistent with an increased RyR2 activity, K180R HET and HOM cardiomyocytes also exhibited an increase in calcium wave frequency compared to WT cardiomyocytes (Figure 7C-7D). The rate of spontaneous RyR2 opening and hence calcium spark frequency increases with increased SR calcium content (Sato *et al.*, 1997). Hence, we next quantified the SR calcium content using a caffeine spritz protocol. The height of the caffeine-induced calcium transient amplitude is a well-established measure of total SR calcium content (Bers, 2001). Total SR calcium content was not significantly different between WT and K180R cardiomyocytes (Figures 8 and 9, indicating that the K180R variants renders RyR2 channels hyperactive without altering total SR calcium content. Next, we quantified the rate of spontaneous SR calcium release events in intact cardiomyocytes using a well-established rapid pacing protocol (Figure 10). Compared to WT, both K180R HET and HOM exhibited significantly higher rates of spontaneous calcium release events (Figure 10), with no differences between the K180R HET and HOM groups. All other calcium handling parameters were not altered in the K180R groups (Table 1). Taken together, the results indicate that the K180R variant in Casq2 causes a dominant gain of function in the RyR2 calcium release unit.

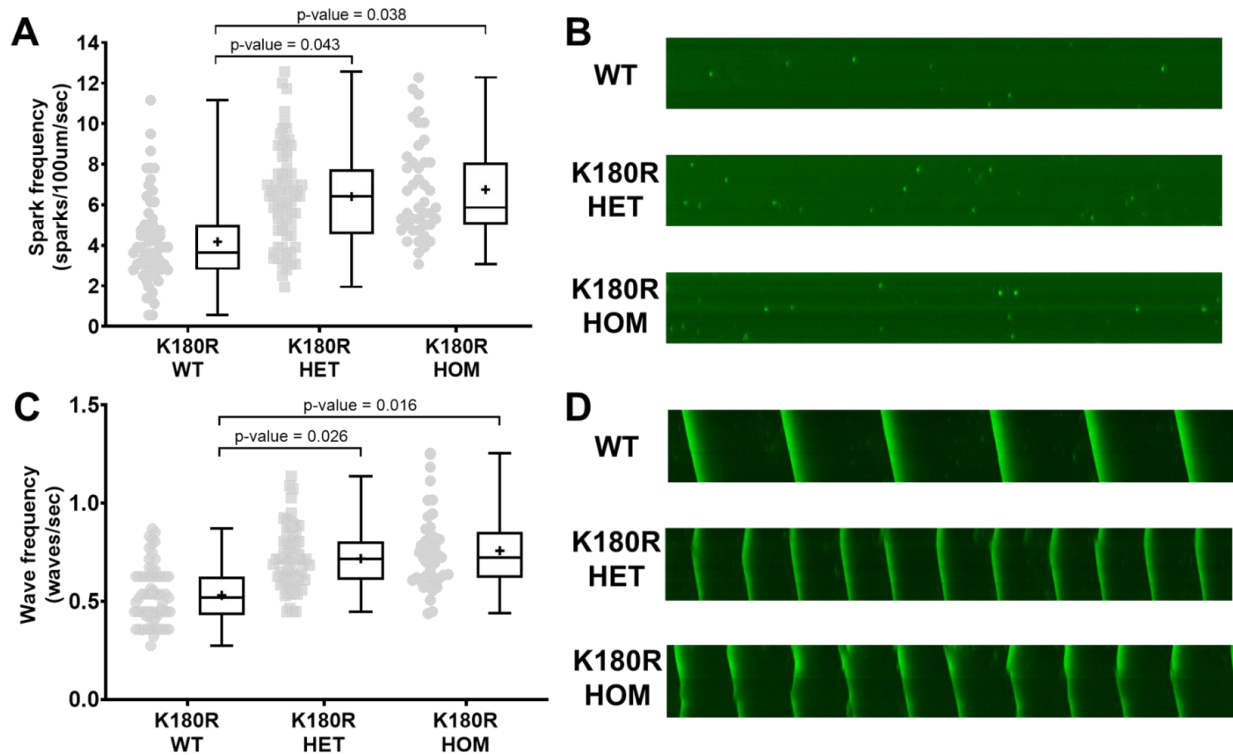


Figure 7. K180R increases spontaneous SR calcium release in single cardiomyocytes. Cardiomyocytes isolated from mouse hearts underwent calcium handling analysis by measuring sparks and waves in permeabilized cardiomyocytes. Briefly, isolated cardiomyocytes underwent permeabilization and were incubated in an internal solution with a calcium indicator (Fluo-4). Cells were imaged using an inverted confocal microscope in line-scan mode and analyzed using ImageJ. **A)** calcium spark frequency in WT, K180R HET, and K180R HOM cardiomyocytes. WT; n = 63 cells from 3 hearts. K180R HET; n = 68 cells from 3 hearts. K180R HOM; n = 43 cells from 2 hearts. **B)** Example line-scan images of calcium sparks in K180R cardiomyocytes. **C)** calcium wave frequency in WT, K180R HET, and K180R HOM cardiomyocytes. WT; n = 71 cells from 3 hearts. K180R HET; n = 67 cells from 3 hearts. K180R HOM; n = 42 cells from 2 hearts. **D)** Example line-scan images of calcium waves. Data displayed as a box and whisker plot. Median is displayed as a line within the box and whisker plot. Mean is displayed as a plus sign within the box and whisker plot. All data were analyzed using a hierarchical statistical model with Bonferroni correction.

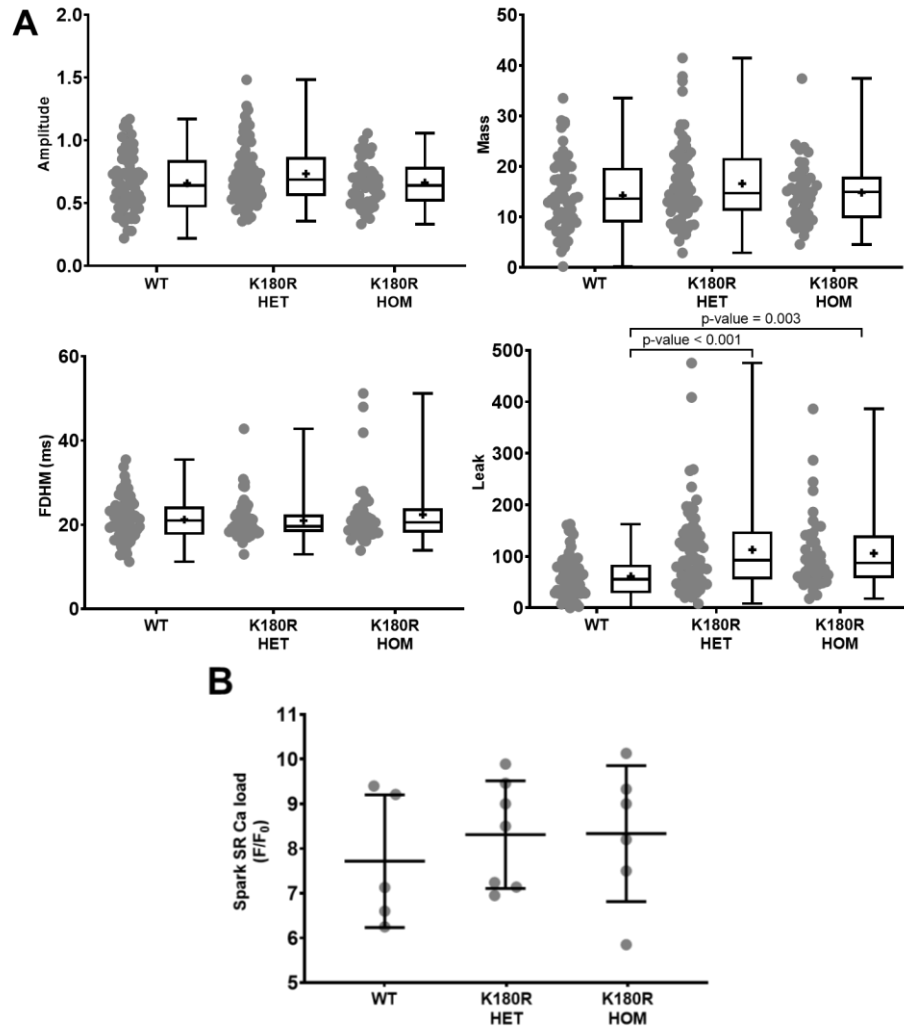


Figure 8. Characteristics of calcium sparks from isolated cardiomyocytes. Briefly, cardiomyocytes isolated from mice underwent permeabilization and were incubated in an internal solution with a calcium indicator dye (Fluo-4). Cells were imaged using an inverted confocal microscope in line-scan mode and analyzed using ImageJ **A**) The parameters measured during spark analysis to investigate the characteristics of calcium sparks in the isolated K180R mouse cardiomyocytes. Amplitude is the peak fluorescence that occurs in the spark. Spark mass is a parameter that is used to understand the three-dimensional nature of a spark. The formula for spark mass is calculated as $1.206 \times \text{amplitude} \times \text{FWHM}^3$. FWHM = full width at half max. Full duration at half maximum (FDHM) is a measure of the length of the spark. Leak is calculated by the formula of mass x frequency to understand the amount of calcium leak that is occurring through the ryanodine receptor type 2. WT; n = 63 cells from 3 hearts. K180R HET; n = 68 cells from 3 hearts. K180R HOM; n = 43 cells from 2 hearts. Data displayed as a box and whisker plot. Median is displayed as a line within the box and whisker plot. Mean is displayed as a plus sign within the box and whisker plot. **B**) At the end of recording, a caffeine spritz was applied to empty the SR and measure relative calcium levels within the isolated cardiomyocytes. WT; n = 5 cells from 3 hearts. K180R HET; n = 5 cells from 3 hearts. K180R HOM; n = 5 cells from 2 hearts. Data displayed as mean \pm SD. All data was analyzed using a hierarchical statistical model with Bonferroni correction.

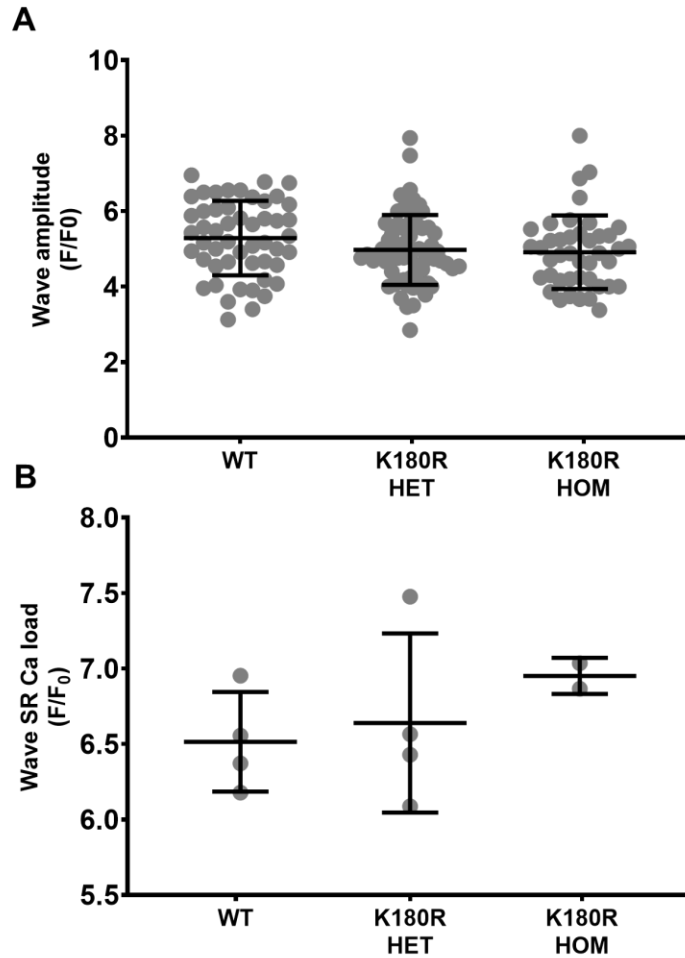


Figure 9. Characteristics of calcium waves from isolated cardiomyocytes. Briefly, cardiomyocytes isolated from mice underwent permeabilization and were incubated in an internal solution with a calcium indicator dye (Fluo-4). Cells were imaged using an inverted confocal microscope in line-scan mode and analyzed using ImageJ **A**) Wave amplitude was measured to analyze the relative amount of calcium that was being released during each excitation-coupling cycle. WT; n = 71 cells from 3 hearts. K180R HET; n = 67 cells from 3 hearts. K180R HOM; n = 42 cells from 2 hearts. **B**) At the end of recording, a caffeine spritz was applied to empty the SR and measure relative calcium levels within the isolated cardiomyocytes. WT; n = 4 cells from 3 hearts. K180R HET; n = 4 cells from 3 hearts. K180R HOM; n = 2 cells from 2 hearts. Data displayed as mean \pm SD. Data analyzed using a hierarchical statistical model with Bonferroni correction.

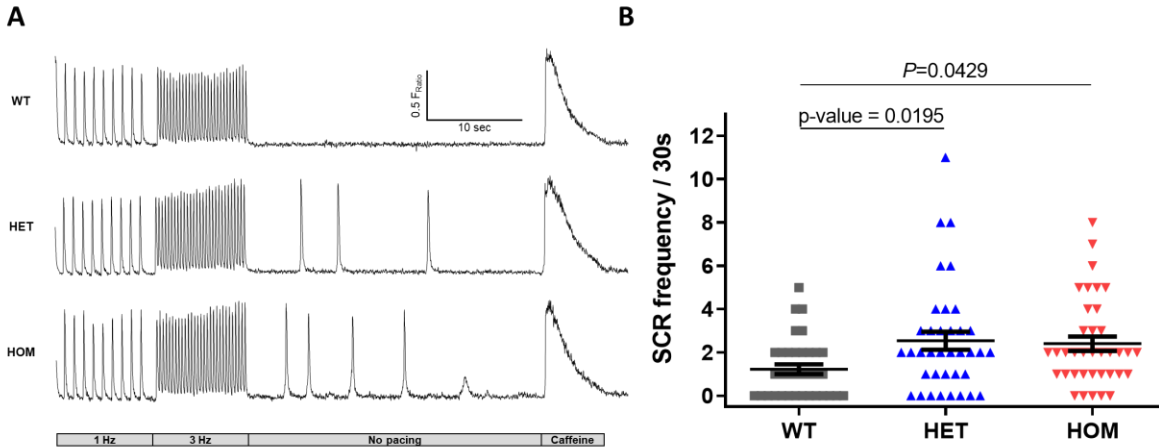


Figure 10. K180R increases rates of spontaneous calcium release events. Ventricular myocytes were isolated and loaded with Fura-2 acetoxymethyl ester to measure spontaneous calcium release (SCR) events. **A)** Example calcium transients from Fura2-loaded myocytes. Myocytes were paced and recorded at 1 and 3 Hz field stimulation followed by no electrical stimulation. Myocytes were exposed to caffeine to estimate total SR calcium contents. **B)** Graph of SCR frequency per 30 seconds. WT; n = 35 cells from 2 hearts. K180R HET; n = 37 cells from 2 hearts. K180R HOM; n = 37 cells from 2 hearts. Data displayed as mean \pm SD. Data analyzed using a hierarchical statistical model with Bonferroni correction.

[Ca²⁺]_i measurements in ventricular myocytes

	WT (n=35)	HET (n=37)	HOM (n=37)
Diastolic Ca (F_{Ratio})	0.539 ± 0.048	0.539 ± 0.041	0.537 ± 0.044
CaT amplitude (F_{Ratio})	0.731 ± 0.132	0.710 ± 0.156	0.790 ± 0.131
Time to peak (ms)	29.7 ± 4.2	30.8 ± 4.1	30.7 ± 5.2
CaT decay rate (ms)	108.4 ± 13.0	113.2 ± 11.2	114.2 ± 11.0
SR Ca content (F_{Ratio})	0.869 ± 0.175	0.838 ± 0.175	0.940 ± 0.130
Caff. Tau (s)	2.619 ± 0.598	2.589 ± 0.396	2.673 ± 0.421
Fractional SR Ca release	0.848 ± 0.075	0.848 ± 0.087	0.853 ± 0.062

Mean ± SD

Table 1. Calcium handling parameters of WT and K180R cardiomyocytes. Calcium handling parameters of isolated WT and K180R cardiomyocytes there were loaded with Fura-2 acetoxymethyl ester to measure spontaneous calcium release (SCR) events. N = 35 cells from 2 hearts for WT; n = 37 cells from 2 hearts for HET; n = 37 cells from 2 hearts for HOM. All data displayed as mean ± SD and analyzed using a hierarchical statistical model with Bonferroni correction.

K180R does not affect levels of Casq2 and other junctional SR proteins

All previously reported *CASQ2* variants cause a decrease in the level of Casq2 protein (Wleklinski *et al.*, 2020). Accordingly, the first report of the K180R variant suggested that even though the variant followed an autosomal dominant inheritance pattern, the most likely cause of K180R-linked CPVT was a decrease in Casq2 levels through a dominant negative mechanism (Gray *et al.*, 2016). A reduction in Casq2 protein causes a reduction of other junctional SR (jSR) proteins including triadin and junctin, which may independently contribute to RyR2 hyperactivity in CPVT (Knollmann *et al.*, 2006). To investigate jSR protein levels, protein lysate was isolated from mouse cardiomyocytes and analyzed via western blotting (Figure 11A). Cardiomyocytes from two autosomal-recessive CPVT models (Casq2 and triadin knockout (KO) mice) were used as positive controls. The absence of one of these jSR proteins can decrease the levels of other jSR proteins (Knollmann *et al.*, 2006; Chopra *et al.*, 2009). GAPDH was used as a loading control to compare protein levels between groups. Consistent with previous reports, Casq2 KO cardiomyocytes have a significant decrease in Casq2, triadin, and junctin protein levels. Knocking out triadin also has a significant effect on Casq2, triadin, and junctin levels. In contrast, the K180R mutation had no effect on Casq2 protein levels (Figure 11B). Recent *in vitro* studies suggested that the K180R variant may affect the ability of Casq2 to form polymers (Ng *et al.*, 2020; Titus *et al.*, 2020). Based on the Casq2 polymers visible on western blot, polymer levels were not significantly decreased in K180R HET and HOM mouse lysates (Figure 11B). Other CRU protein levels (RyR2, triadin, and junctin) were also not significantly different in the K180R HET and HOM mouse cardiomyocytes (Figure 11C). Taken together, these results indicate that the K180R mutations causes CPVT without altering jSR proteins or Casq2 polymers and therefore via a novel mechanism.

K180R does not affect subcellular localization of Casq2

Casq2 is found in the junctional SR where it co-localizes with RyR2, triadin, and junctin. Together, these four proteins form the SR component of the calcium release unit (Jones *et al.*, 1995; Kobayashi & Jones, 1999). CPVT caused by loss of triadin is likely caused not only by a decrease in Casq2 protein levels, but also impaired localization of Casq2 to the jSR (Chopra *et al.*, 2009). With Casq2 protein levels being normal in K180R mice, one potential mechanism for K180R causing altered calcium handling could be abnormal subcellular localization of Casq2 or other CRU proteins. To test if K180R Casq2 localization is altered, K180R mouse cardiomyocytes were isolated, plated, fixed, and stained for Casq2, RyR2, and triadin (Figure 12A). Co-localization was calculated in ImageJ between Casq2-RyR2 and triadin-RyR2. Staining density was measured for each protein and the density of overlapping pixels between the two proteins calculated. The ratio between the overlapping density and the total density was used as the percent co-localization between the two proteins. Triadin KO cardiomyocytes were included as a positive control. There were no significant differences for Casq2-RyR2 and triadin-RyR2 co-localization in K180R HET cardiomyocytes compared to K180R WT cells (Figure 12B). On the other hand, Triadin KO cardiomyocytes, consistent with previous studies, exhibited decreased Casq2-RyR2 co-localization. To corroborate the results of our immunostaining experiments, we next examined electron micrographs of ventricular sections from WT and K180R HET hearts. K180R HET and HOM hearts had normal SR structure, and Casq2 polymers were visible in all jSR cross-sections examined (Figure 13). Taken together, the normal localization of Casq2 in K180R HET myocytes indicates that K180R localizes correctly in the jSR and likely can interact with other jSR proteins.

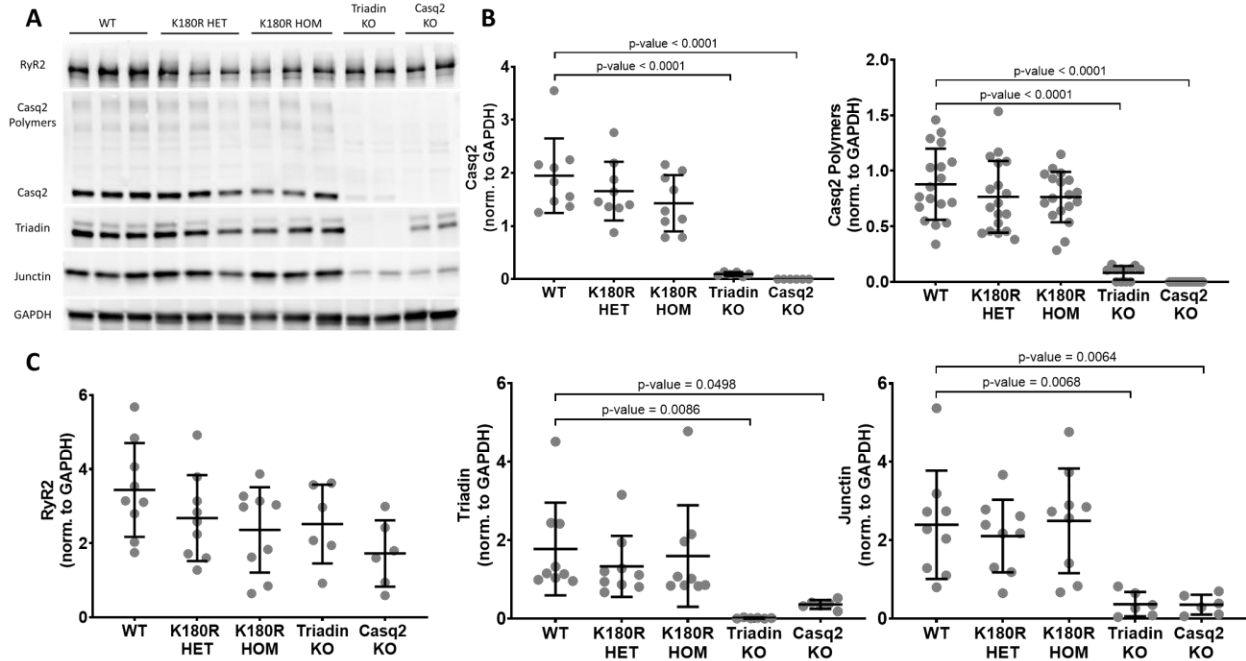


Figure 11. Levels of junctional SR proteins are normal in K180R mice. Ventricular cellular lysate was collected from isolated mouse hearts and analyzed using western blotting techniques. **A)** Raw western blot image. Triadin knockout and Casq2 knockout mice were used as positive controls. **B)** Analysis of Casq2 and Casq2 polymers band density using ImageJ. There is no significant difference between Casq2 and Casq2 polymer protein levels in K180R mice and WT mice. **C)** Quantification of junctional SR protein band density using ImageJ. There is no significant difference in junctional SR protein levels in K180R mice compared to WT. All values were normalized to GAPDH. $n = 9$ lysates for WT, K180R HET, and K180R HOM. $N = 6$ lysates for Triadin KO and Casq2 KO. Data displayed as mean \pm SD. Data were analyzed using one-way ANOVA with Tukey's multiple comparison test.

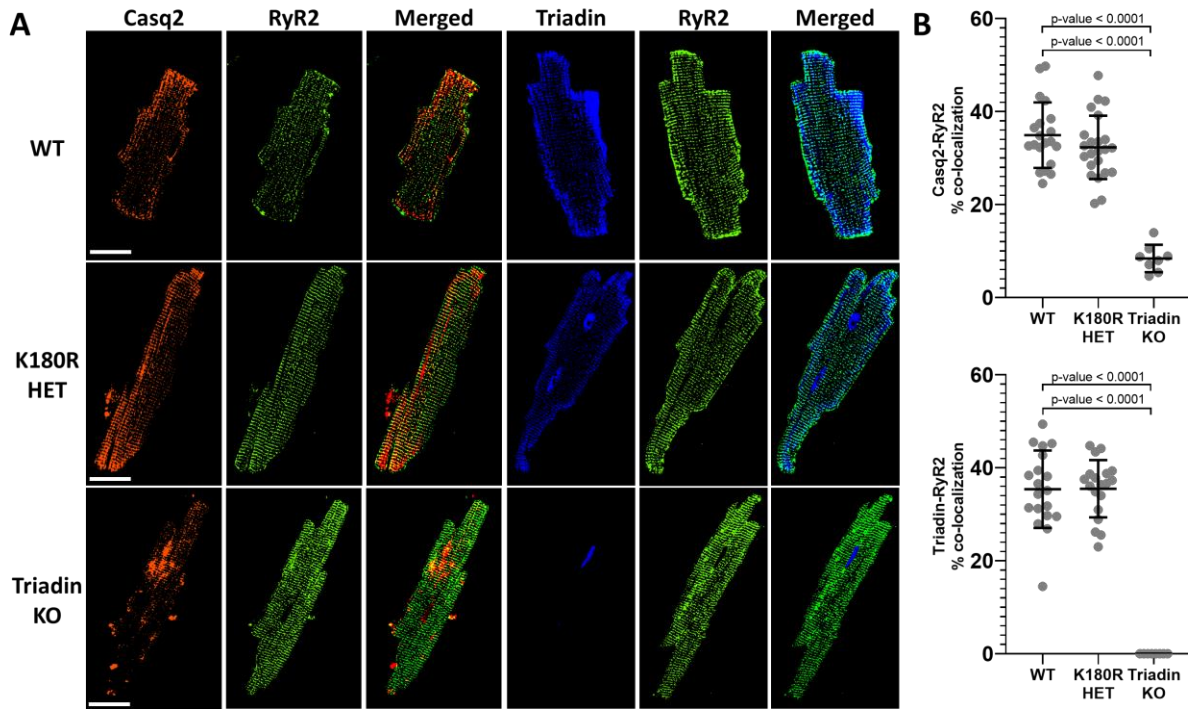


Figure 12. K180R does not change intra-SR localization of Casq2. Hearts isolated from K180R mice were prepared for immunohistochemistry. Hearts were sectioned and stained for Casq2 and RyR2 or triadin and RyR2 to analyze co-localization between calcium release unit proteins. Co-localization analysis was conducted in ImageJ. **A)** Immunostaining displaying representative images from each genotype. Antibodies against Casq2, RyR2, and triadin were used. **B)** Co-localization analysis was performed and displayed as a percent of overlapping pixels between images. WT n = 39 cells total from 4 hearts, K180R n = 42 total cells from 4 hearts, Triadin KO n = 16 cells total from 2 hearts. Data displayed as mean \pm SD. Data analyzed using a hierarchical statistical model with Bonferroni correction. Scale bar = 50 μ M.

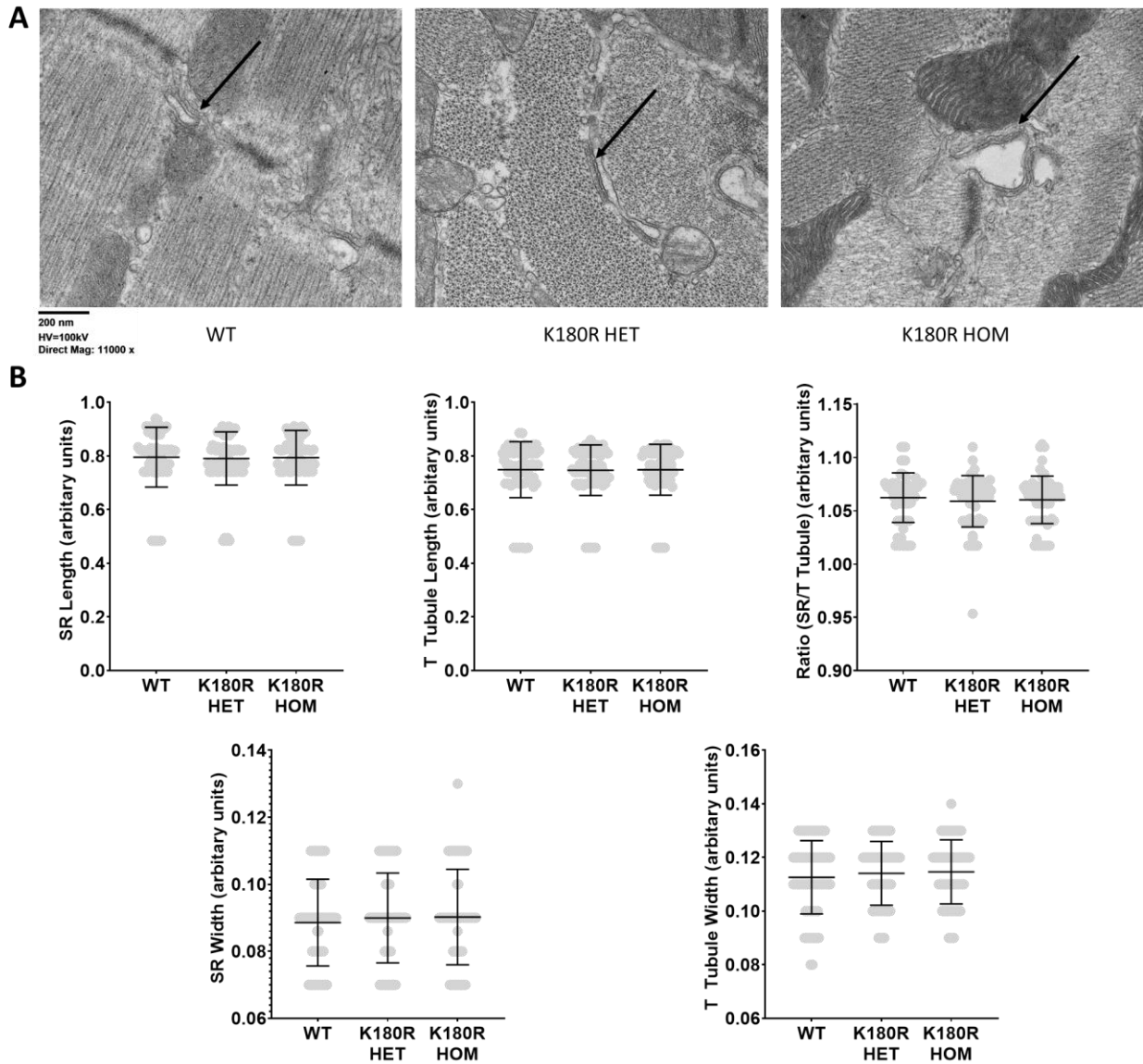


Figure 13. Electron microscopy of WT and K180R cardiomyocytes. Thin section low power electron microscopy of cardiac muscle showing Casq2 (arrows) filled junctional SR in wild-type (WT) and the 2 K180R mutants.

K180R does not alter total SR calcium levels under steady-state conditions

Given its role as the major calcium buffer in the SR, a decrease in Casq2 protein causes a reduction in total SR calcium content (Knollmann *et al.*, 2006). Due to the abnormal calcium handling that occurs in the K180R cardiomyocytes, we would hypothesize that total SR calcium content is altered. Surprisingly, our experiments in permeabilized and intact cardiomyocytes suggest that K180R does not alter total SR calcium content (Figures 8B and 9B; Table 1). To quantify total SR calcium content more accurately in intact K180R cardiomyocytes, we measured NCX currents (Figure 14A) generated during the rapid application of caffeine, which releases the total amount of calcium stored in the SR. The integral of NCX currents generated by the SR calcium release is a well-established quantitative measure of total SR calcium content (Bers, 2001). In contrast to Casq2 KO cardiomyocytes, which exhibited a significant decrease in the NCX integral, the NCX integral of K180R cardiomyocytes was not significantly different from WT cardiomyocytes (Figure 14B). Taken together, our data indicate that unlike autosomal-recessive CPVT2 cardiomyocytes, K180R cardiomyocytes have normal total SR calcium content.

K180R decreases SR calcium release refractoriness

One of the roles of Casq2 is to regulate the refractory period during each EC coupling cycle. By buffering free calcium in the SR, Casq2 helps to prevent the premature release of calcium during diastole. Absence of Casq2 decreases the refractory period of calcium release which could lead to premature calcium release and arrhythmias (Korneyev *et al.*, 2012). Our experiments showed that the K180R variant produces CPVT *in vivo* and increases spontaneous calcium release *in vitro* without affecting Casq2 levels or total SR calcium content. To test if K180R alters SR calcium release refractoriness, isolated cardiomyocytes were loaded with fluo-4 calcium

fluorescent indicator, patched in voltage clamp mode, and underwent an established stimulation protocol that is described in Figure 15A (Kryshtal *et al.*, 2015). Calcium transients from WT and K180R HET mice were recorded and normalized to first peak amplitude (Figure 15A). The amplitude from the premature beat (S2) was measured and compared to the amplitude of the first peak (S1) to calculate a fractional recovery of the calcium transient (ratio of S2/S1, Figure 15B). The ratio was then plotted as a function of the coupling interval between S1 and S2 to assess the amount of calcium release occurring during different periods of diastole. K180R HET myocytes had a significantly higher fractional recovery of calcium transients at shorter coupling intervals compared to WT myocytes (Figure 15C). The higher amount of calcium being released at shorter coupling intervals indicates that the K180R variant impairs calcium release refractoriness, which would render the cell prone to release calcium prematurely.

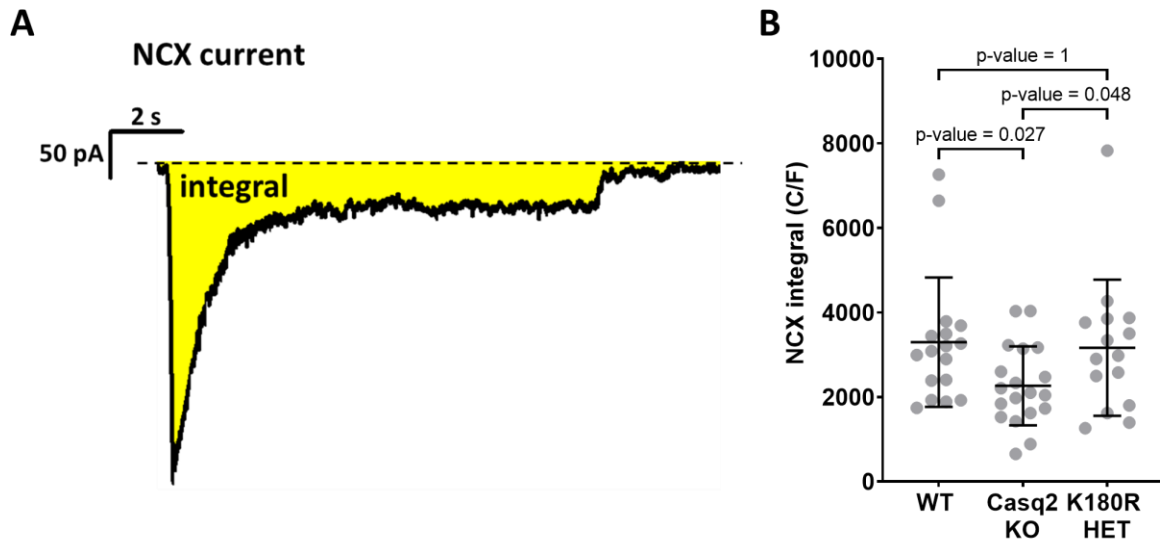


Figure 14. K180R does not change total SR calcium content. Total SR calcium content was quantified by integration of NCX current elicited in response to rapid caffeine application. NCX current integrals were normalized by cell capacitance, a measure of cell size. **A)** Representative trace of the NCX current. **B)** Average values for each group. WT n = 17 cells from 6 hearts, Casq2 KO n = 16 cells from 5 hearts, K180R HET n = 18 cells from 5 hearts. Data displayed as mean \pm SD. Data analyzed using a hierarchical statistical model with Bonferroni correction.

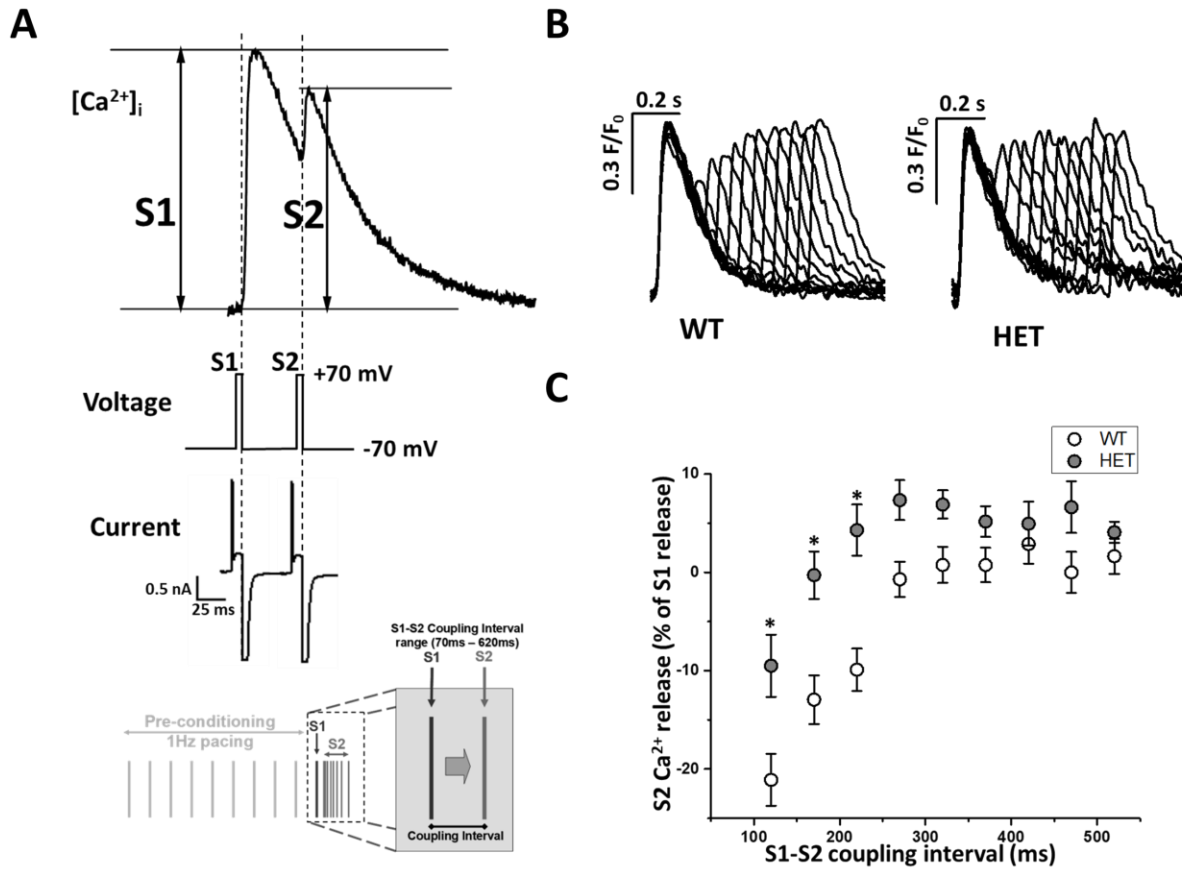


Figure 15. SR calcium release refractoriness is impaired in K180R cardiomyocytes. To measure the refractoriness of SR Ca release, isolated cardiomyocytes were loaded with fluo-4 Ca indicator, patched in voltage clamp mode, and a voltage stimulation protocol used as described in Kryshtal et. al 2015. A. SR Ca release was triggered by L-type Ca tail currents elicited by stepping membrane potential from +70 to -70mV. Example $[Ca]_i$ fluorescent trace indicates how S1 and S2 were calculated following restitution protocol. B. Representative Ca transients recorded with cytosolic Ca indicator fluo-4 for K180R WT and K180R HET cells. Traces were normalized to the amplitude of the first peak and superimposed over each other. C. Average S2 SR Ca release fraction plotted as a function of varying the S1–S2 coupling interval. $n = 10$ cells from 3 hearts for WT, white circles; $n = 10$ cells from 3 hearts for HET, grey circles. Data displayed as mean \pm SD. Data was analyzed using a hierarchical statistical model with Bonferroni correction. $*p < 0.05$. P values = 0.0084, 0.0002, and 0.0140, respectively.

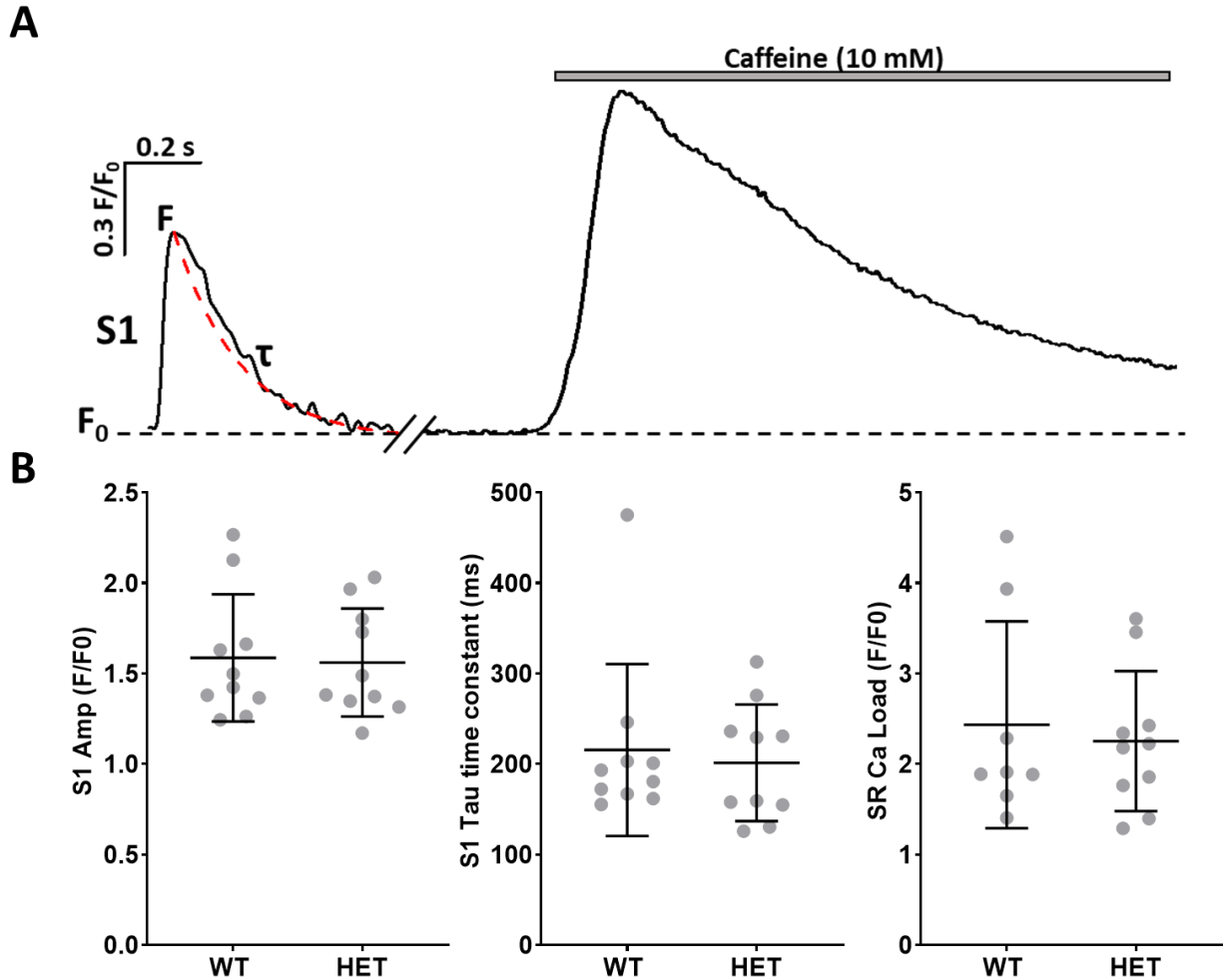


Figure 16. Cytosolic calcium transient and SR calcium content handling in intact K180R cells. Isolated cardiomyocytes were loaded with fluo-4 pentapotassium salt and studied using patch clamp in voltage-clamp mode using the stimulation protocol described in (Kryshtal *et al.*, 2015). **A**) Example recording traces. S1 tau was measured in the last S1-S2 pair (with the longest S1-S2 interval) using single-exponential fit. SR calcium load was estimated by caffeine (10 mM) spritz at the end of experiment. **B**) Bar graphs displaying measured variables. No differences were seen between K180R WT and HET cells for S1 amplitude, S1 tau, and SR calcium load. $n = 10$ cells from 2 hearts for WT; $n = 10$ cells from 2 hearts for K180R HET. Data displayed as mean \pm SD. Data analyzed using a hierarchical statistical model with Bonferroni correction.

K180R alters dynamic intra-SR calcium buffering

Given that K180R reduced refractoriness of SR calcium release, we reasoned that K180R impairs the ability of the SR to buffer calcium appropriately following calcium release. To quantify intra-SR calcium buffering, we next measured cytosolic and intra-SR free calcium simultaneously. A low-affinity esterified calcium indicator, Calbryte 520L-AM, was loaded into the SR of the cardiomyocytes. A high-affinity calcium indicator, Calbryte 590 potassium salt, was used to measure free calcium in the cytosol (Figure 17A) and was loaded via permeabilization of the cell membrane with saponin. Calcium waves in the cytosol and corresponding calcium depletions in the SR were recorded concurrently via confocal line scans (Fig 17A). Following calcium release, the free calcium concentration in the SR rose more quickly in K180R cardiomyocytes compared to WT cardiomyocytes. The rate of SR calcium uptake, measured by the decay of the cytosolic calcium transient (Figure 17B, Table 2), was identical in both groups. In other words, for the same amount of calcium entering the SR, the free SR calcium concentration increased significantly faster in K180R compared to WT myocytes. These results directly demonstrate that K180R impairs the dynamic buffering of calcium by Casq2. On the other hand, the amplitude of the SR calcium depletion signal (i.e., the maximal change in intra-SR free calcium concentration during the SR calcium release event) was not different between the groups. This result indicates that steady-state SR calcium buffering is NOT altered by K180R, consistent with our finding that total SR calcium content is unchanged in K180R cardiomyocytes (Figures 8B, 9B, and 14; Table 1). We next measured intra-SR calcium buffering in intact cardiomyocytes at a fixed pacing rate of 1 Hz (Figure 18). Corroborating our results from the permeabilized cardiomyocytes, the K180R variant caused a more rapid rise of intra-SR calcium after each paced beat without altering the amplitude of the intra SR calcium depletion signal (Figure 18). Taken together, our results indicate

that the K180R variant causes spontaneous calcium release by impairing the rate of calcium binding to Casq2 (i.e., dynamic calcium buffering) without changing steady-state calcium buffering by Casq2.

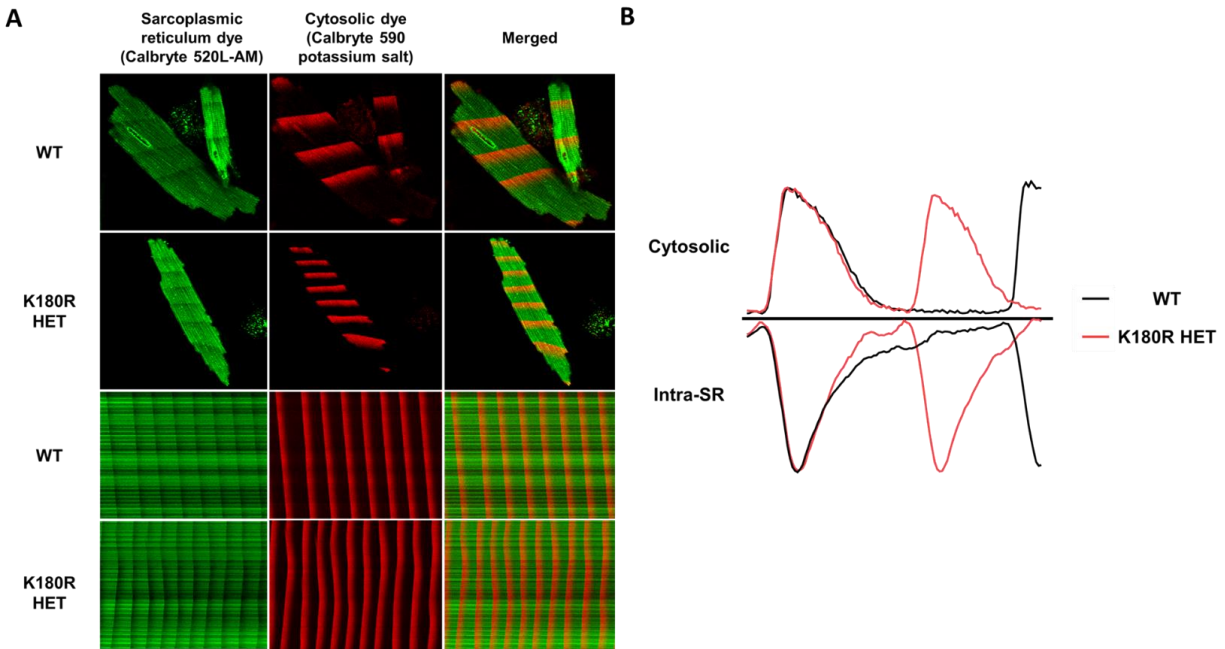


Figure 17. K180R decreases dynamic SR calcium buffering without affecting steady-state SR calcium buffering. Isolated cardiomyocytes underwent sarcoplasmic reticulum (SR) calcium handling analysis by measuring calcium waves using a dual-indicator approach. Briefly, cardiomyocytes were first loaded with an esterified low-affinity calcium indicator that could access the SR (Calbryte-520L, AM). Cells were then permeabilized and loaded with the high-affinity calcium indicator Calbryte-590, potassium salt, to measure cytosolic calcium levels. Cells were imaged using an inverted confocal microscope in line-scan mode. calcium transients were analyzed using LabChart 8. **A)** Representative images of indicator loading and wave propagation in permeabilized cardiomyocytes. Example line scan images from both SR and cytosolic fluorescent calcium indicators during calcium waves. **B)** Example trace of fluorescent signal over time during calcium release from the SR.

	K180R WT n = 35	K180R HET n = 35		
Sarcoplasmic reticulum			Significant?	p-value
Ca²⁺ transient				
Amplitude (F _{min} - F ₀)	-0.178 ± 0.040	-0.190 ± 0.040	No	0.1863
Time to peak (ms)	44.3 ± 9.39	40.2 ± 4.41	No	0.2064
Time to 10% peak (ms)	169 ± 38	140 ± 21	Yes	0.0174
Time to 50% peak (ms)	70.2 ± 9.8	63.6 ± 10.8	Yes	0.0084
Time to 70% peak (ms)	45.4 ± 6.5	41.1 ± 6.9	Yes	0.0085
Tau time constant (ms)	54.2 ± 13.5	46.4 ± 11.5	Yes	0.0102
Cytosolic			Significant?	p-value
Ca²⁺ transient				
Amplitude (F _{min} - F ₀)	2.18 ± 0.32	2.35 ± 0.36	No	0.1626
Time to peak (ms)	37.0 ± 11.1	37.8 ± 8.3	No	0.7491
Time to 10% peak (ms)	133 ± 17	131 ± 18	No	0.6584
Time to 50% peak (ms)	79.0 ± 11.6	80.3 ± 11.8	No	0.6516
Time to 70% peak (ms)	54.0 ± 10.0	54.6 ± 8.8	No	0.7993
Tau time constant (ms)	61.5 ± 12.3	61.5 ± 8.3	No	0.9966

Table 2. Analysis of cytosolic and intra-SR calcium handling in K180R cardiomyocytes. Cytosolic and intra-SR free calcium was measured simultaneously in permeabilized cardiomyocytes. n = 35 cells from 3 hearts for WT; n = 35 cells from 3 hearts for HET. Data displayed as mean ± SD. All data were analyzed using a hierarchical statistical model with Bonferroni correction.

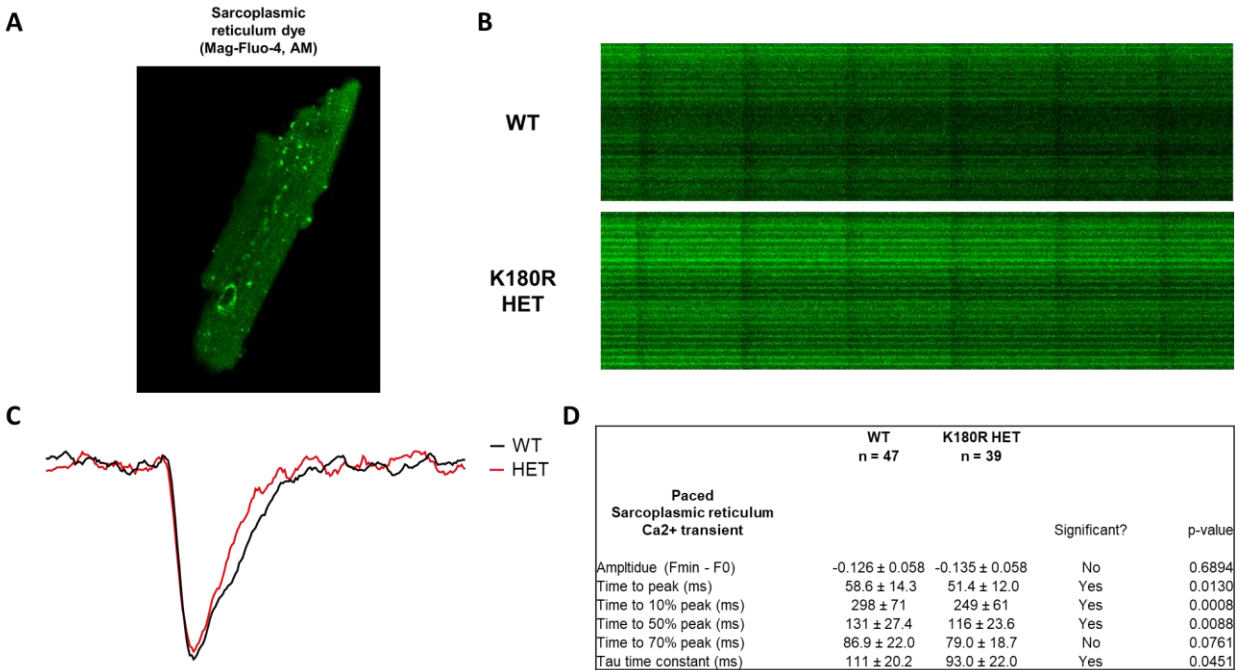


Figure 18. SR calcium buffering in intact K180R cardiomyocytes paced at 1 Hz. Cardiomyocytes isolated from mouse hearts underwent SR calcium handling analysis by pacing cells. Briefly, cardiomyocytes isolated from two different mice per group underwent SR dye loading with a calcium indicator dye that could access the SR (Mag-Fluo-4, AM). During the experiment, cells were incubated in 2 mM calcium normal Tyrode solution and paced at 1 hertz. Cells were imaged using an inverted confocal microscope in line-scan mode and analyzed using ImageJ. **A)** Example image of an isolated cardiomyocyte loaded with Mag-Fluo-4, AM. **B)** Example line-scan images of paced calcium waves in intact cardiomyocytes. **C)** Representative trace of fluorescent signal over time during calcium release from the SR. **D)** Table of characteristics of calcium transients from the SR. n = 47 cells from 3 hearts for WT; n = 39 cells from 3 hearts for K180R HET. Data reported as mean ± SD. Data analyzed using a hierarchical statistical model with Bonferroni correction.

Conclusion

Casq2 is a calcium binding protein with the function of regulating calcium release in various parts of the body. In the heart, Casq2 acts within the sarcoplasmic reticulum (SR) to manage free calcium levels and calcium release during the excitation-contraction (EC) coupling cycle. Variants in *CASQ2* have been found to cause a lethal arrhythmia syndrome, catecholaminergic polymorphic ventricular tachycardia type 2 (CPVT2). The current understanding is that CPVT2 follows an autosomal recessive inheritance pattern and causes CPVT by decreasing levels of Casq2. The absence of Casq2 reduces the ability of the SR to buffer calcium appropriately, resulting in a propensity to release calcium prematurely and cause delayed afterdepolarizations, triggered beats and ultimately CPVT (Wleklinski *et al.*, 2020). The first autosomal dominant variant in Casq2, K180R, was reported in 2016 (Gray *et al.*, 2016). The proposed hypothesis was that K180R, analogous to autosomal recessive variants, would decrease Casq2 protein levels and cause CPVT. With the variant being in only one allele, protein reduction would occur through a dominant negative mechanism where the mutated Casq2 would bind to WT Casq2, ultimately resulting in the degradation of the Casq2 multimer. Prior to our experiments reported here, the proposed dominant negative hypothesis had not been examined and the pathophysiology of the K180R variant was unknown. Here, we developed a K180R mouse model to study the pathophysiology of the K180R-linked autosomal dominant CPVT. We find that K180R produces a CPVT phenotype in both mice and isolated cardiomyocytes. Analogous to autosomal recessive Casq2 variants, K180R also decreases calcium release refractoriness. However, the underlying mechanism is fundamentally different, because K180R does NOT alter Casq2 protein levels, Casq2 polymers, or steady-state calcium buffering in the SR. Rather, K180R appears to reduce the rate of calcium binding to Casq2, resulting in a more rapid rise of free calcium

within the SR after a heartbeat. In other words, K180R alters the dynamic ability of Casq2 to regulate buffering of calcium ions as they move in and out of the SR during the E-C coupling cycle. Static buffering (e.g., steady-state calcium levels in the SR) appears to be not altered by the K180R variant, which is fundamentally different from Casq2 variants that reduce Casq2 protein levels and hence total SR calcium buffering. By affecting the dynamic buffering, K180R is decreasing the SR calcium release refractoriness of the cell. As calcium is re-entering the SR during diastole, the SR is now prone to having a faster rise in free calcium levels, which can lead to premature calcium release.

How does the K180R cause an impairment of dynamic SR calcium buffering? While the reported findings give insight into the pathophysiology of the SR calcium handling caused by K180R Casq2, the variant itself is quite small and is a conserved amino acid change within the structure of the protein. Recent studies have suggested that the K180R variant may affect the polymerization of Casq2 (Ng *et al.*, 2020; Titus *et al.*, 2020). Casq2 has been found to form monomers, dimers, and polymers through a calcium dependent process (Park *et al.*, 2003). The polymerization of Casq2 plays an important role in the ability of Casq2 to bind calcium and to provide a structural component for the SR (Park *et al.*, 2004). Recently, a manuscript was published where the authors were able to crystallize the Casq2 polymer and study it to gain a better idea of how Casq2 can cause CPVT. The study investigated potential autosomal dominant variants in *CASQ2* that have been linked to families with CPVT (Titus *et al.*, 2020). Based on the results of *in vitro* turbidity assays, the authors concluded that K180R and the other autosomal dominant *CASQ2* variants decreased the ability of Casq2 to polymerize. Further investigation of the crystallized polymer mapped the K180 amino acid onto a potential inter-dimerization site of Casq2. Based on the finding of impaired Casq2 polymerization, the authors hypothesized that the

K180R variant will cause the depletion of part of the wild-type and variant protein populations due to their inability to polymerize in the SR appropriately. The removal of WT or variant protein would affect the protein levels of Casq2 in K180R cells. However, we found that this hypothesis is not correct. Based on our western blot analysis, Casq2 protein levels are not decreased in K180R HET or HOM mice (Figure 11). Furthermore, K180R-Casq2 is also capable of forming polymers *in vivo*, as evidenced by our western blot and electron microscopy data (Figures 11 and 13). Polymerization is critical for trafficking and retention of Casq2 to the SR, since alterations in Casq2 polymerization, due to the addition of tags or fluorescent markers, lead to an inability of the protein to localize to the SR appropriately (Milstein *et al.*, 2009; McFarland *et al.*, 2010; Sleiman *et al.*, 2015). If K180R was disrupting the polymerization of Casq2, it would be expected that Casq2 would not be retained in the SR. Based on our results from K180R HET and HOM mice, K180R Casq2 appears to be trafficked correctly and able to polymerize. Our data indicate that *in vivo*, the K180R mutations cause a more subtle defect in the Casq2 polymer, whereby the rate of calcium binding to Casq2 is reduced. As previously discussed, Casq2 is a high-capacity, low-affinity calcium-binding protein that binds 40–50 calcium ions mainly through the 60–70 negatively charged amino acid residues within the monomer (Yano & Zarain-Herzberg, 1994). The initial polymerization studies suggested that the ability for Casq2 to bind calcium may also be dependent on polymerization state with an increase in calcium affinity as the polymer forms (Park *et al.*, 2004). The recent Casq2 polymer crystal structure also revealed novel potential calcium binding sites within the polymer and found a large cavity within the center of the polymer where calcium ions could bind (Titus *et al.*, 2020). Currently, there are no studies that have measured the calcium binding affinity (Kd) of the different states of Casq2. The location of K180 within the Casq2 polymer is proposed to be an inter-dimer region. The same region was also found to have

two potential calcium binding sites located near K180 (Titus *et al.*, 2020). It is possible that K180R could affect the ability of the Casq2 polymer to bind calcium given its involvement in the inter-dimer region. This mechanism would help explain how K180R is affecting the dynamic buffering capabilities of the SR. As the polymerization of Casq2 is a calcium dependent process, when calcium is re-entering the SR during diastole, K180R could be increasing the calcium K_d of the polymer. The decreased calcium affinity would allow for the decreased refilling kinetics in the SR that were observed (Figure 17). The faster refilling would then lead to a decrease in calcium release refractoriness (Figure 15), an increase in the potential for spontaneous calcium release events (Figures 7 and 10), and ultimately the possibility of CPVT (Figure 6).

The results of our experiments have broader implications regarding the pathophysiology of *CASQ2* variants. Recently, a large multi-center study was conducted to look for prevalence of autosomal-dominant *CASQ2* variants within CPVT families (Ng *et al.*, 2020). Of 36 probands, 12 had heterozygous *CASQ2* variants. The penetrance of heterozygous variants was lower than that of homozygous variants, 33.3% vs. 97.1%, but heterozygous patients still experienced similar symptoms and severity of arrhythmias as homozygous patients (e.g., aborted cardiac arrest). The study identified several other autosomal-dominant *CASQ2* variants that could be the target of future studies to confirm if other autosomal-dominant variants follow a similar mechanism as K180R.

Here we have shown that K180R is an autosomal-dominant *CASQ2* variant that is able to produce CPVT in mice. The K180R variant disrupts cellular calcium handling by altering the dynamic intra-SR buffering of calcium without reducing the levels of Casq2 or other junctional SR proteins. K180R had no effect on the static calcium buffering of the SR. The impaired dynamic buffering increases the rate of calcium rise in the SR and thereby decreases SR calcium release

refractoriness. The reduced SR calcium release refractory period can lead to spontaneous calcium release, delayed after depolarizations, triggered beats, and CPVT. Hence, our experimental work has uncovered a novel mechanism responsible for autosomal-dominant CPVT2 and thereby provides a template to investigate if other heterozygous variants in CPVT2 follow a similar pathophysiology.

CHAPTER II[†]

Targeting Casq2 to discover the tissue mechanism of CPVT

Introduction

As previously discussed, catecholaminergic polymorphic ventricular tachycardia (CPVT) is an inherited disorder characterized by emotional or physical stress-induced arrhythmias in structurally normal hearts (Leenhardt *et al.*, 1995). The more common autosomal-dominant form has been linked to mutations in the gene encoding the cardiac calcium release channel (*RYR2*) (Swan *et al.*, 1999a; Priori *et al.*, 2002). A less common, but more severe autosomal-recessive form is caused by loss of function mutations in the gene encoding cardiac calsequestrin (*CASQ2*), the major calcium-binding protein in the sarcoplasmic reticulum (SR) (Lahat *et al.*, 2001b; Postma *et al.*, 2002). Both *RYR2* and *CASQ2* mutations cause spontaneous premature SR calcium releases in ventricular myocytes (Knollmann *et al.*, 2006; Fernandez-Velasco *et al.*, 2009) that facilitate the generation of delayed afterdepolarizations (DAD) and focal ventricular arrhythmias (Priori *et al.*, 2001; Postma *et al.*, 2002). Hyperactive *RYR2* channels and an increased rate of spontaneous calcium release has also been observed in ventricular myocytes isolated from failing human hearts (Luo & Anderson, 2013; Dries *et al.*, 2018) and animal models of heart failure (Hoeker *et al.*, 2009). Since increased *RYR2* activity and spontaneous diastolic calcium release is an accepted

[†] This chapter is adapted from “The Purkinje-myocardial junction is the anatomic origin of ventricular arrhythmia in CPVT” published in *JCI Insight* and has been reproduced with the permission of the publisher and my co-authors: Dan Blackwell, Michela Faggioni, Nieves Gomez-Hurtado, Raghav Venkataraman, Chelsea Gibbs, Franz Baudenbacher, Shiaoqing Gong, Glenn Fishman, Patrick Boyle, Karl Pfeifer, and Bjorn Knollmann. Blackwell DJ, Faggioni M, Wleklinski MJ, Gomez-Hurtado N, Venkataraman R, Gibbs CE, Baudenbacher FJ, Gong S, Fishman GI, Boyle PM, Pfeifer K & Knollmann BC. (2022). The Purkinje-myocardial junction is the anatomic origin of ventricular arrhythmia in CPVT. *JCI Insight* 7.

cellular mechanism for the generation of ectopic ventricular beats, CPVT can be considered as a model to study calcium-triggered ventricular arrhythmia (Knollmann & Roden, 2008).

Experimental and modeling studies have suggested that Purkinje cells in the cardiac conduction system are the cellular source responsible for arrhythmia generation in CPVT (Cerrone *et al.*, 2007; Herron *et al.*, 2010; Kang *et al.*, 2010). Purkinje cells have differential protein expression (e.g. ion channels) and structural properties (lack of T-tubules) that make them particularly prone to develop spontaneous calcium releases (Vassalle & Lin, 2004; Li & Rudy, 2011). Modeling studies demonstrate increased sodium load and susceptibility to calcium overload, enhanced SR load, and lower action potential threshold. Experiments in isolated Purkinje cells and intact hearts from the *Ryr2/Ryr2^{R4496C}* mouse model have suggested that the Purkinje cells in the cardiac conduction system are the cellular source responsible for triggering CPVT (Cerrone *et al.*, 2007; Kang *et al.*, 2010; Li & Rudy, 2011). On the other hand, ventricular cardiomyocytes carrying CPVT mutations also exhibit spontaneous calcium release in response to catecholamine challenge and can generate DADs and spontaneous action potentials (Knollmann *et al.*, 2006; Fernandez-Velasco *et al.*, 2009). Optical mapping, commonly used to study the anatomical origin of ventricular arrhythmias, cannot resolve the Purkinje cells from the surrounding ventricular cardiomyocytes in the sub-endocardium. Thus, the anatomical and cellular origin of focal activation in CPVT remains uncertain.

To answer this question experimentally, we utilized an established *Casq2*^{-/-} mouse model of CPVT (Knollmann *et al.*, 2006). *Casq2* null mutations cause a severe CPVT phenotype in mice and humans. Our experiments aimed to achieve the following objectives: 1) determine the *cellular* origin of ventricular ectopy using a tissue-targeted genetic approach that selectively ablates *Casq2* gene expression either in the specialized conduction system or in the ventricular working

myocardium, 2) determine the *anatomical* origin of ventricular ectopy in the *Casq2*^{-/-} mouse CPVT model using optical voltage mapping of isolated hearts, and 3) model the Purkinje-myocardial junction and determine if and how subthreshold DADs generate ectopic beats.

Methods

Generation of tissue-specific Casq2^{-/-} mice

The generation of conditional *Casq2* has been reported (Flores *et al.*, 2018). Briefly, to modify *Casq2* expression, mice were generated with the promoter and exon 1 of *Casq2* in the forward (*fCasq2*) or reverse (*rCasq2*) orientation flanked by loxP sites. The *rCasq2* allele is similar to the modified *Casq2* allele used to generate *Casq2* null mice in a previous report (Knollmann *et al.*, 2006). However, in the reverse orientation there are three important differences: first, the promoter and first exon sequences between the *loxP* sites are inverted relative to the rest of the *Casq2* gene. Thus, no functional *Casq2*-encoding RNA can be generated, making *rCasq2* effectively a null-allele. Second, the *loxP* sites are inverted relative to each other (whereas in the *fCasq2* gene they are in the conventional tandem orientation). Consequently, Cre-mediated recombination results in inversion and not deletion of the intervening sequences. Thus, the cre enzyme acts on the *rCasq2*- allele to restore normal gene structure. Third, the *loxP* sites used in the *rCasq2*- allele each carry a single point mutation. Cre mediated recombination between these two *loxP* elements generates two new *loxP* elements: one wild-type and one carrying both point mutations. These two *loxP* elements do not recombine with each other, thus making the Cre-mediated inversion unidirectional and permanent. The *fCasq2* allele contains loxP sites in tandem orientation, resulting in Cre-mediated deletion of the intervening sequence.

To generate the *rCasq2* allele, mouse ES cells (RI line, 129SV) were transformed with linearized plasmid, pKP700. Plasmid pKP700 included a 2.1 kb 5' homology flank and a 2.0 kb 3' homology flank to direct insertion of a *loxP* element at -561 bp and an inverted *loxP* element and a 2.1 kb NeoR cassette at +538 bp inside of intron 1. In addition, the entire 1.1 kb region between the *loxP* elements was inverted relative to the external flanks. Plasmid pKP700 also contained a 3.0 kb *Diphtheria toxin A* gene for negative selection. G418 resistant colonies were isolated and scored for homologous recombination by PCR amplification using 1 primer from outside the flanking sequences present in pKP700 and one primer from within the *NeoR* cassette. Targeted clones were injected into C57BL/6J blastocysts and chimeric animals crossed with C57BL/6J females to establish the *rCasq2-Neo* line. These males were crossed with Rosa26-Flp transgenic females (Jackson Labs strain 003946) to remove the *NeoR* cassette and thereby generate mice carrying the *rCasq2* allele.

To generate transgenic mice expressing *cre* under the control of the Purkinje-specific *Cntn2* gene, we employed BAC recombineering, like the approach used in the GENSAT program to generate *Cntn2-EGFP* BAC reporter mice (Gong *et al.*, 2003). *Cntn2-cre* BAC DNA was injected into FVB/N pronuclei. Founders were screened by crossing with a floxed dTomato reporter and one line with expression that best co-localized with the *Cntn2-EGFP* reporter strain (Pallante *et al.*, 2010) was identified.

All transgenic lines were backcrossed into the C57BL/6J strain at least ten times before they were used in our studies. Mice homozygous for the *fCasq2* or *rCasq2* were crossed with mice heterozygous for *Cntn2-cre* to generate tissue specific Casq2 knockout lines, as described in Figure 19.

Arrhythmia induction in anesthetized mice

Arrhythmia susceptibility was tested in mice with a catecholaminergic challenge during surface ECG recording. Mice were selected by an individual blinded to the genotype, anesthetized with 3% (v/v) isoflurane inhalation, and needle electrodes were placed subcutaneously into all four limbs. Isoflurane was titrated to the lowest possible setting (~1.25% v/v) to maintain stable sedation and ECGs were recorded using a 16-channel PowerLab with 10 kHz sampling rate (AD Instruments). After stabilization of the baseline heart rate (1 – 5 minutes) mice were injected intraperitoneally (i.p.) with 3 mg/kg isoproterenol + 60 mg/kg caffeine. ECG traces were recorded for an additional 10 minutes. Arrhythmia susceptibility was quantified as ventricular ectopic beats (VEB) per minute per mouse and as the number of mice with ventricular tachyarrhythmias (VT; >2 consecutive VEB) in each group. ECG analysis was conducted by two reviewers blinded to the genotype and then compared for precision. A third observer analyzed 2 ECG traces where the discrepancy was more than 0.5% of the total VEB count.

Western blotting

Cell lysates were prepared from hearts in homogenization buffer (50 mM TRIS, 320 mM sucrose, 1 mM DTT, 0.1% IGEPAL CA-630, pH = 7.0) containing 1% protease inhibitor cocktail (Sigma P8340) and phosphatase inhibitor (Sigma P0044). Two hearts from C57BL/6J and one heart from a congenital *Casq2*^{-/-} mouse (Knollmann *et al.*, 2006) were included as controls. Samples were separated on a 4 – 20% polyacrylamide gel (Bio-Rad Mini-PROTEAN), transferred to a polyvinylidene difluoride membrane, blocked in TBST + 5% milk for 1 hour at room temperature, and incubated overnight at 4 °C with primary antibody. Blots were washed 3X in TBST and incubated with secondary antibody for 1 hour at room temperature, washed 3X in TBST,

and then developed with ECL reagent (GE Healthcare) and imaged using a ChemiDoc MP (Bio-Rad). For calsequestrin 2 immunolabeling, blots were incubated with 1:2,000 anti-calsequestrin2 (Abcam ab108289) and 1:5,000 anti-rabbit HRP conjugate (Promega W401B). For GAPDH, blots were incubated with 1:10,000 anti-GAPDH (ThermoFisher AM4300) and 1:5000 anti-mouse HRP conjugate (Invitrogen 31430). Full uncropped/unedited blots were provided to the reviewers.

Immunostaining

Murine hearts were isolated, hung on a Langendorff apparatus, and perfused with Tyrode's solution for one minute. Hearts were dissected in half, embedded in optimal cutting temperature compound (Fisher Scientific), and flash frozen on dry ice. A cryostat (Leica CM1950) and high-profile microtome blades (Accu-Edge 4685) were used to generate 8 μ m sections on charged slides (Denville M1021). Frozen sections were fixed in 2% paraformaldehyde for 20 minutes, blocked with 5% goat serum in DPBS + 0.4% triton for 1 hour at room temperature, and incubated with primary antibodies overnight. Casq2 (Pierce PA1-913 or Proteintech 18422-1-AP), Contactin-2 (R&D AF4439), and GFP (AbCam 9F9.F9) antibodies were diluted in DPBS+triton at 1:500, 1:20, and 1:1000, respectively. Blocking solution was used as a negative control. Secondary antibodies were diluted in DPBS + triton 1:400 for Casq2 and Cntn2 and 1:500 for GFP. Slides were incubated with Alexa Fluor 488 or 568 secondary antibody for 1 hour at room temperature. Cover slides were mounted using ProLong Gold antifade with DAPI (Invitrogen P36941) and left to dry overnight. Imaging was carried out on a Zeiss LSM 880 confocal microscope (provided by Dr. Laura Dugan, Vanderbilt University, Nashville, TN). Excitation was elicited using a 488 nm Argon laser or 561 nm diode pumped solid state laser and emission was collected from 493 – 556 nm and 568 – 712 nm. The images were reviewed and scored by an individual blinded to the genotype and phenotype.

Casq2- and Cntn2-immunostained images were opened in ImageJ (version 1.52i) and free polygons were hand-drawn around areas with positive staining by a reviewer blinded to the genotype and phenotype. Images were converted to binary masks and exported as text image files. Nearest neighbor distances for corresponding Casq2 and Cntn2 masks were calculated on a pixel-by-pixel basis in R (version 3.6.0) using the `nncross()` function available in the `spatstat` package (version 1.59-0). Histograms were generated with a bin-width of 15 μm . The percent of the PF having contiguous Casq2 expression in ventricular myocytes juxtaposed to the fiber was analyzed using the “freehand line” tool in ImageJ to measure fiber length.

Optical mapping and electrocardiogram (ECG) recordings in Langendorff-perfused hearts

Mice were anaesthetized with 5% isoflurane inhalation. After achieving a surgical plane of anesthesia, a thoracotomy was performed and the heart harvested and retrogradely perfused in the Langendorff mode with oxygenated Tyrode’s buffer (pH = 7.4; 1.5 mM calcium, 37 °C). Hearts were equilibrated for 5 minutes and then stained with 10 – 15 μl of the transmembrane potential dye di-4-ANEPPS (0.5 mg/ml in dimethyl sulfoxide) by slow injection of dye stock into a bubble trap directly above the cannula, followed by an additional 5-minute equilibration period. di-4-ANEPPS was excited using a diode-pumped solid-state 532 nm laser (Coherent, CA) focused onto the heart through 4 liquid light guides and the fluorescence signal was collected with a 14-bit, 80 \times 80 pixel, 1000 FPS CCD camera (RedShirtImaging, GA). Hearts were imaged from the anterior epicardial surface, both at baseline and during arrhythmia induction.

To facilitate induction of ventricular arrhythmia, the intrinsic sinus heart rate was reduced by adding 1 μM carbachol to the perfusate. After 5 – 10 minutes equilibration, ventricular

arrhythmias were induced with repeated 0.1 mL boli of 100 nM isoproterenol (ISO) injected into the perfusion line. Ventricular arrhythmic events typically occurred within 5 – 10 seconds after a bolus injection of ISO. Optical recordings were acquired for up to 2 minutes after injection; each recording lasting 4 seconds. ECG traces were continuously recorded and were used to determine the end of an arrhythmic burst and hence the end of optical data acquisition.

LV and RV endocardial ablation in Casq2^{-/-} Langendorff-perfused hearts

After equilibration in the 37 °C bath and acquisition of basal sinus activation maps, the perfused heart was arrested in cold buffer (4 °C). 8 *Casq2^{-/-}* and 8 WT hearts received an injection of Lugol's solution (~30 µl) into the left ventricular cavity through an incision in the left auricle. Both the endocardial and epicardial surface were thoroughly washed with buffer before the heart was repositioned in the warm bath. The ablation was considered successful if the left ventricular breakthrough of sinus activation disappeared while the right sided breakthrough was still present, and conduction of the activation wavefront on the epicardial surface of both ventricles remained unchanged after the procedure. The incidence of ectopic activity in Lugol-treated *Casq2^{-/-}* hearts was compared to that of *Casq2^{-/-}* hearts undergoing the same procedure (i.e. equilibration, immersion in 4 °C buffer, auricle incision) but receiving an injection of vehicle instead of Lugol's solution. The same experiment was repeated on another 8 *Casq2^{-/-}* mice with right ventricle (RV) endocardial ablation with Lugol's.

Following the experiments with endocardial ablation, the hearts were perfused with triphenyl tetrazolium chloride dye, sectioned, and imaged. The depth of the endocardial ablation in the thickness of the LV wall was measured as a ratio between purple-stained and unstained

(necrotic) tissue. Intact *Casq2*^{-/-} hearts receiving an intra-ventricular injection of vehicle were used as controls.

Analysis of optical data

Optical data analysis was performed using custom algorithms implemented in MATLAB (Mathworks, MA). Recordings were first temporally filtered with a 3-frame running-average and spatially filtered with a 3x3 pixel Gaussian low-pass filter. Fluorescence maps were generated by calculating the difference in fluorescence between the frame of interest and a background frame selected when the heart was fully repolarized. Isochronal activation maps were generated using an automated algorithm that scanned through user-defined time intervals to calculate the action potential (AP) activation at each point; the activation time at each point was then plotted to generate the map. AP activation was defined at the time at which the absolute rate of change of fluorescence was maximal during the AP upstroke.

Arrhythmia analysis in isolated hearts

ECG records were reviewed and ventricular ectopic beats (VEB) identified based on standard criteria (i.e., wide QRS complex, AV dissociation). In experiments where the heart rate was lowered by carbachol, ventricular rhythms with cycle lengths longer than 150 ms (intrinsic cycle lengths of isolated mouse hearts) were considered ventricular escape beats and were not included in the analysis. The ventricular origin of abnormal beats on the ECG was verified on the optical map. Only ectopic beats with a visible full activation ring were used for the analysis.

Computational modeling of DAD-Like Activity in the Ventricles or Purkinje fiber

All modeling was conducted in openCARP (Plank *et al.*, 2021) (<http://opencarp.org>; free for non-commercial use), a finite element software custom-designed to simulate electrophysiological phenomena at the cell, tissue, and organ scale. The Purkinje-myocardial junction was modeled as a geometric tissue expansion between two regions with distinct cell- and tissue-scale electrophysiological characteristics. Specifically, the model was a rectangular prism-shaped block of ventricular tissue (dimensions: $1 \times 1 \times 0.475 \text{ cm}^3$) with a PF-like structure ($1 \text{ cm} \times 500 \mu\text{m} \times 125 \mu\text{m}$), attached at a single junction (Figure 29). Membrane kinetics were represented by a well-validated human ventricular action potential model (ten Tusscher & Panfilov, 2006). To represent differences in excitability, the simulated sodium channel conductance (G_{Na}) was fixed at $0.5\times$ of its default value in ventricular cells; the same parameter was fixed at $5\times$ in PF-like cells. Myofiber orientations in the PF region were uniform, parallel to the long axis of the structure; in ventricular tissue, myofibers ran in the perpendicular direction, as shown in Figure 29. To account for heterogeneity of inter-cellular coupling between tissues, we adjusted conductivity values (PF vs. ventricular: longitudinal = 2.336 vs. 0.2336 S/m ; transverse = 0.1761 vs. 0.01761 S/m).

To simulate DAD-like activity, the ventricular tissue was initialized in a refractory state, then a short stimulus was applied to elicit a subthreshold response. The refractory steady state was obtained by pre-pacing the model at 2 Hz then freezing state variable values at the time point corresponding to APD_{90} . We empirically calibrated a transmembrane current pulse (20 ms long; amplitude = $4.3740234375 \text{ pA/pF}$) that produced a transient depolarization without triggering a new action potential. A buffer region of ventricular cardiomyocytes adjacent to the PF was modeled in an identical manner to other ventricular cells, but without the electrical stimulus; to

gauge how this affected the propensity for retrograde excitation, the buffer region's radius was varied from 0 to 300 μm in 75 μm steps.

Statistics

Statistical analyses were performed using Prism v7.04 (GraphPad Software, Inc.). Statistical tests were used as reported in the figure legends. A P value of 0.05 was used as the threshold to reject the null hypothesis.

Study approval

The use of animals was approved by the Animal Care and Use Committee of Vanderbilt University, USA (animal protocol #'s M1600090-00 and M1600259-00) and performed in accordance with NIH guidelines.

Results

Generation of Purkinje-specific and ventricular myocardium-specific Casq2^{-/-} mouse models

To selectively delete Casq2 expression either in Purkinje cells (PC-Casq2^{-/-} mice) or in the ventricular myocardium (VM-Casq2^{-/-} mice), mice with conditional deletion or with conditional rescue Casq2 alleles (Flores *et al.*, 2018) were crossed with mice expressing Cre recombinase under control of the contactin-2 (*Cntn2*) promoter (see methods section). Immunostaining and western blot from selected hearts confirmed successful Purkinje- or cardiomyocyte-specific Casq2 deletion in our tissue-targeted murine models (Figure 19B, 20C, and 21).

Arrhythmia susceptibility in tissue-targeted Casq2^{-/-} mice

Arrhythmia susceptibility was tested in 8 – 38 weeks old, anesthetized mice injected intraperitoneally with 3 mg/kg isoproterenol (iso) or 3 mg/kg iso + 60 mg/kg caffeine during continuous surface electrocardiogram (ECG) recording. As expected, “wild-type” mice had no ventricular arrhythmias (Figure 20D-F). Global knockout of Casq2 caused a full-blown CPVT phenotype characterized by PVCs and bidirectional and polymorphic VT (Figure 20D-F), comparable to what we have previously observed in a germline whole heart Casq2^{-/-} model (Knollmann *et al.*, 2006). One Casq2 knockout mouse had zero PVCs (Figure 20E), but had supraventricular tachycardia immediately following catecholamine injection, an observation we have noted that may protect these mice from ventricular ectopy (Faggioni *et al.*, 2013; Kannankeril *et al.*, 2020).

Deletion of Casq2 in the ventricular myocardium is both necessary and sufficient to cause a CPVT phenotype; deletion of Casq2 in the His-Purkinje system is not

To determine whether loss of Casq2 only in Purkinje cells is sufficient to induce a CPVT phenotype, we tested arrhythmia susceptibility in our selective Casq2^{-/-} models. When Casq2 was knocked out only in the Purkinje cells (PC-Casq2^{-/-}), no ventricular arrhythmias were observed, despite injection with both 3.0 mg/kg iso and 60 mg/kg caffeine (Figure 20D-F). Normally, 1.5 mg/kg iso alone is sufficient to induce a CPVT phenotype in global Casq2^{-/-} mice (Knollmann *et al.*, 2006). These results suggest that Casq2 loss in the conduction system alone is not sufficient to cause ventricular arrhythmias. To test whether the ventricular cardiomyocytes are the cellular origin for CPVT we examined arrhythmias in mice where Casq2 was selectively knocked out in the VM but maintained in the PC. VM-Casq2^{-/-} mice had significant ventricular arrhythmias, with

similar arrhythmia burden as whole-heart *Casq2*^{-/-} mice (Figure 20E-F, P = 0.29). Taken together, these data indicate that loss of Casq2 in the ventricular working myocardium is both necessary and sufficient to cause ventricular ectopy in CPVT, even when Casq2 is appropriately expressed in the conduction system.

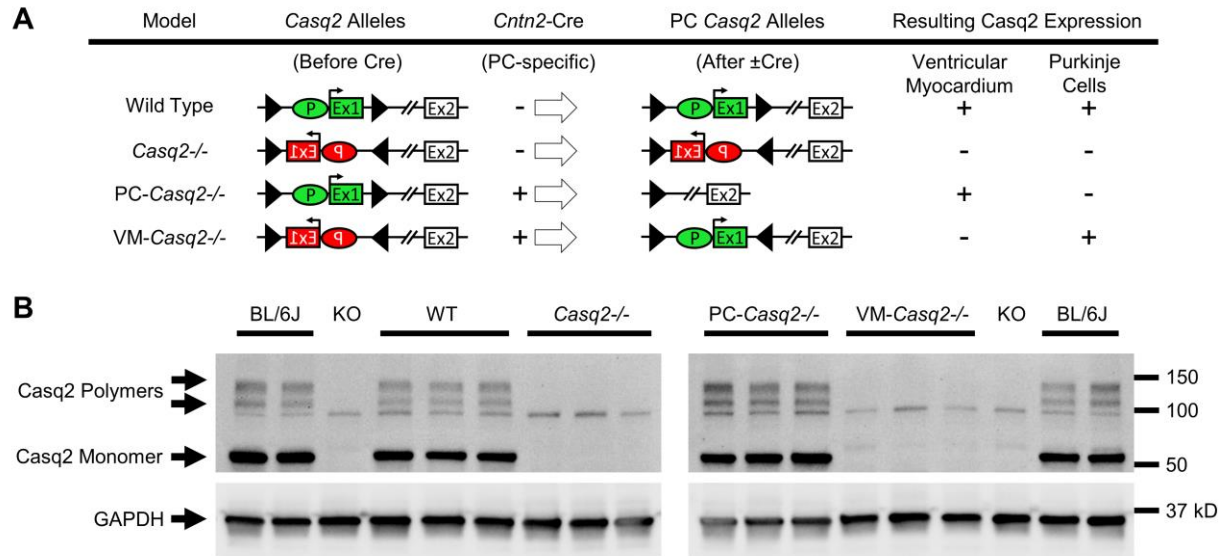


Figure 19. Generation and characterization of cardiac calsequestrin (Casq2) tissue-specific mouse models part 1. **A)** Each mouse model is shown with its representative *CASQ2* alleles before and after Cre expression in the Purkinje Cells (PC) and resulting Casq2 protein expression in the ventricular myocardium (VM) and PC. The *Casq2* floxed allele contains the promoter (P) and exon 1 (Ex1) in either the forward or reverse gene orientation flanked by loxP sites (triangles). Cre expression (if present) flips the orientation of the promoter and exon 1, resulting in four models: “wild-type” (global Casq2^{+/+} expression); “*Casq2*^{-/-}” (global *Casq2*^{-/-}); “PC-*Casq2*^{-/-}” (Casq2 knocked out only in PC); and “VM-*Casq2*^{-/-}” (Casq2 knocked out only in the VM). Contactin-2 (*Cntn2*) is only expressed in PC. **B)** Western blots from *Casq2* tissue-specific mouse hearts. C57BL/6J (BL/6J) was included as a positive control. Casq2 null (KO) is an independent *Casq2* germline deletion model (Knollmann *et al.*, 2006) and was included as a negative control (the same BL/6J and KO samples were loaded on both gels). GAPDH was used as a loading control.

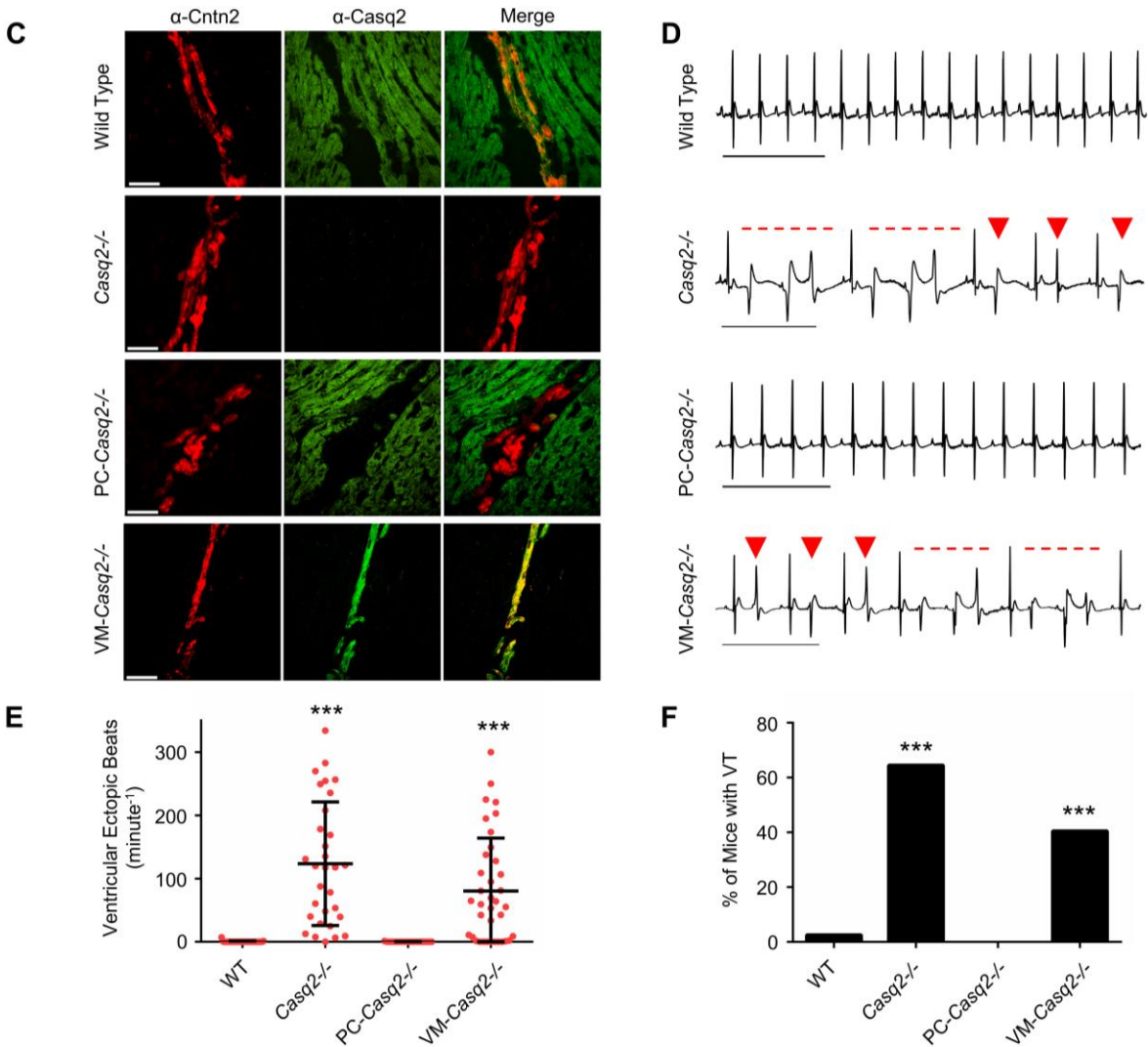


Figure 20. Generation and characterization of cardiac calsequestrin (Casq2) tissue-specific mouse models part 2. **C)** Representative immunostaining for Cntn2 and Casq2 from sectioned mouse hearts. Scale bar = 50 μ m. **D)** Representative electrocardiogram traces from each mouse model after intraperitoneal administration of 3 mg/kg isoproterenol + 60 mg/kg caffeine. Arrows denote premature ventricular complexes and dashed lines denote episodes of ventricular tachycardia (VT). Scale bar = 500 ms. **E)** Quantification of ventricular ectopic beats (VEB) and **F)** VT incidence in 8 – 38 week old mice. Sample number for E and F: WT n = 39, Casq2KO n = 31, PC-Casq2^{-/-} n = 16, VM-Casq2^{-/-} n = 28. Data in E shown with mean \pm SD. *** p < 0.001 vs WT or PC-Casq2^{-/-} by Kruskal-Wallis test followed by Dunn’s multiple comparisons post-hoc test (panel E) or Fisher’s Exact test (panel F).

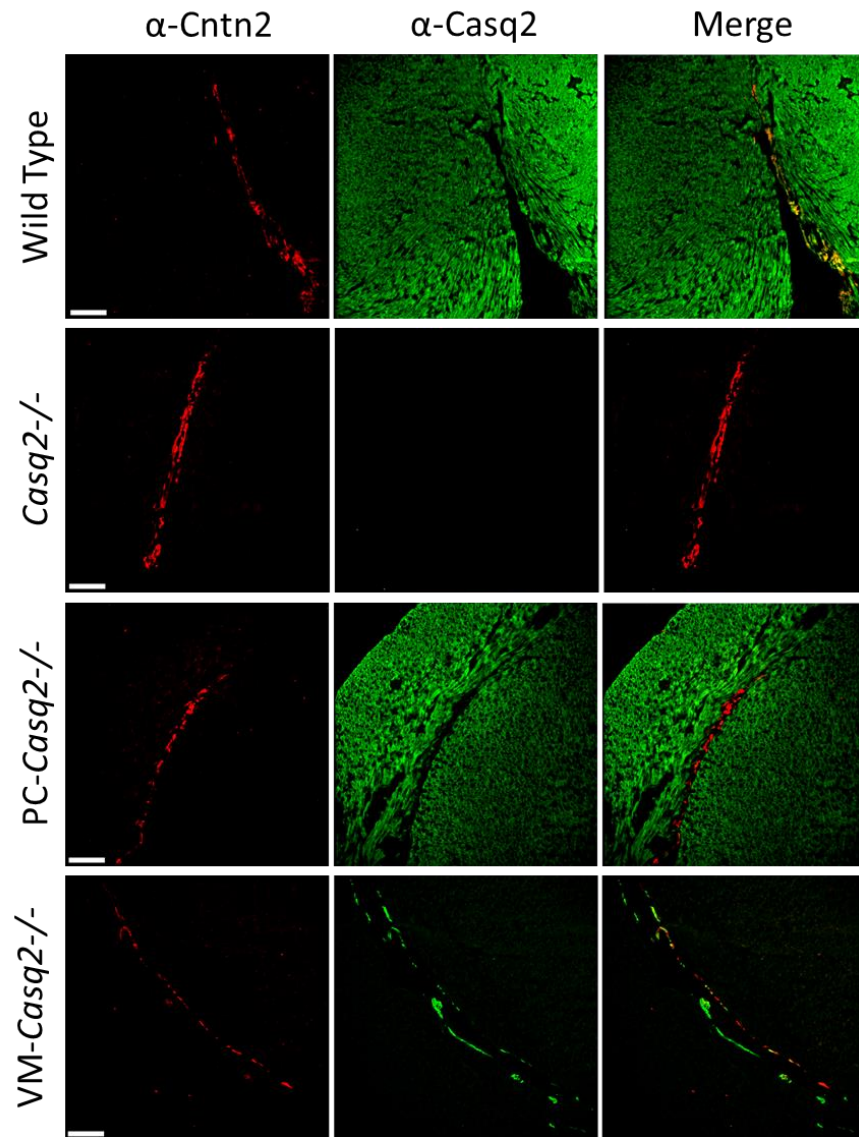


Figure 21. Representative images of contactin-2 (Cntn2; a Purkinje cell maker) and calsequestrin-2 (Casq2) immunostaining in tissue-specific *Casq2*^{-/-} mouse lines. Scale bar = 200 μ m. PC = Purkinje cell; VM = Ventricular myocardium.

Optical voltage mapping indicates focal origin of ventricular arrhythmias in Casq2^{-/-} mouse hearts

To examine the anatomical origin of ventricular ectopy in CPVT, hearts were isolated from *Casq2^{-/-}* mice and perfused in Langendorff mode with oxygenated Tyrode's solution and the transmembrane potential dye di-4-ANEPPS. Voltage mapping showed normal sinus rhythm bundle branch breakthroughs at baseline (Figure 22A). Upon stimulation with perfused isoproterenol (iso), the hearts developed mono- and multi-focal ventricular arrhythmias in the form of single premature ventricular complexes (PVCs), couplets, bigeminy, bidirectional VT, and polymorphic VT (Figure 22B-D). All ventricular arrhythmias were focal in origin, without any evidence for reentrant circuits. The focal activity originated from both ventricles, with RV foci significantly more common than LV foci (Figure 22E-F), which mirrors observations from humans diagnosed with CPVT (Sumitomo *et al.*, 2003). Importantly, the breakthrough sites of all ventricular ectopic beats were outside and distinct from the normal sinus rhythm breakthrough sites of the left and right bundle branches. This result corroborates the results from our tissue-targeted *in vivo* experiments (Figures 19 and 20) and further confirms that the ventricular ectopy in CPVT does not originate exclusively from Purkinje cells in the bundle branches, as previous modeling studies had suggested (Cerrone *et al.*, 2007; Baher *et al.*, 2011).

Endocardial ablation prevents ventricular arrhythmia in Casq2^{-/-} mouse hearts

To identify the origin of ventricular ectopy within the working ventricular myocardium, we first mapped ventricular activation of the epicardial surface of *Casq2^{-/-}* hearts during sinus rhythm and during isoproterenol-induced ventricular arrhythmias. Then, we injected Lugol's solution into the left or right ventricle (LV or RV) to chemically ablate the endocardial surface and

underlying myocardium and repeated the isoproterenol challenge (Figure 23A-B). All *Casq2*^{-/-} hearts displayed loss of the left sided breakthrough during sinus activation after LV endocardial ablation, thereby establishing the successful disruption of the conduction system and endocardial activation in the LV. However, the activation wavefront originating from the RV breakthrough was still homogeneously conducted on the epicardial surface of both ventricles (Figure 23B). The QRS complex duration after the procedure was significantly prolonged (10.5 ± 0.4 ms before LV ablation vs. 13.7 ± 0.9 ms after LV ablation), with a QRS morphology consistent with a left bundle branch block (Figure 23C). Importantly, the endocardial lesion produced by the chemical ablation did not increase the incidence of ventricular ectopy in 8 WT hearts, ruling out chemical ablation as a cause of arrhythmogenesis. After LV endocardial ablation in *Casq2*^{-/-} hearts, ventricular ectopic beats (VEBs) originating from the LV were almost completely suppressed (only 0.4% of the total number of VEBs in Lugol-treated hearts) and RV VEBs accounted for 99.6% of all ectopic beats recorded (Figure 23D). Conversely, when the RV endocardium was ablated, the RV breakthrough for sinus beats was abolished and all ectopic ventricular activity was generated from the LV (Figure 23D). Although chemical ablation by Lugol's does not discriminate between the ventricular conduction system and the working endocardium, these results, together with the evidence from the selective *Casq2* knockout models (Figures 19 and 20), indicate that the subendocardial myocytes are the likely cellular source of ventricular ectopy.

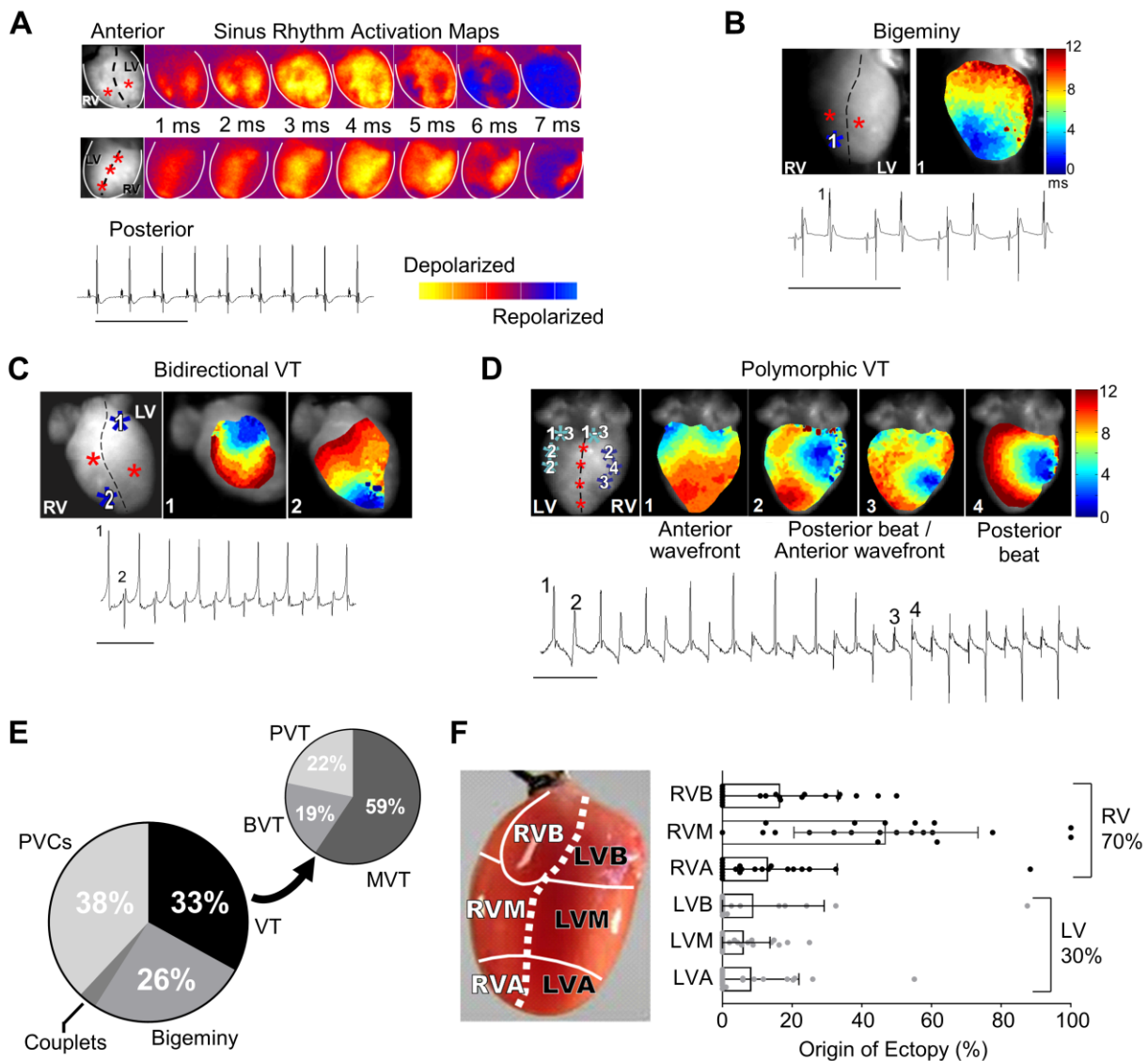


Figure 22. *Ex vivo* optical mapping and continuous electrocardiogram (ECG) recording in Langendorff-perfused calsequestrin-2 (Casq2) null mouse hearts. **A**) ECGs were continuously recorded while optical voltage maps were acquired from anterior and posterior epicardial surfaces during sinus rhythm. Sinus rhythm epicardial breakthroughs are denoted by red stars in the left-most panel. **B**) Example temporal activation maps and associated ECG traces of bigeminy; **C**) bidirectional ventricular tachycardia; and **D**) polymorphic ventricular tachycardia following perfusion of 100 nM isoproterenol bolus. Ectopic foci are denoted by blue stars and indicated numerically on the accompanying ECG traces. **E**) Classification of arrhythmia episodes from 8 hearts captured by ECG and optical mapping (n = 246 total episodes). PVC = premature ventricular complex. VT = ventricular tachycardia. PVT = polymorphic VT. BVT = bidirectional VT. MVT = monomorphic VT. ECG scale bars = 500 ms. **F**) Quantification of the site of epicardial breakthroughs (n = 21 for each group) during voltage mapping from the same recordings as E. Data shown as mean \pm SD. R/LVB = right/left ventricular base, R/LVM = mid right/left ventricle, R/LVA = right/left ventricle apex.

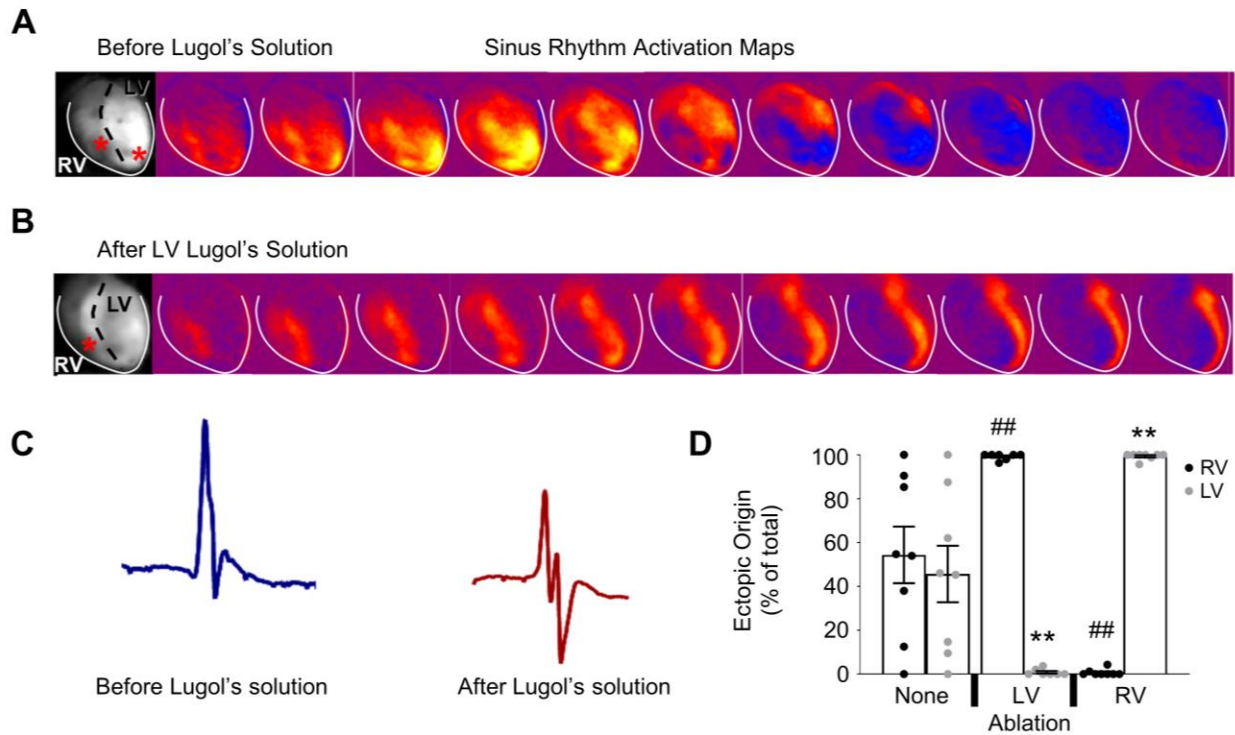


Figure 23. Endocardial ablation reduces arrhythmia burden in caspase-2 (Casq2) null hearts. Lugol's solution was injected either into the left (LV) or right (RV) ventricle to ablate the endocardial wall. Optical mapping **A**) before and **B**) after injection of Lugol's solution into the LV. Breakthroughs are denoted in the left-most panels by red stars. Activation of the LV epicardium was maintained even after endocardial ablation. **C**) Representative QRS waveform morphology before and after injection with Lugol's solution. **D**) Origin of ventricular ectopic beats (VEB) after injection of vehicle or Lugol's solution into the LV or RV. Arrhythmias were stimulated by perfusion with 100 nM isoproterenol (n = 8 hearts per group). Data shown as mean \pm SD. ## P < 0.01 by two-sided Student's t-test when comparing ectopic origin percentage from the RV to no ablation. ** P < 0.01 by two-sided Student's t-test when comparing ectopic origin percentage from the LV to no ablation.

Juxta-Purkinje ventricular cardiomyocytes located in the subendocardium are the cellular origin for CPVT

During our investigation, we noted that several VM-*Casq2*^{-/-} mice had no ventricular ectopy *in vivo* (Figure 19E-F). To determine whether *Casq2* was completely knocked out in the ventricular myocytes of these mice, hearts were examined by co-immunostaining for *Casq2*, and *Cntn2* to identify Purkinje cells. We found that, alongside *Casq2* expression in the conduction system, some VM-*Casq2*^{-/-} hearts still expressed *Casq2* in ventricular myocytes juxtaposed to the conduction system (Figure 24A), an expression pattern which we termed “juxta-Purkinje *Casq2*.” A reviewer blinded to the genotype classified hearts based on the *Casq2* immunostaining relative to *Cntn2* staining as either complete VM knockout or “juxta-Purkinje *Casq2*” (Figure 24A-B). Hearts classified as having juxta-Purkinje *Casq2* expression had *Casq2*-positive myocytes almost contiguous with the PF (Figure 24C, mean = 87.4%). To quantify the relative colocalization in each group, we calculated the nearest neighbor distance (NND) for each positive *Casq2* pixel relative to the nearest *Cntn2* pixel. The median NND in complete VM knockout hearts was 0.0 μm (perfect colocalization) whereas it was 34.07 μm in hearts classified as having juxta-Purkinje *Casq2* expression (Figure 24D-E, individual NND distributions for each heart are show in Figure 25). As shown by the NND distributions, ventricular cardiomyocytes that expressed *Casq2* were only near Purkinje cells. Incidence of positive staining for *Casq2* decreased as distance from the nearest Purkinje cell increased, showing that additional *Casq2* expression was only in the subendocardial myocytes juxtaposed to the Purkinje cells. No *Casq2* expression was observed in the epicardial tissue of any heart.

Notably, mice expressing *Casq2* in myocytes juxtaposed to Purkinje cells had significantly lower rates of ectopy ($P = 0.006$) and accounted for most of the zero values within the VM-*Casq2*-

/- (shown in Figure 20E) that were immunostained (Figure 24F-G). The arrhythmia rates in the complete VM knockout group were essentially the same as the whole-heart *Casq2*^{-/-} model (P = 0.94) whereas the juxta-Purkinje group had significantly fewer ectopic beats and reduced arrhythmia burden compared to the whole-heart *Casq2*^{-/-} group (P < 0.001). Although it is unclear why in a subset of VM-*Casq2*^{-/-} mice Cre was turned on in cardiomyocytes adjacent to Purkinje cells, this serendipitous finding provides direct evidence that subendocardial ventricular myocytes near PFs are the cellular origin for CPVT. Expression of *Casq2* in ventricular myocardium juxtaposed to Purkinje cells protected against arrhythmias, whereas *Casq2* expression only in the Purkinje cells did not (Table 3).

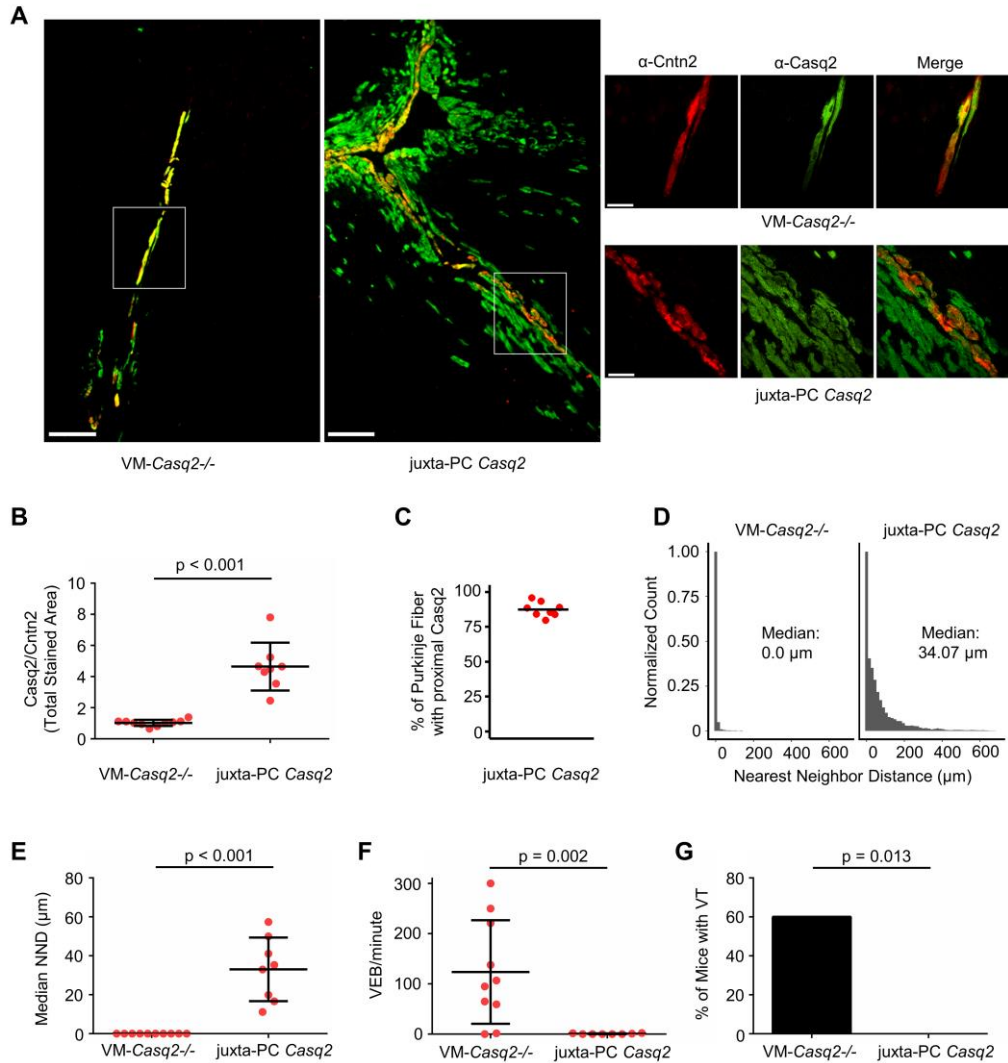


Figure 24. Calsequestrin-2 (Casq2) expression in subendocardial ventricular myocytes juxtaposed to Purkinje cells reduces premature ventricular contraction (PVC) burden and prevents arrhythmia. **A**) Immunostaining for contactin-2 (Cntn2; a Purkinje cell marker) and Casq2 in selected hearts from ventricular myocardium *Casq2*^{-/-} mice (VM-*Casq2*^{-/-}). A subset of mice expressed Casq2, in addition to the Purkinje cells, also in ventricular myocytes next to Purkinje cells, denoted as “juxta-PC Casq2” (example shown in “b”). Other mice co-expressed Casq2 only in Cntn2-positive cells (example shown in “a”). Scale bar = 200 μm. Scale bar in “a” and “b” = 50 μm. **B**) Ratio of Casq2:Cntn2 positive immunostaining in hearts categorized as VM-*Casq2*^{-/-} or “juxta-PC Casq2” by a reviewer blinded to the genotype. **C**) Percent of Cntn2-labeled fiber having contiguous Casq2 staining in ventricular myocytes juxtaposed to the fiber. **D**) Nearest neighbor distance (NND) distributions for Casq2-positive immunostaining relative to Cntn2-positive immunostaining. Data are displayed in 15 μm bins (individual distributions are shown in Supplemental Figure 2). **E**) Median NND for each heart. **F**) Ventricular ectopic beats (VEBs) and **G**) VT incidence (>2 consecutive VEB). Sample number n = 10 and 8 hearts per group, respectively. Data in panels B, D, and E shown with mean ± SD and compared using a two-sided Mann-Whitney test. Panel F compared using Fisher’s exact test.

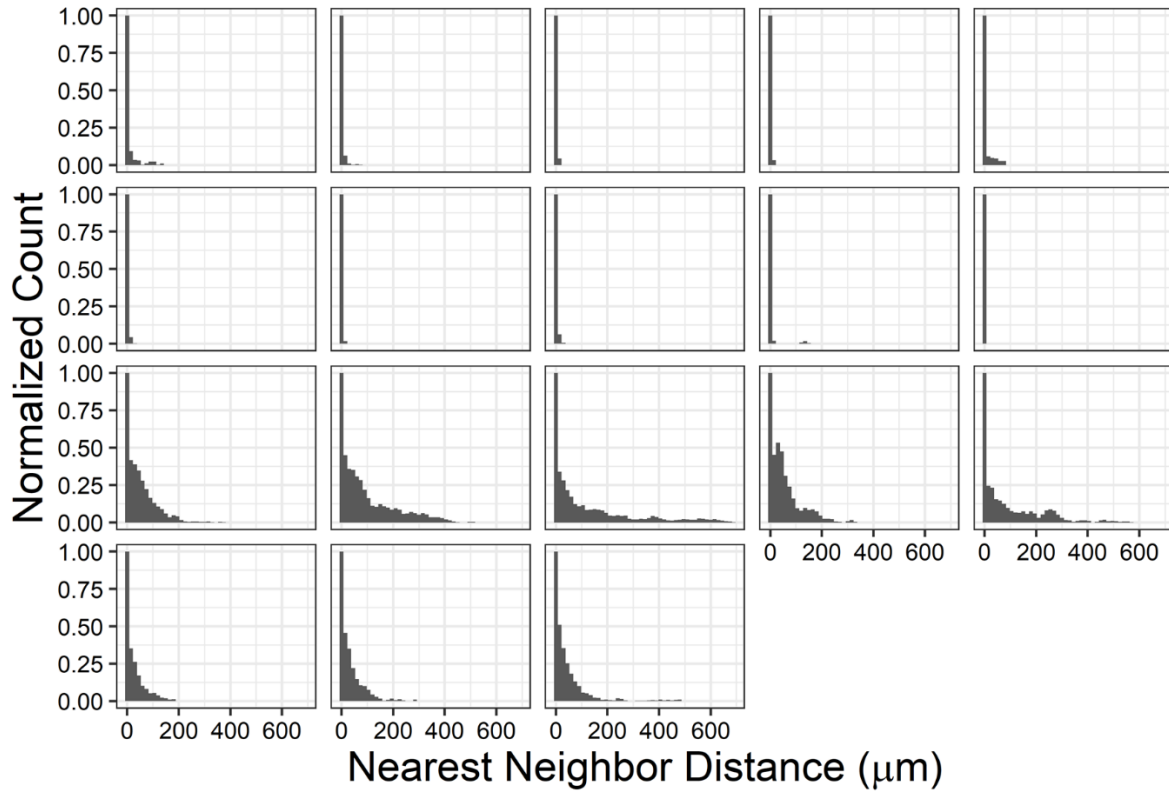


Figure 25. Nearest neighbor distance (NND) distributions calculated on a pixel-by-pixel basis for cardiac calsequestrin (Casq2) staining relative to contactin-2 (Cntn2) staining for each heart shown in Figure 24. Data are displayed in 15 μm bins. Data were analyzed from a single 2-dimensional plane. n = 18 hearts.

Calsequestrin-2 Mouse Model	Casq2 Expression		Phenotype
	VM	Purkinje	CPVT
Wild-Type	100%	100%	No
<i>Casq2</i> ^{-/-}	0%	0%	Yes
PC- <i>Casq2</i> ^{-/-}	100%	0%	No
VM- <i>Casq2</i> ^{-/-}	0%	100%	Yes
juxta-PC <i>Casq2</i>	<1%	100%	No

Table 3. Summary of calsequestrin-2 (Casq2) tissue specific mouse models. Resulting Casq2 protein expression (% of total cells) and whether the catecholaminergic polymorphic ventricular tachycardia (CPVT) phenotype was observed. PC = Purkinje cell; VM = Ventricular myocardium.

Juxta-Purkinje Casq2 positive cardiomyocytes are not transitional cells

We next examined expression of markers associated with transitional cells, a cell population intermediate between Purkinje cells and ventricular cardiomyocytes (Tranum-Jensen *et al.*, 1991), to determine whether juxta-ventricular myocytes represent a unique cellular subtype. A recent study conducted transcriptomic profiling on the cardiac conduction system of developing mouse hearts to identify genes that could characterize the various parts of the conduction system (Goodyer *et al.*, 2019). Transitional cells were identified by a gene expression pattern that included lower levels of Cx40, higher levels of Cx43, and high levels of Cpne5. Other studies though have suggested that Cx40 levels are increased in both Purkinje and transitional cells (Garcia-Bustos *et al.*, 2017). We first examined wild-type hearts to determine whether any differential expression of connexin 40 (Cx40), connexin 43 (Cx43), and copine-5 (Cpne5) could be established in myocardium juxtaposed to the PF. In all examined sections from wild-type hearts, Cx40 was only associated with the PF and Cx40 staining did not extend beyond the boundary defined by Cntn2 staining (Figure 26). Conversely, Cx43 staining was observed in all Cntn2-negative juxta-Purkinje ventricular myocytes. Cpne5 staining mirrored that observed by Cx40. These findings indicate that the ventricular myocardium surrounding the PF is not part of a transitional cell population. To determine whether cells with juxta-Purkinje Casq2 may be part of a unique transitional cell population that erroneously arises during development, we repeated the immunostaining for Cx40 and Cx43 in all four remaining groups (*Casq2*^{-/-}, *PC-Casq2*^{-/-}, *VM-Casq2*^{-/-}, and juxta-Purkinje *Casq2*). There were no differences in Cx40 or Cx43 immunostaining, indicating that the ventricular myocardium expressing Casq2 is not part of the transitional cell population (Figure 27, Table 4). Furthermore, morphometric analysis of juxta-Purkinje myocytes showed that they are distinct from Purkinje-cells, but not significantly different from adjacent ventricular myocytes (Figure 28).

Hence, the juxta-Purkinje myocytes represent the ventricular myocardium at the Purkinje-myocardial junction.

<i>Casq2</i> tissue model	Colocalization (%)		
	Cntn2 > Casq2	Cx40 > Cntn2	Cx43 > Cntn2
<i>Casq2</i> <i>-/-</i>	0	89	0
PC- <i>Casq2</i> <i>-/-</i>	0	91	4
VM- <i>Casq2</i> <i>-/-</i>	88	95	0
juxta-PC <i>Casq2</i>	87	89	1

Table 4. Colocalization data of cardiac-specific proteins. Frozen sections from the hearts of each tissue-specific calsequestrin-2 (*Casq2*) mouse model were stained for *Casq2*, connexin-40 (Cx40), or connexin-43 (Cx43). All sections were co-stained with contactin-2 (Cntn2). Using the Just Another Co-localization Plugin (JACoP) in ImageJ, images were analyzed for the percent colocalization of various protein pairs. Within JACoP, images were assessed using the M1 and M2 coefficients. M1 is defined as the ratio of the "summed intensities of pixels from the image for which the intensity in the green channel is above zero" to the "total intensity in the red channel" and M2 is defined conversely for red. The output from the M1 and M2 coefficients ranges from 0 to 1 and is represented as a percent colocalization for the protein pair being analyzed.

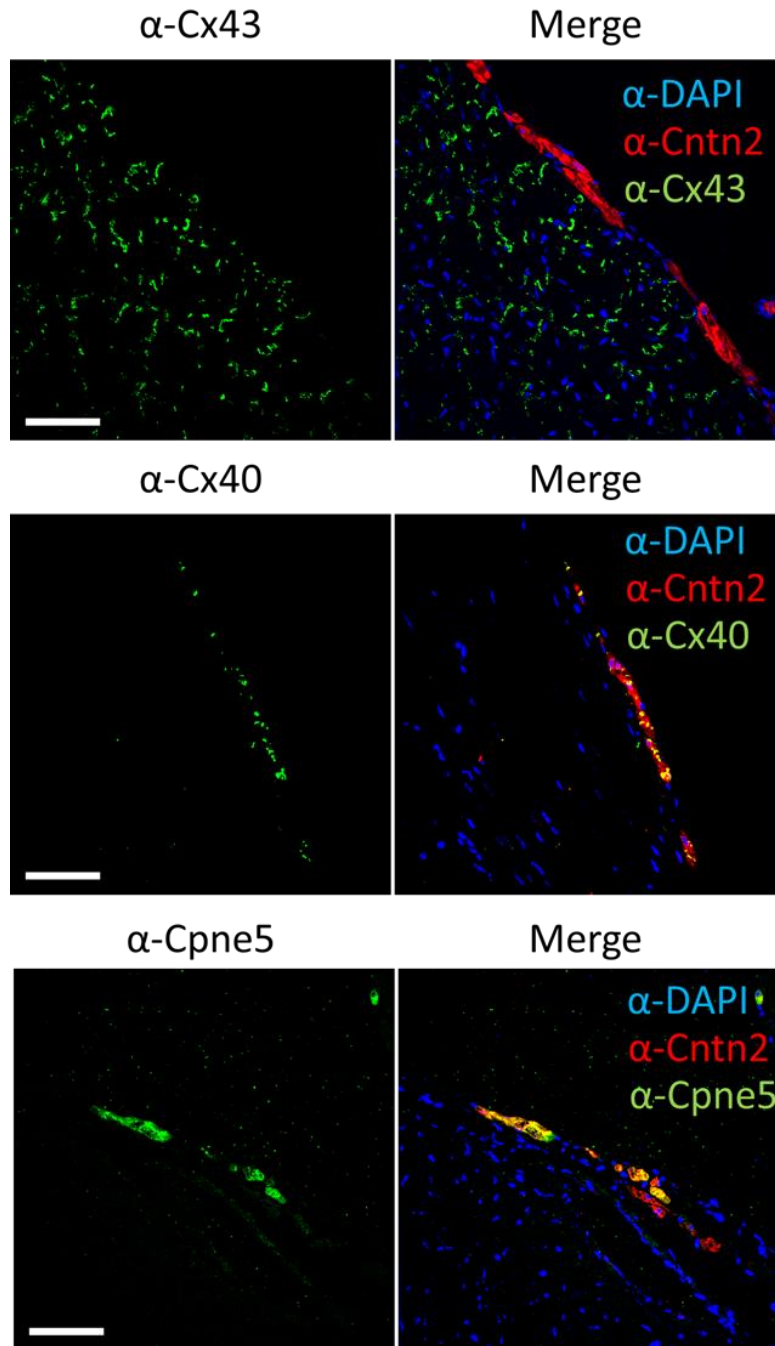


Figure 26. Contactin-2 (Cntn2) positive cells are positive for the ventricular cardiomyocyte marker Connexin-43 (Cx43) and negative for the Purkinje and transitional cell markers Connexin-40 (Cx40) and Copine 5 (Cpne5). Cx43 is a gap junction protein expressed only in the ventricular myocardium but not the atria and conduction system. Cx40 is another gap junction protein that is expressed in atrial myocytes as well as the His-Purkinje system including transitional cells. Cpne5, is a calcium-dependent membrane-binding protein that is expressed in the conduction system including transitional cells. Frozen sections from a C57BL/6 mouse heart tissue were stained. For each antibody, a representative 40x image of the antibody alone is shown (left panel) together with a merged image (right panel) of co-staining with DAPI (blue) and Cntn2 (red). Scale bar = 50 μ m.

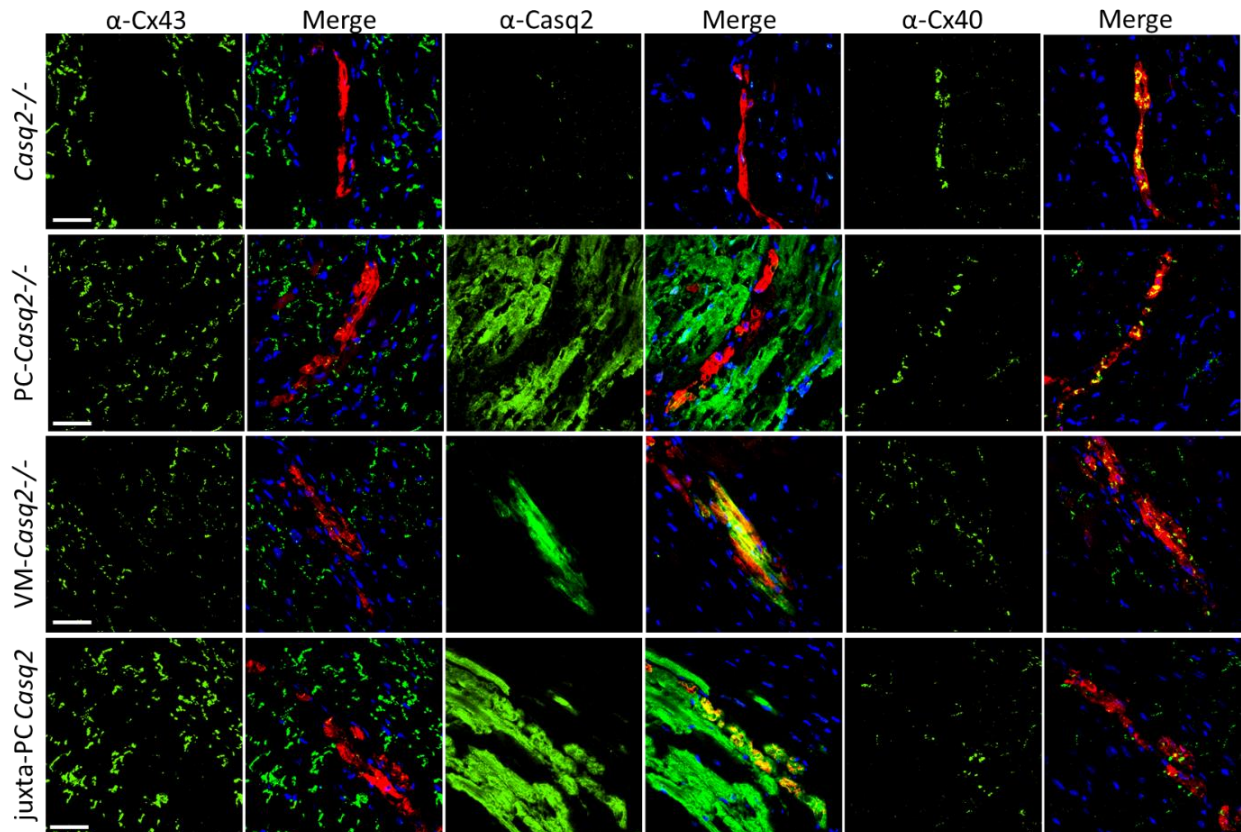


Figure 27. Juxta-Purkinje cells expressing calsequestrin-2 (Casq2) are positive for the ventricular cardiomyocyte marker Connexin-43 (Cx43) and negative for the Purkinje and transitional cell markers Connexin-40 (Cx40) and Contactin-2 (Cntn2). Frozen sections from the hearts of each tissue-specific Casq2 mouse model were stained for the cardiac proteins mentioned above. For each antibody, a representative 40x image of the antibody alone is shown (left panel) together with a merged image (right panel) of co-staining with DAPI (blue) and Cntn2 (red). Scale bar = 50 μ m.

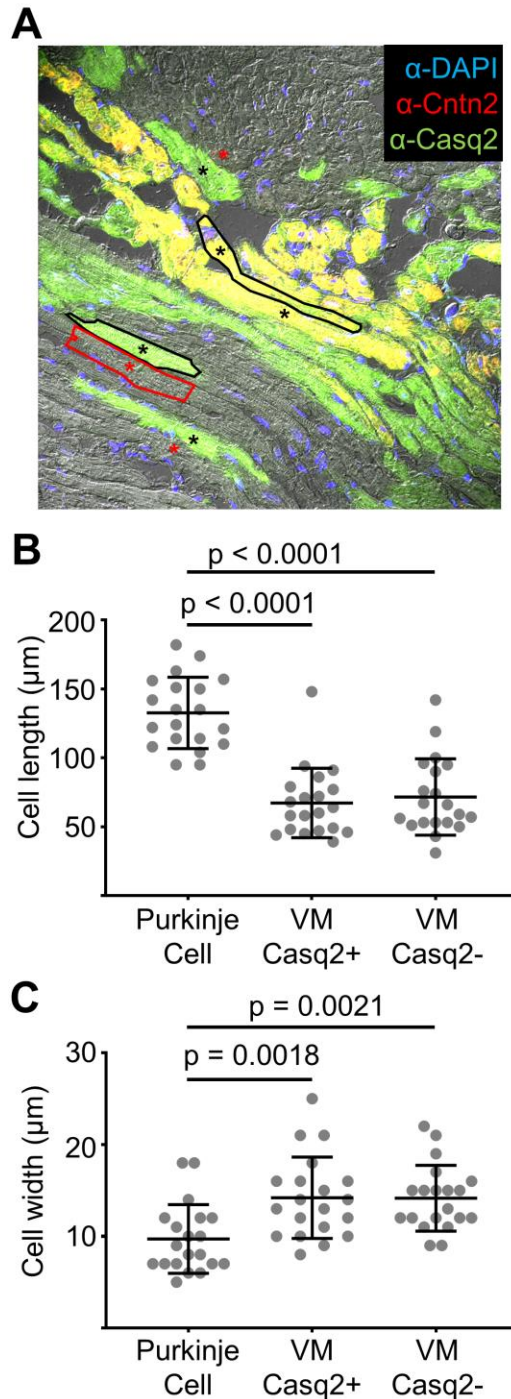


Figure 28. Juxta-Purkinje ventricular myocytes expressing cardiac calsequestrin (Casq2) are morphometrically like ventricular myocytes lacking Casq2. **A)** Representative image showing Purkinje cells stained by contactin-2 (Cntn2; resulting in yellow) alongside ventricular myocytes expressing Casq2 (green) or lacking Casq2 (gray). Cell boundaries are drawn for one cell of each type and selected cells used for analysis are marked (*). Scale bar = 50 μm . **B)** Cell length. **C)** Cell width. Data collected from six fields of view for a total of $n = 20$ cells per group. Data shown with mean \pm SD and compared using one-way ANOVA with Tukey's multiple comparisons test.

In silico modeling of the Purkinje-myocardial junction

Taken together, our experimental data indicate that ectopic beats in the CPVT mouse model are generated near or at the Purkinje-myocardial junction. Given the unique geometric properties of the Purkinje-myocardial junction, which facilitates retrograde conduction (Wiedmann *et al.*, 1996; Huelsing *et al.*, 1998), we hypothesized that ectopic beats are triggered by subthreshold membrane depolarizations (i.e., DADs) in the juxta-Purkinje ventricular myocytes. DADs are a well-established cellular consequence of spontaneous calcium release due to activation of the electrogenic Na-calcium exchanger (Priori & Corr, 1990). To test this hypothesis, we used a computational model to examine the effect of the unique tissue geometry at the Purkinje-myocardial junction. Simulations were set to conditions reflecting the selective expression of Casq2 in either the Purkinje cells or ventricular myocardium alone – that is, DAD-like activity in only one of the tissue subtypes. In the first model, we chose initial conditions in which the entire block of ventricular tissue was prone to DAD-like activity, but the coupled PF structure was not. From this starting point, we allowed electrophysiological activity in the model to evolve by itself and monitored for the incidence of retrograde excitation. Retrograde excitation occurred as subthreshold DADs in the ventricular myocardium triggered action potentials in the PF (Figure 30A). When electrophysiological properties of the two regions were reversed (i.e., the conditions for DAD-like activity were in the PF instead of the surrounding myocardium), antegrade excitation did not occur (Figure 30B). Thus, in this model, the asymmetric propensity for DAD-induced ectopic beats initiated by retrograde versus antegrade conduction is a consequence of Purkinje-myocardial junction geometry. These findings establish a mechanism for triggered activity and explain how selective knockout of Casq2 only in the myocardium still leaves the PF vulnerable to triggered activity by the DAD-prone ventricular myocyte.

To test our hypothesis that the presence of non-DAD-prone juxta-Purkinje ventricular cells could inhibit retrograde excitation, we simulated a hemispherical region around the Purkinje-ventricular junction (with radius r_{Juxta} ranging from 0 to 300 μm in steps of 75 μm ; Figure 30C left inset) of ventricular cells that did not undergo DADs. When most of the ventricular tissue ($r_{Juxta} = 0$ or 75 μm) underwent a DAD-like excitation, retrograde excitation of the PF was observed, even as the local bulk of the ventricular tissue remained sub-threshold. For larger values of r_{Juxta} , the PF was buffered from DAD-like activity and retrograde excitation did not occur (Figure 30C). These observations demonstrate how expression of Casq2 within close proximity of the PF is sufficient to prevent any DAD-like activity in the mid- or epi-myocardium from retrograde excitation and illustrate that only DADs from subendocardial myocytes at the Purkinje-myocardial junction trigger action potentials.

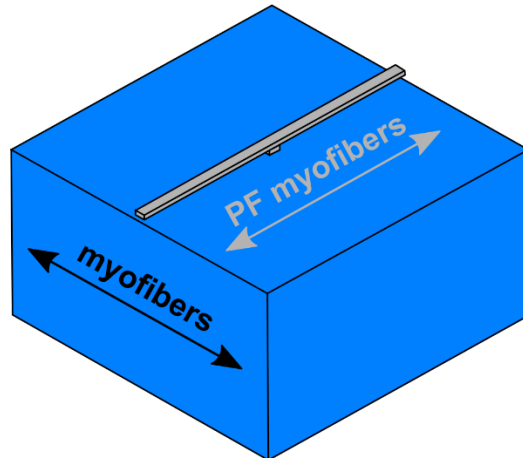


Figure 29. Schematic representation of the computational model, with Purkinje fiber (PF) primed for delayed afterdepolarization (DAD)-like behavior and ventricular tissue ready to be excited (i.e., cell-scale ionic model conditions).

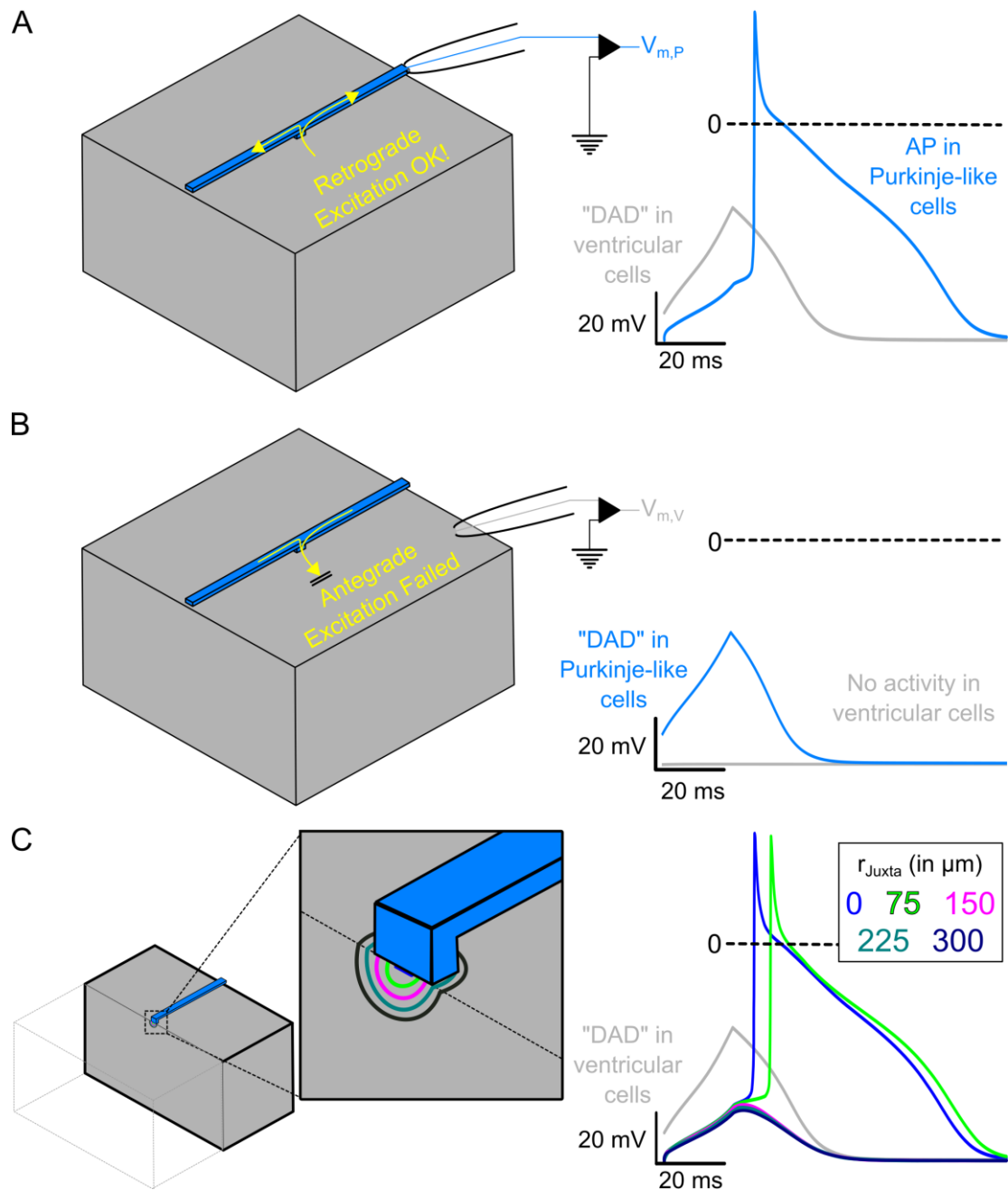


Figure 30. Subthreshold delayed afterdepolarization (DAD)-like activity in ventricular cells of the Purkinje-myocardial junction cause retrograde excitation of Purkinje fibers. **A)** Representation of the tissue block (left) used in the computational model. Recording electrode is illustrated for the ventricular (gray) and Purkinje (blue) tissue subtypes. The membrane voltage recording (at right) shows a ventricular DAD (gray) triggering an action potential in the Purkinje fiber (blue). **B)** Reciprocal experiment demonstrating that Purkinje DADs fail to generate ventricular action potentials. **C)** Schematic representation of the computational model. Clipping plain and zoomed-in inset are used to show the boundaries of the hemispherical Juxta cell region with characteristic r_{Juxta} . Membrane voltage traces (right), showing DAD-like activity in ventricular tissue (gray; identical regardless of r_{Juxta} value) and the response in a coupled Purkinje fiber for various r_{Juxta} values.

Conclusion

Our experimental work supports three important conclusions regarding the cellular and anatomical origin of polymorphic ventricular tachycardia in this model of CPVT: 1) The cell type responsible for triggering arrhythmogenesis in CPVT is the ventricular cardiomyocyte. We found that VM-*Casq2*^{-/-} mice have equivalent arrhythmia burden to global *Casq2*^{-/-} mice (Figure 19 and 20), whereas expression of *Casq2* only in the Purkinje cells did not protect against catecholamine-induced VT. In silico modeling suggests that, at the Purkinje-myocardial junction, subthreshold ventricular DADs cause full Purkinje action potentials capable of propagation. In contrast, antegrade excitation from DADs in the PF does not take place. 2) Subendocardial cardiomyocytes juxtaposed to Purkinje cells are the cellular source for arrhythmogenesis. Histological analysis allowed us to relate the type of cells expressing *Casq2* with arrhythmia susceptibility to catecholamine challenge or exercise. Subendocardial expression of *Casq2* near Purkinje cells was sufficient to prevent CPVT, further supporting the modeling data that subthreshold DADs rather than action potentials in the ventricular myocardium are the underlying mechanism. Moreover, ablation of the endocardial surface confirmed previous reports that the endocardial wall and not the epicardium is the arrhythmogenic focus in CPVT. Finally, in silico modeling further supported the experimental findings, showing that only DADs near the Purkinje-myocardial junction trigger action potentials in the PF. 3) CPVT foci predominately arise from the right side of the heart. Voltage mapping showed right-sided epicardial breakthrough in 70% of all arrhythmogenic ventricular ectopy, analogous to observations in humans with CPVT.

Evidence on the pathophysiology of CPVT has been used to better understand arrhythmogenesis in several acquired heart conditions characterized by impaired calcium trafficking such as heart failure and hypertrophic cardiomyopathy. For this reason, the cellular

origin of focal arrhythmias in CPVT has been a matter of interest and debate for years. Experimental evidence has led some investigators to conclude that Purkinje cells are the cellular foci in CPVT based on the morphology of its trademark arrhythmia: bidirectional ventricular tachycardia. The 180° QRS axis shift that characterizes the bidirectional pattern on the ECG suggested that the ectopic activity originated alternatively from right and left bundle branches (Cerrone *et al.*, 2007). Indeed, voltage activation maps in *Casq2*^{-/-} isolated hearts often show alternating right and left ventricular activation during ventricular tachycardia. *In vitro* studies, highlighting the higher rates of spontaneous calcium releases in isolated Purkinje cells compared to VM, seemed to support this hypothesis (Kang *et al.*, 2010).

However, several reports challenge this model: observations from human patients frequently show anatomical foci outside of PFs (Kaneshiro *et al.*, 2012) that could be successfully silenced via ablation (Kaneshiro *et al.*, 2017). Interestingly, one study found an inverse correlation between sudden death and arrhythmogenic focal distance from the conduction system, although both the sudden death cohort and surviving cohort had foci near the conduction system (Sumitomo *et al.*, 2003). Additional support comes from cellular studies: Purkinje cells have a prolonged refractory period which would make them less likely to generate triggered ectopic activity *in vivo* during normal sinus rhythm. Our genetic approach reported here points towards the incidence of DADs in a specific subset of the working myocardium – ventricular myocytes juxtaposed to Purkinje cells – as the critical prerequisite for arrhythmia initiation. Our results from activation map experiments with ablation of the endocardial layer (Figures 22 and 23) corroborate that conclusion.

Why are subendocardial ventricular cardiomyocytes juxtaposed to Purkinje cells capable of triggering ventricular ectopy *in vivo*, but Purkinje cells are not? Both cell types are capable of

triggering DADs and spontaneous beats in single cell experiments after enzymatic isolation (Liu *et al.*, 2006; Cerrone *et al.*, 2007). Previous reports highlighted the susceptibility of Purkinje cells to calcium overload and indicated their high rate of DADs as evidence that these cells are the cellular trigger. However, as shown in our modeling experiments (Figure 30), DAD-like activity in PF cannot excite the myocardium, whereas sub-threshold excitation of the ventricular bulk myocardium can initiate retrograde excitation of the PF due to the favorable source-sink relationship at the Purkinje-myocardial junction. Observations in superfused preparations suggest source-sink mismatch and the presence of a resistive barrier at Purkinje-myocardial junctions leads to longer delay times for antegrade compared to retrograde conduction (Wiedmann *et al.*, 1996; Huelsing *et al.*, 1998). Many factors at the junction influence the “safety factor” for conduction (Boyle & Vigmond, 2010; Boyle *et al.*, 2019) from PF to ventricles and vice-versa. Propagation from high- to low-conductivity tissue (i.e., PF to VM) enjoys a high safety margin, which confers a slight advantage for antegrade transmission. But this slight increase in safety margin is more than offset by the reduction of the safety factor when the electrical impulse propagates across thin-to-thick tissue expansions (i.e., at the Purkinje-myocardial junction). Thus, retrograde transmission is favored overall. The present findings suggest that these suppositions hold true in the context of subthreshold excitations (as might be caused by a DAD) able to retrogradely excite the PF with a comfortable margin of safety, even while transmission in the opposite (antegrade) direction fails.

Although our simulation studies favor retrograde excitation by subthreshold membrane depolarizations in the ventricular myocardium, we cannot exclude that ectopic foci could also be caused by full ventricular action potential. Any action potentials arising from the mid-myocardium or epicardium must compete with a large sink, whereas juxta-Purkinje ventricular myocytes can more easily conduct into the nearby Purkinje cells. Regardless of whether ventricular DADs or

ventricular action potentials are the cellular trigger, ventricular cells at the Purkinje-myocardial junction still produce an apparent activation and QRS morphology consistent with Purkinje cell origin, as previously described in activation maps. Our data showed that restoration of Casq2 at a median (non-zero) distance of 53.8 μm from the nearest Cntn2-positive (Purkinje) cells was sufficient to prevent arrhythmias, indicating that distal (epicardial) cardiomyocytes – despite lacking Casq2 – are not the cellular trigger for CPVT. The observation that cardiomyocytes distal from the Purkinje-myocardial junction do not trigger ventricular ectopy (Figures 23 and 24) further support the hypothesis that subthreshold myocardial DADs rather than full myocardial action potentials are the cellular mechanisms responsible for focal ectopic activity in CPVT.

Recent work by Flores *et al.* suggested that concurrent loss of Casq2 in both the myocardium and Purkinje system was required to generate a CPVT phenotype (Flores *et al.*, 2018). In that study, conditional deletion or rescue of Casq2 was achieved in adult mice using a tamoxifen-induced *cre* expression system under the control of a *Hcn4* promoter to target the cardiac conduction system (Flores *et al.*, 2018). Analogous to our results, Casq2 deletion only in the cardiac conduction system was not sufficient to generate a CPVT phenotype. In contrast to the data presented here, turning on *Casq2* gene expression with *Hcn4-cre* in adult mice prevented catecholamine-induced VT (Flores *et al.*, 2018). One explanation for this discrepancy could be that *Casq2* expression was also activated in the ventricular myocardium outside the conduction system by the *Hcn4-cre*. This is a distinct possibility, because although *HCN4* gene expression is much higher in the conduction system, the *HCN4* gene is expressed in the ventricular myocardium, especially in failing hearts (Borlak & Thum, 2003). As shown here (Figure 24), even a small number of myocytes expressing Casq2 in the subendocardial myocardium is sufficient to prevent CPVT. Furthermore, Flores *et al.* reported that Casq2 rescue in the sinoatrial node caused a sinus

tachycardia. The association of slow sinus heart rate with CPVT susceptibility has been previously shown by our group and others (Leenhardt *et al.*, 1995; Priori *et al.*, 2002; Knollmann *et al.*, 2006; Sumitomo *et al.*, 2007; Wang *et al.*, 2017); a fast sinus rhythm is protective against catecholamine or exercise induced ventricular arrhythmia (Faggioni *et al.*, 2013; Kannankeril *et al.*, 2020). The low rate of ventricular arrhythmias observed by Flores *et al.* after Casq2 rescue in the sinoatrial node could be attributed to the sinus tachycardia in this model.

The identification of subendocardial cardiomyocytes juxtaposed to PFs as the cellular driver and the Purkinje-myocardial junction as the anatomical origin of focal ventricular ectopy has important mechanistic and therapeutic implications beyond CPVT. DADs caused by spontaneous calcium release are considered the underlying cellular mechanism for ventricular arrhythmias following myocardial infarction or in the failing heart, based on studies of ventricular myocytes isolated from failing human hearts (Luo & Anderson, 2013; Dries *et al.*, 2018) and animal models of heart failure (Hoeker *et al.*, 2009). Our data suggest that, as in CPVT, the ectopic beats in heart failure may also be generated at the Purkinje-myocardial junction via a heretofore unrecognized *tissue mechanism*, whereby subthreshold membrane depolarizations caused by spontaneous RyR2 calcium release in the ventricular myocardium generate full action potentials in the adjacent PF. Hence, intervention with pharmacological agents that target RyR2 can prevent arrhythmias not only in CPVT but also in heart failure models (Kubalova *et al.*, 2005).

CHAPTER III

Generation and characterization of the CASQ2 knockout human induced pluripotent stem cell-derived cardiomyocytes

Introduction

Cardiac calsequestrin (Casq2, encoded by *CASQ2*) is a low-affinity high-capacity calcium binding protein located in the sarcoplasmic reticulum (SR) of cardiomyocytes (Knollmann *et al.*, 2006; Chopra *et al.*, 2007). In the heart the SR functions as a regulator of calcium storage and release. Calcium within the SR is stored by binding largely to Casq2. Casq2 binds calcium through the 60-70 negatively charged amino acids within the protein (Yano & Zarain-Herzberg, 1994). Casq2 monomers increase their ability to bind calcium by forming polymers (Park *et al.*, 2003). The polymerization process is calcium dependent with Casq2 being polymerized at rest and depolymerized as calcium is depleted in the SR (Manno *et al.*, 2017). Within the SR, Casq2 interacts with other calcium handling proteins such as the ryanodine receptor 2 (RyR2), triadin, and junctin (Györke *et al.*, 2004). The interactions of Casq2 with the RyR2-triadin-junctin complex form the SR calcium release unit and are important for regulating calcium release during the excitation-contraction (EC) coupling cycle in the heart, where electrical activation is coupled to mechanical force via calcium (Bers, 2002).

The EC coupling cycle begins when the membrane depolarizes during the cardiac action potential opening L-type calcium channels and bringing in calcium. The calcium will then bind to cardiac ryanodine receptors (RyR2) and open them, a process called calcium-induced calcium-release (CICR) (Fabiato, 1985). The rise in cytosolic calcium initiates myofilament contraction which is terminated by the removal of calcium through either the sodium-calcium exchanger located on the cell membrane or the sarco/endoplasmic reticulum calcium-ATPase on the SR.

Perturbations in proteins that handle calcium within the SR of the heart have been found to cause a lethal, stress-induced cardiac channelopathy, catecholaminergic polymorphic ventricular tachycardia (CPVT) (Leenhardt *et al.*, 1995). Mutations in the *CASQ2* gene are the second most common cause of CPVT (Lahat *et al.*, 2001a; Lahat *et al.*, 2001b). The first variants associated with CPVT occurred when missense mutations were discovered in *CASQ2* in a family with CPVT in 2001 and nonsense mutations in another family in 2002 (Postma *et al.*, 2002). Studies published on *CASQ2* mutations have found that *CASQ2*-linked CPVT is a result of a decrease in Casq2 protein levels, impairing the ability of Casq2 to buffer calcium in the SR. The result is a faster rise of the intra-SR free calcium concentration close to RyR2 release channels. The increased free calcium leads to hyperactive RyR2 channels, impaired calcium-release termination, shortened calcium release refractory period, and enhanced spontaneous release of calcium (Knollmann *et al.*, 2006; Chopra *et al.*, 2007; Kryshnal *et al.*, 2015).

While a majority of *CASQ2*-linked CPVT research has been conducted in mouse models, hiPSC-CMs research has increased over the last decade. Recently, hiPSC-CMs have been utilized due to the ability to generate patient-specific models. Multiple hiPSC lines have been created from patients with mutations in *CASQ2* (Novak *et al.*, 2012; Novak *et al.*, 2015; Sasaki *et al.*, 2016; Maizels *et al.*, 2017). After iPSC generation, the lines are differentiated and have been shown to recapitulate a CPVT phenotype. The advantages of hiPSC-CMs are their cost compared to transgenic mouse models, their genetic background, and the ability to perform drug screens to identify potential therapeutic compounds that could be used in patient care. While these studies have been crucial to show that hiPSC-CMs are useful for studying CPVT, all CPVT hiPSC lines are from families with a specific *CASQ2* mutation (Itzhaki *et al.*, 2012). The generation of a *CASQ2*^{-/-} mouse model showed that the absence of Casq2 could cause CPVT in mice and provided

a mechanism of action for *CASQ2*-linked CPVT (Knollmann *et al.*, 2006). A *CASQ2*^{-/-} hiPSC line would provide a human model that would continue advancing our understanding of CPVT and could be used to screen for novel compounds to treat diseases where calcium handling is dysregulated.

In this study, we used CRISPR/Cas9 to generate *CASQ2* homozygous (*CASQ2*^{-/-}) and heterozygous (*CASQ2*^{+/-}) knockout hiPSC lines. We show that *CASQ2*^{-/-} and *CASQ2*^{+/-} hiPSC-CMs have the reduced expression or complete deletion of Casq2 but no significant changes in other calcium handling proteins. Despite absent Casq2, hiPSC-CMs maintain relatively normal calcium release and contractile function, which we attribute to unprecedented increases in SR volume, and increased gain of calcium-induced SR calcium release. We conclude that even a modest reduction in Casq2 protein levels can increase arrhythmia susceptibility in hiPSC-CMs. Similar to *CASQ2*^{-/-} mice, the underlying mechanism seems to be a direct modulation of the RyR2 SR calcium release complex caused by the absence of Casq2.

Methods

Human-induced pluripotent stem cell (hiPSC) lines were approved by Vanderbilt University Medical Center Institutional Review Board. Data were averaged from three independent cardiac differentiation events.

sgRNAs design and cloning

pSpCas9(BB)-2A-Puro (PX459) V2.0 was a gift from Feng Zhang (Addgene plasmid # 62988) (Ran *et al.*, 2013). According to human *CASQ2* gene sequence (NG_008802.1 RefSeqGene, NCBI), two pairs of single-guide RNAs (sgRNAs) were designed using CRISPOR online program (<http://crispor.tefor.net>) for high on-target efficiency and low off-targeting score

(Concordet & Haeussler, 2018): (1) sgRNA 1 was to target the proximal promoter of *CASQ2*; (2) sgRNA 2 was to target *CASQ2* exon 1 near the 5' end. The sequences of sgRNAs are: (1) sgRNA 1, forward CACCGTTAGATACGACACTGAGA and reverse AAACCTCTACAGTGTTCGTA TCTAAC; (2) sgRNA2, forward CACCGTGCTTGAGGTAAGTAACCAA and reverse AAACCT TGGTTACTTACCTCAAGCAC. SgRNAs were inserted into the pSpCas9 vector and the insertion of sgRNAs was confirmed by sequence analysis (Wang *et al.*, 2018).

Generation of the CASQ2- allele

Generation and characterization of control hiPSCs is described previously in (Wang *et al.*, 2018). Control hiPSCs were grown in feeder-free homemade E8 medium (BurrIDGE *et al.*, 2014). For gene editing, 1×10^6 control hiPSCs were electroporated with 10 μ g of pSpCas9-sgRNA1 and 10 μ g of pSpCas9-sgRNA2 using Neon transfection system (ThermoFisher Scientific). 36 hours after electroporation, 0.5 μ g/ml puromycin was added to the culture medium. After two days of puromycin selection, hiPSCs were fed with the regular E8 medium until distinct colonies were established. Then, single colonies were manually picked and plated individually in wells of 24-well plates. Colonies were grown over 12 days, at which point they were dissociated using 0.5 mmol/L EDTA. A small portion of cells was harvested for the validation of genome editing. *CASQ2*- allele was screened by PCR with a pair of primers flanking the deletion. The sequences of primers are: Forward: 5'- TGAGGGGACAGGCTGAGTTACCACCCTGGGGTGATTTAAC-3'; Reverse: 5'- CCCCAGTGCCAGGTTACAAACAGGCAGGCCATGTAATGCG-3'. We screened 57 hiPSC clones and 5 clones exhibited mutations in the *CASQ2* allele: 3 clones were confirmed with double *CASQ2*⁻ alleles (*CASQ2*^{-/-}) and 2 clones with one *CASQ2*⁻ allele (*CASQ2*^{+/-}).

). All *CASQ2*^{-/-} and *CASQ2*^{+/-} hiPSC lines were screened for chromosomal abnormalities by karyotype analysis (Genetics Associates, Nashville, TN).

hiPSC maintenance and cardiac differentiation

All hiPSC lines were maintained in the home-made E8 medium (Wang *et al.*, 2021). Cardiac differentiation was induced from hiPSC monolayers using small molecules CHIR99021 (Selleck Chemicals) and IWR-1 (Sigma) (Wang *et al.*, 2021). On day 15, hiPSC-CMs were dissociated and replated on 1:200 Matrigel-coated plates. From day 16 to day 30, hiPSC-CMs were treated with 100 nmol/L triiodothyronine (Sigma) and 1 μmol/L Dexamethasone (Cayman) (Wang *et al.*, 2021).

RNA sequencing

Total RNA was extracted from day 30th hiPSC-CMs with RNeasy Mini Kit (QIAGEN) followed by DNase treatment. Each demultiplexed sample was analyzed using FASTqc for overall quality, followed by trimming low quality or biased reads using seqtk (<https://github.com/lh3/seqtk>). Transcript abundances were calculated using Salmon 0.8.2, the recently developed pseudomapping algorithm for rapid RNAseq analyses (Patro *et al.*, 2017). Reads were mapped to the GRCh38.p12 build of the human genome using the parameters -k 31, -seqBias, -gcBias, -posBias. Differential expression was determined using the DESEQ2 R package using default parameters (Love *et al.*, 2014). Gene Enrichment Analyses were performed using the GeneAnalytics Suite, which used the binomial distribution-based enrichment analysis and reported Benjamini-Hochberg-adjusted p values (Ben-Ari Fuchs *et al.*, 2016).

Impedance-based contractility measurement

Day 30 hiPSC-CMs were seeded on 0.6mm CardioExcyte 96 sensor (Nanon Technologies) coated with 1:200 Matrigel at 40,000 cells per well (Wang *et al.*, 2018). 2 days after plating, hiPSC-CMs were transduced with the adeno-associated virus (AAV)1 expression of channelrhodopsin-2 (ChR2) with H134R mutation fused to mCherry at a multiplicity of infection (MOI) of 1.2×10^4 viral genome/cell (Addgene viral prep #100054-AAV1) (Chavali *et al.*, 2019). 10 days after plating, impedance (IMP) was recorded in a 30-s sweep at a 10 kHz sampling rate at 37 °C and 5% CO₂ in RPMI 1640 medium (Gibco, Thermo Fisher Scientific) with B-27 supplement (Gibco, Thermo Fisher Scientific). The spontaneous beating rate was determined by the beating frequency of the sweep. To evaluate cellular triggered activity, 5 µmol/L tetrodotoxin and 50 µmol/L lidocaine was used to block voltage-gated sodium channels and prevent the spontaneous beating of hiPSC-CMs. The 470-nm blue light pulse was applied to activate ChR2 and initiate the contraction of hiPSC-CMs at the pacing rate of 3 Hz. To investigate the effects of Casq2 on the contractile function, hiPSC-CMs were paced at 3 Hz for 5 s in the presence of 1 µmol/L isoproterenol, followed by a 25-s pause. Pause-dependent triggered beats were determined by the occurrence of spontaneous beating activity in the 25-s pause.

Intracellular calcium transient measurement

Day 30 hiPSC-CMs were dissociated and plated on Matrigel Mattress for an additional 3 to 5 days before experiments (Feaster *et al.*, 2015). HiPSC-CMs were loaded with Fura-2 AM (ThermoFisher Scientific) as described previously in (Parikh *et al.*, 2017). Briefly, hiPSC-CMs were incubated with 2 µmol/L Fura-2 AM for 8 min and then washed twice for 10 min with Tyrode's solution containing 1.2 mmol/L calcium and 250 µmol/L probenecid. Calcium transient

measurements were performed with a 40x objective using a Nikon Eclipse T5100 fitted with an IonOptix video microscopy system (Ionoptix). Calcium transients were recorded in Tyrode's solution with 2 mmol/L calcium for 20 s during 1 Hz electrical field stimulation. Stimulation was then stopped, and the external solution was quickly switched to 0 mmol/L Na and 0 mmol/L calcium (0Na0Ca) solution for 30 s to quantify spontaneous SR calcium release. RyR2 channels were inhibited by 1 mmol/L tetracaine in 0Na0Ca solution for 10s and SR calcium content was assessed by the application of 10 mmol/L caffeine for 5 s. All solutions contained 1 μ mol/L isoproterenol, and experiments were conducted at room temperature. Calcium transients were analyzed using commercially available analysis software (IonWizard, IonOptix, Milton, MA). For each hiPSC-CM, the following parameters were determined: (1) baseline and peak amplitude of calcium transient, (2) time to peak and baseline, and tau of A) field stimulated calcium transients, B) caffeine transients, and C) zero Na zero calcium caffeine transients. Analyses of calcium transients and calculation of calcium flux balance was completed as described previously. Time zero for time to peak measurements were defined as the time of electrical stimulation. The tetracaine-induced drop in fluorescence ratio was defined as SR calcium leak, which is the change of minimum ratio before and after tetracaine application.

Tyrode's solution was composed of (mmol/L): (134) NaCl, (5.4) KCl, (1) MgCl₂, (10) Glucose, and (10) HEPES, pH adjusted to 7.4 with NaOH. A zero Na zero Ca solution contained the following (mmol/L): (134) LiCl, (5.4) KCl, (1) MgCl₂, (1) EGTA, (10) glucose, and (10) HEPES, pH 7.4 with LiOH. Caffeine (10 mmol/L), isoproterenol (1 μ mol/L), and tetracaine (1 mmol/L) solutions were prepared in Tyrode solution with 2 mmol/L calcium. All stock solutions were freshly diluted in recording solutions before use.

Calcium spark measurement

Calcium spark measurement was performed as described previously in (Parikh *et al.*, 2017). Briefly, hiPSC-CMs on Matrigel Matress were washed for 30 seconds in a relaxation solution, permeabilized with 20 µg/mL saponin for 35 seconds, and then bathed in a freshly made internal solution for 60 seconds. Confocal imaging was performed on a Zeiss LSM 510 inverted laser scanning confocal microscope equipped with a 40X / 1.30 NA planar oil immersion objective. Fluo-4 was excited by an argon laser line at 488 nm, and the fluorescence emission was passed through a 505 nm long-pass filter to PMT detectors. Cell sparks were imaged in the line-scan mode in isolated cells with no contact with other cells. Lines were positioned longitudinally near the center of the cell, avoiding nuclei. Image analysis was performed in ImageJ with the SparkMaster plugin using a background setting of 5 and criteria of 3.8. Spark mass was calculated from the equation: spark mass = 1.206 * Amplitude * FWHM³. FWHM = full width at half-maximum.

Relaxing solution was composed of (mmol/L): (10) HEPES, (150) L-aspartic acid potassium salt, (0.1) EGTA, (0.25) MgCl₂, and (5) Na₂ATP, pH adjusted to 7.2 with KOH. Internal solution contained the following (mmol/L): (120) K-aspartate, (15) KCl, (5) K₂HPO₄, (5.6) MgCl₂, (10) HEPES, (5) MgATP, (10) Phosphocreatine-Na₂, (10) reduced L-glutathione, (0.3) EGTA, (0.12) CaCl₂, (0.03) Fluo-4, 4% dextran (w/v), and 10 U/mL creatine phosphokinase, pH adjusted to 7.2 with KOH.

Western blotting

Day 30 hiPSC-CMs were lysed with homogenization buffer (50 mmol/L TRIS, 320 mmol/L sucrose, 1 mmol/L DTT, 0.1% IGEPAL CA-630, pH = 7.0) supplemented with 1% protease inhibitor cocktail (Sigma P8340) and 1% phosphatase inhibitor (Sigma P0044). All

lysates were centrifuged at 13000 rpm for 20 min at 4°C. Protein concentrations were quantified using the Bradford protein assay (Bio-Rad). 20 µg of protein lysates were resolved on a 4-20% polyacrylamide gel (Bio-Rad Mini-PROTEAN) and transferred onto nitrocellulose membranes for immunoblotting. Membranes were blocked in TBST (Tris-buffered saline, 0.1% Tween 20) with 5% milk for 1 hour at room temperature. Membranes were incubated with primary antibody overnight at 4°C, and then in secondary antibody for 1 hour. The information of primary and secondary antibodies is listed in Table 5. Membranes were incubated with ECL substrate (Thermo) for 5 min and developed on ChemicDoc MP imaging system (Bio-Rad).

Immunostaining

Immunostaining of hiPSC-CMs was carried out as previously described in (Parikh *et al.*, 2017). Briefly, hiPSC-CMs on Matrigel Mattress were fixed in 4% paraformaldehyde for 20 minutes. Fixed cells were permeabilized and blocked in DPBS with 0.2% saponin, 5% goat serum, and 0.5% bovine serum albumin (BSA) for 1 hour at room temperature and then incubated with primary antibodies overnight at 4°C. Casq2 antibody (Proteintech 18422-1-AP) and α -actinin antibody (Sigma-Aldrich A7811) were diluted in DPBS with 0.2% saponin and 0.5% BSA at 1:500. Secondary antibodies were diluted in DPBS with 0.2% saponin and 0.5% BSA at 1:500. Cells were incubated with an Alexa Fluor 488 or 556 secondary antibody for 1 hour at room temperature. Cover slides were mounted using ProLong Gold antifade with DAPI (Invitrogen P36941) and left to dry overnight. Imaging was carried out at 40x magnification on an Olympus confocal microscope (IXplore SpinSR). Excitation was elicited using a LS 100 mw diode laser at either 488 nm or 561 nm (Coherent Obis laser lines). Images were acquired using Olympus cellSens Dimension 2.3 software and were analyzed in ImageJ.

Statistical analysis

Data are presented as mean \pm SD. Statistical comparisons were made using GraphPad Prism 8 (GraphPad Software). Statistical differences were assessed with one-way ANOVA followed by posthoc Tukey's comparisons. $p < 0.05$ was considered as statistical significance.

Antibody target	Manufacturer	Product number	Host species	Primary dilution	Secondary dilution
RyR2	Thermo Fisher	MA3-916	Mouse	1:1,000	1:5000
Casq2	Proteintech	18422-1-AP	Rabbit	1:2,000	1:5000
Triadin	Dr. Isabelle Marty	N/A	Rabbit	1:10,000	1:5,000
Junctin	Dr. Karl Pfiefer	N/A	Rabbit	1:2,000	1:10,000
GAPDH	Invitrogen	AM4300	Mouse	1:20,000	1:20,000

Table 5. Antibody concentrations used during Western blotting of CASQ2 hiPSC lines.

Results

Generation of *CASQ2*^{-/-} and *CASQ2*^{+/-} hiPSC lines

Using the human *CASQ2* gene structure (Reyes-Juárez *et al.*, 2007), we designed two pairs of sgRNAs to flank the promoter and exon 1 of *CASQ2* (Figure 31A): (1) sgRNA1 was designed to cleave 37 bp from the upstream promoter; (2) sgRNA2 was designed to cleave 8 nucleotides from the downstream exon 1. A total of 57 hiPSC colonies were sequenced, 5 were found to have mutations corresponding to the inversion or deletion of the promoter and exon 1.

Polymerase chain reactions (PCR) was done to screen colonies to be sent off for sequencing. In Figure 31B, the band sized 906 bp indicates the deletion of promoter and exon 1, in *CASQ2*^{-/-} hiPSC lines 1 and 3. The band sized 1500 bp indicates the wild type allele is present in the hiPSC lines control, *CASQ2*^{+/-} line 1 and 2, and *CASQ2*^{-/-} line 2. Further sequencing was done and *CASQ2*^{-/-} was found to have an inversion of promoter and exon 1. A second PCR that was specific to the promoter of *CASQ2* was used to confirm that *CASQ2*^{-/-} line 2 was homozygous (Figure 31B). We subsequently examined whether the genetic hiPSC lines had altered chromosomal structure. HiPSCs were found to have normal karyotypes (Figure 31C).

RNA sequencing

To examine whether the deletion in *CASQ2* affects cardiac gene expression, we compared the gene expression profiles among control and two *CASQ2*^{-/-} hiPSC-CMs. In a total of 7826 genes, 674 genes were significantly changed compared to the control. To account for multiple hypothesis testing, adjusted p-values were calculated using the false discovery rate method and were reported as Q-values. When a Q-value of less than 0.05 was used as a cutoff we instead only found 12 genes that were significantly different (Figure 32D). *CASQ2* was found to have the smallest p and q value. RNA sequencing results from each line were analyzed and displayed using volcano plots

(Figure 32A-B). Due to the large variability that can occur between samples in RNA sequencing, the data from both lines were pooled together to find the changes that were significant (Figure 32C).

Expression of proteins associated with Casq2 in hiPSC-CMs

Next, we used western blotting techniques to detect the protein expression of Casq2 in hiPSC-CMs. It is well known that Casq2 interacts with multiple proteins within the SR such as RyR2, triadin, and junctin (Zhang *et al.*, 1997). With a significant decrease in *CASQ2* gene expression detected, we wanted to see if Casq2 and the other intra-SR calcium handling protein levels were affected. Lysates from each hiPSC-CM line was collected and analyzed. The protein levels of RyR2, triadin, and junctin were not altered in any of the mutant lines, but there was a significant decrease in Casq2 protein levels in the *CASQ2*^{-/-} and *CASQ2*^{+/-} lines (Figure 33A-B).

To further verify the levels of Casq2 were decreased, we performed immunostaining on isolated hiPSC-CM. Cells were stained with Casq2 and as a control, alpha-actinin to visualize the cytoskeleton structure within the cardiomyocytes. Casq2 was not visible in the *CASQ2*^{-/-} differentiated cardiomyocytes but was observed in the *CASQ2*^{+/-} myocytes (Figure 33C). Together, the western blot and immunostaining confirms that Casq2 is absent in our *CASQ*^{-/-} lines but is still present in the *CASQ2*^{+/-} lines.

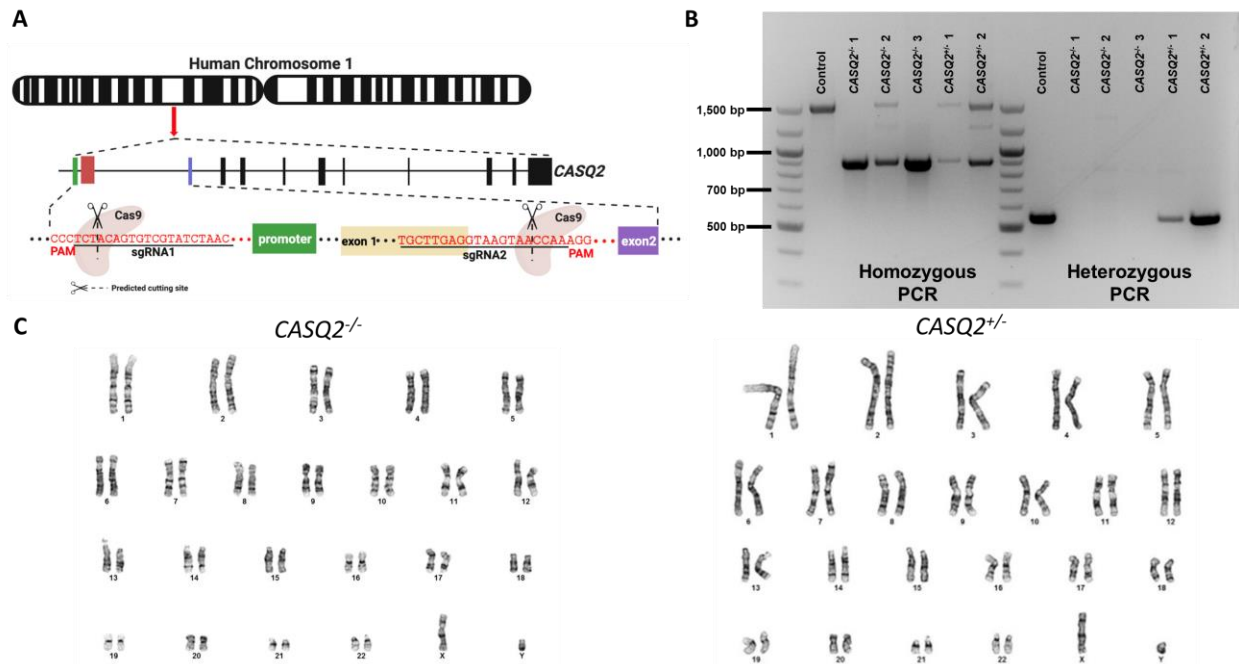


Figure 31. Generation of mutated *CASQ2* hiPSC lines. **A)** Genetic editing strategy using CPRISR/Cas9. Guide RNAs were designed to flank the promoter of exon 1. sgRNA1 was designed to cleave 37 bp from the upstream promoter; sgRNA2 was designed to cleave 8 nucleotides from the downstream exon 1. **B)** Agarose gel showing PCR amplification of exon 1 in the *CASQ2* hiPSC lines (homozygous PCR). Top band represents a wild-type allele and the bottom band represents the *CASQ2* allele without exon 1. Another PCR amplification (heterozygous PCR) for the promoter of *CASQ2* was used to confirm the mutations present in each hiPSC line. **C)** Representative karyotyping from a *CASQ2*^{-/-} line and a *CASQ2*^{+/-} line.

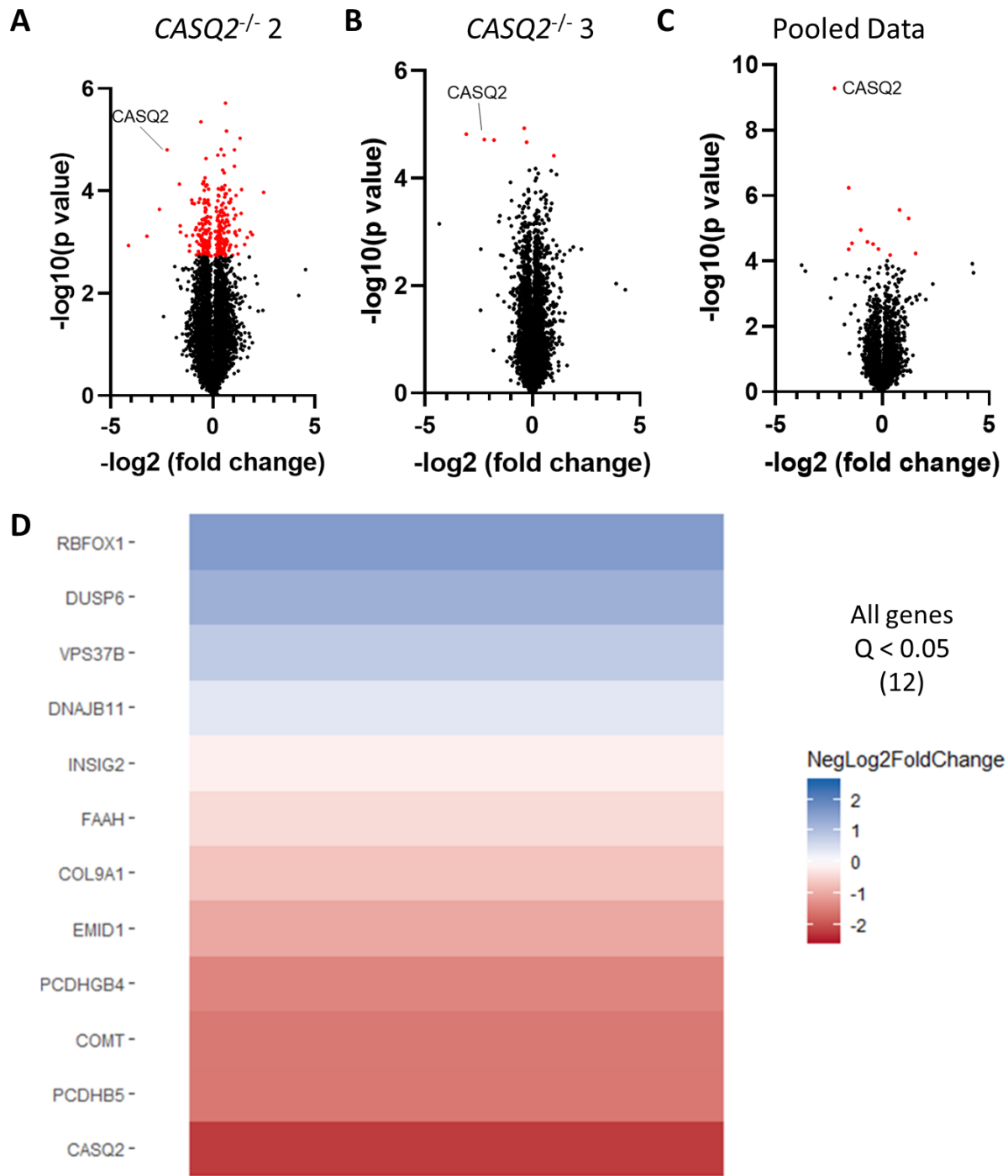


Figure 32. RNA sequencing data of *CASQ2*^{-/-} hiPSC lines. Sequencing runs were performed in triplicate. RNA-seq data analyzed by aligning to reference genome (HiSat), quantifying transcripts (Stringtie) and association tests performed between groups (Ballgown). **(A, B)** Volcano plots of two independent *CASQ2*^{-/-} lines compared to control. **(C)** Data pooled from both independent *CASQ2*^{-/-} lines. **(D)** Data showing absolute fold change of knockout groups compared to control with adjusted p-value (Q). A total of 7826 genes were analyzed.

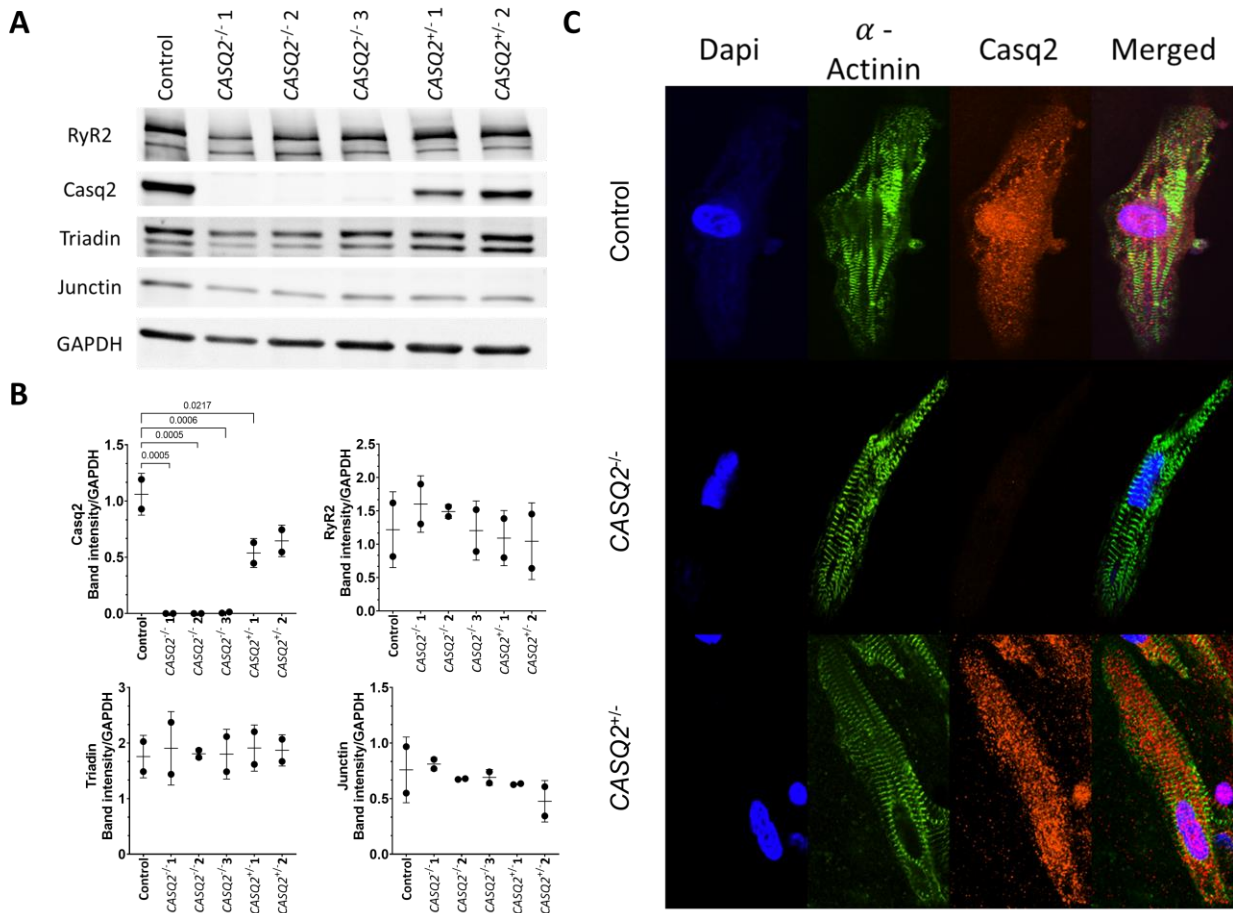


Figure 33. Casq2 protein levels are decreased in *CASQ2*^{-/-} and *CASQ2*^{+/-} hiPSC cardiomyocytes. **A)** Cellular lysate was collected from hiPSC cardiomyocytes and analyzed using western blotting techniques. Representative western blot image is shown. **B)** Quantification of junctional SR protein band density using ImageJ. All values were normalized to GAPDH. n = 2 lysates. Data displayed as mean ± SD. Data were analyzed using one-way ANOVA with Tukey's multiple comparison test. **B)** hiPSC cardiomyocytes were prepared for immunohistochemistry. Myocytes were fixed and stained for Casq2, alpha-actinin, and dapi to visualize Casq2 expression. Example representative immunostaining images from each genotype.

Impedance-based contractility

Ablation of Casq2 has been reported to be linked to an increase in spontaneous calcium release events, causing the formation of delayed after depolarization (DAD), triggered beats, and CPVT (Knollmann *et al.*, 2006). We wanted to test if the *CASQ2*^{-/-} hiPSC-CMs had a similar phenotype. *CASQ2*^{-/-} lines were plated in monolayers and transfected with channel rhodopsin and optically paced. The pacing was then stopped, and the monolayer was recorded for spontaneous activity, signifying DADs (Figure 34A). It was found that both the *CASQ2*^{-/-} and *CASQ2*^{+/-} lines had significantly more spontaneous activity per well, and a larger percentage of wells that had spontaneous activity compared to the control cells (Figure 34B-C). We also assessed the spontaneous beating rate of each cell line and found that mutated *CASQ2* lines had a significantly higher spontaneous beating rate than control cardiomyocytes (Figure 34D). Together the increase in events and the higher spontaneous beating rate suggest that the mutated *CASQ2* cardiomyocytes have a CPVT phenotype.

Intracellular calcium handling

CPVT is a disease that is caused by abnormal calcium handling leading to an increase in the spontaneous calcium release events that are pathologic (Knollmann *et al.*, 2006; Cerrone *et al.*, 2009). With mutated *CASQ2* hiPSC-CMs having a CPVT phenotype, we wanted to investigate the calcium handling properties of the cells. To examine the effect of Casq2 deletion on RyR2 function and intracellular calcium release, we performed intracellular calcium spark measurements in permeabilized hiPSC-CMs using previously established protocols (Parikh *et al.*, 2017). Cells were permeabilized with saponin and incubated with the calcium dye, Fluo-4, in internal solution containing 120 nM free calcium. Kymographs were generated to illustrate the calcium spark

release events that occur in the permeabilized cardiomyocytes (Figure 35A). HiPSC-CMs with mutated *CASQ2* had significantly more sparks, calcium release per spark, and total calcium leak compared to control hiPSC-CMs (Figure 35B). These data are congruent with previous findings in mice (Knollmann *et al.*, 2006) and suggest that loss of Casq2 increases RyR2 calcium release.

We next tested how the absence of Casq2 would affect intact single cells. To test whether *CASQ2* deletion in intact single cell hiPSC-CMs promotes pro-arrhythmic triggered activity, we loaded hiPSC-CM with the cell-permeable, ratiometric calcium indicator, Fura-2 AM, to measure spontaneous calcium release events. To perform this experiment, graphically displayed in Figure 36A, single cells were paced for 60 seconds to equilibrate cellular conditions and ensure calcium loading. Calcium recordings were made during the last 20 seconds before cessation of pacing and then for 60 additional seconds. During that 60-second interval, spontaneous action potentials were recorded for the first 5 seconds. Following that, the external solution was exchanged for a 0Na0Ca solution (to prevent any calcium release events due to calcium entry or depolarization of the cell) so that intracellular spontaneous calcium release (SCR) events could be recorded. After 30 seconds, cells were perfused with tetracaine (RyR2 inhibitor) to measure the inherent SR calcium leak. Finally, caffeine was applied to measure the total SR calcium content. *CASQ2*^{-/-} hiPSC-CMs lines were found to have a significant increase in SCR frequency, SR calcium leak, and SR calcium leak normalized to SR calcium content (Figure 36C; Table 6).

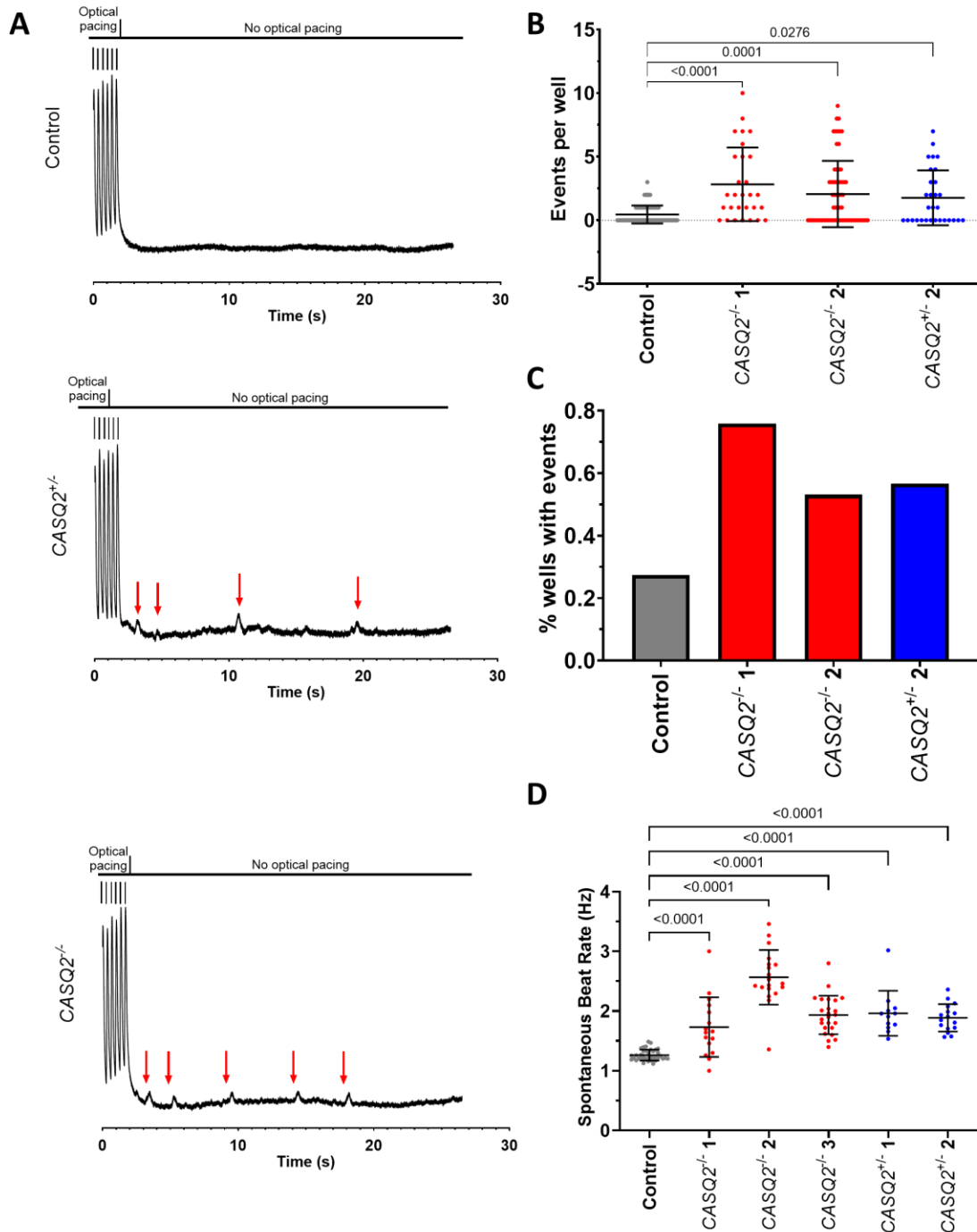


Figure 34. Impedance-based contractility measurements. *CASQ2*^{-/-} and *CASQ2*^{+/+} lines were plated in monolayers and transfected with channel rhodopsin and optically paced. Pacing was stopped and spontaneous activity was recorded. **A)** Representative trace showing spontaneous events occurring after pacing is stopped. **B)** Measurements of events that occurred per well. **C)** Graph of the percent of wells that had events in each line. **D)** Spontaneous beating rate of each cell line was measured. Spontaneous beat rates were measured using changes in impedance of the monolayer. Data displayed as mean ± SD. Data were analyzed using one-way ANOVA with Tukey’s multiple comparison test.

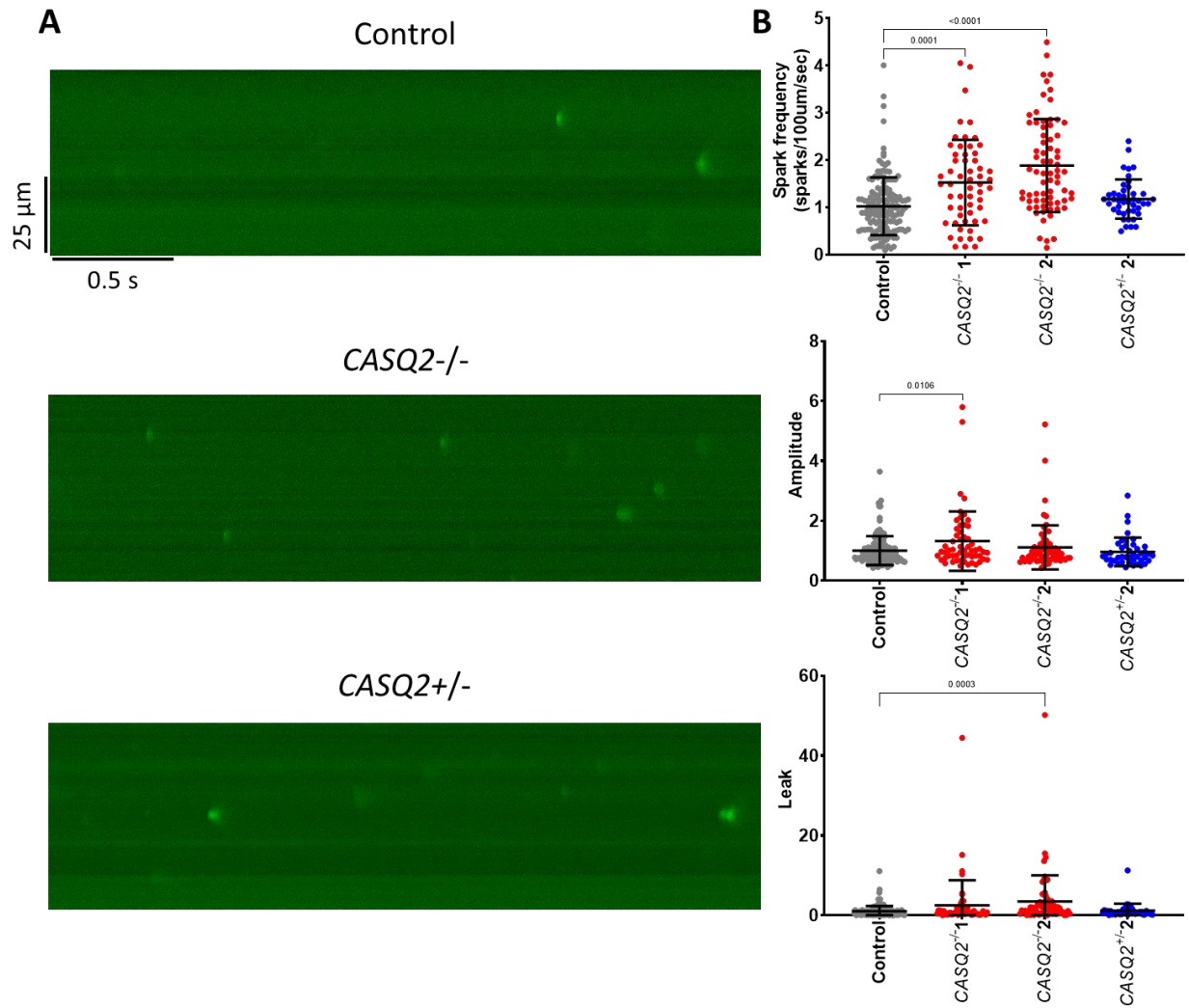


Figure 35. Calcium handling is altered in *CASQ2* hiPSC cardiomyocytes. **A)** Representative line scans showing calcium sparks in isogenic control and *CASQ2*^{-/-} cells. **B)** Calcium spark parameters measured in *CASQ2* hiPSC cardiomyocytes. Data displayed as mean \pm SD. Data were analyzed using one-way ANOVA with Tukey's multiple comparison test.

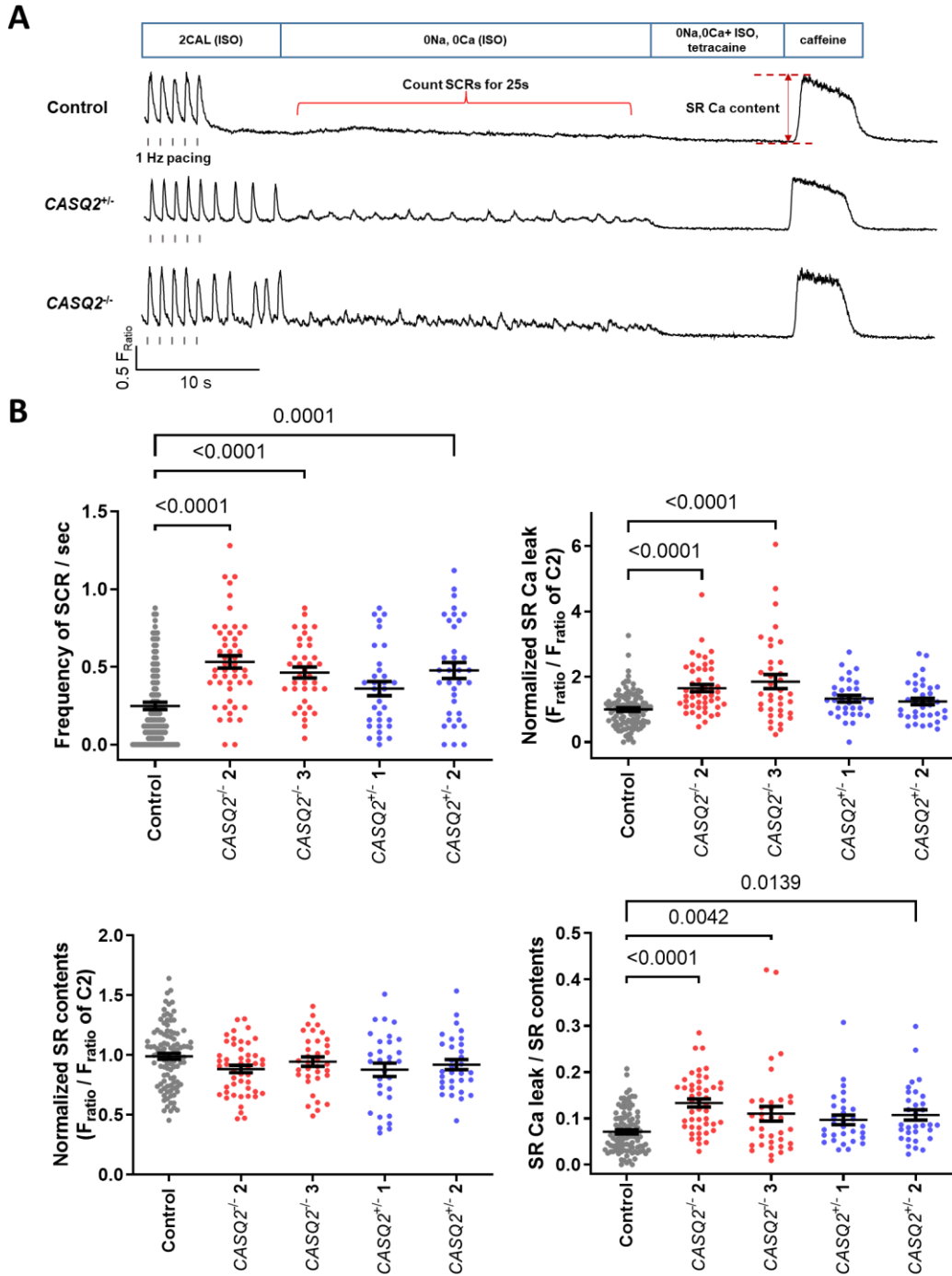


Figure 36. *CASQ2*^{+/-} and *CASQ2*^{-/-} have increased calcium leak and spontaneous/fractional calcium release in the presence of 1 μ M isoproterenol. **A)** Representative traces of each *CASQ2* genotype. **B)** Measurements taken from calcium traces with 1 Hz field stimulation. Frequency of spontaneous calcium release, measured as calcium inflections >10% from diastolic levels in 0Na, 0Ca. SR calcium leak, measured as ratio of diastolic calcium levels before and after application of tetracaine. Total SR calcium content, measured as amplitude after caffeine application. Data displayed as mean \pm SD. Data were analyzed using one-way ANOVA with Tukey's multiple comparison test.

Ca²⁺ transient measurements in hiPSC-cardiomyocytes

	Control (n=108)	CASQ2 ^{-/-} 1 (n=33)	CASQ2 ^{-/-} 2 (n=36)	CASQ2 ^{-/-} 2 (n=36)	CASQ2 ^{-/-} 3 (n=48)
Diastolic Ca	1.000 ± 0.173	1.038 ± 0.246	0.911 ± 0.083 ^{**}	1.038 ± 0.264	1.105 ± 0.135 ^{***}
CaT amplitude	1.000 ± 0.281	1.013 ± 0.394	1.103 ± 0.277	1.052 ± 0.267	1.041 ± 0.236
Time to peak	1.000 ± 0.173	0.981 ± 0.181	0.959 ± 0.194	0.921 ± 0.195	0.906 ± 0.196 [§]
CaT decay rate	1.000 ± 0.173	0.878 ± 0.346	0.725 ± 0.258 ^{***}	0.896 ± 0.267	0.911 ± 0.331
Fractional SR Ca release	0.813 ± 0.137	0.912 ± 0.178 ^{**}	0.998 ± 0.145 ^{***}	0.872 ± 0.179 [§]	0.983 ± 0.146 ^{***}

Mean ± SD; § p-value<0.05, **p-value<0.01 and ***p-value<0.001 compared with Control

Table 6. Calcium transient properties in *CASQ2* hiPSC cardiomyocytes. Paced calcium transient parameters in the presence of 1 μM isoproterenol to stimulate adrenergic response. Data were compared using Brown-Forsythe and Welch ANOVA tests with post-hoc Dunnett's T3 multiple comparisons test with adjusted p-value and 95% confidence interval of the difference compared to control.

Conclusion

Cardiac calsequestrin (Casq2, encoded by *CASQ2*) is a major calcium-binding protein with the function of regulating calcium release within the sarcoplasmic reticulum (SR) during the excitation-contraction (EC) coupling cycle. Variants in *CASQ2* have been found to cause a lethal arrhythmia syndrome, catecholaminergic polymorphic ventricular tachycardia (CPVT) (Lahat *et al.*, 2001a; Lahat *et al.*, 2001b). *CASQ2* variants cause CPVT by decreasing levels of Casq2, reducing the ability of the SR to buffer calcium appropriately, and resulting in a propensity to release calcium prematurely, cause delayed afterdepolarizations, triggered beats and ultimately CPVT (Cerrone *et al.*, 2005; Knollmann *et al.*, 2006; Rizzi *et al.*, 2008; Uchinoumi *et al.*, 2010). Understanding how the ablation of Casq2 affects human cardiomyocytes is important because a majority of Casq2 research has been conducted in mouse models, but it is currently not known if *CASQ2* variants are truly causal for a potential life-threatening disorder or merely incidental and noncausal genomic background noise, which is notably high in the *CASQ2* gene (Jabbari *et al.*, 2013).

Recently, hiPSC-CMs have been utilized to investigate the mechanism of CPVT in patient-specific models. Multiple hiPSC lines have been created and differentiated from patients with mutations in *CASQ2* (Novak *et al.*, 2012; Novak *et al.*, 2015; Sasaki *et al.*, 2016; Maizels *et al.*, 2017). Having a human model is important to identify potential therapeutic compounds that could be used for patients that are resistant to common CPVT treatments, but a major limitation is that current hiPSC lines have been generated directly from patients with CPVT. It is possible that the patient's genetic background could affect the resulting phenotype that is present in the hiPSC-CM. A genetically engineered *CASQ2*^{-/-} hiPSC line provides a human model specific for *CASQ2* that could be used to both advance our understanding of CPVT and serve as a target for future drug screens for diseases that have abnormal calcium handling.

Here we used CRISPR/Cas9 to generate both homozygous and heterozygous *CASQ2* knockout (*CASQ2*^{-/-} and *CASQ2*^{+/-}) hiPSC lines. Our data show that *CASQ2*^{-/-} hiPSC-CMs recapitulate human disease features. *CASQ2*^{-/-} hiPSC-CMs were found to have increased spontaneous calcium release events in both single cells and monolayers because of hyperactive RyR2 channels. The increase in proarrhythmic events was a result of a decrease in Casq2 levels, confirmed by RNA-sequencing, western blotting, and immunostaining.

Despite absent Casq2, we observed that cardiomyocytes lacking Casq2 had normal contractility and SR calcium release in basal conditions. Despite normal baseline contractility and calcium handling, in the presence of catecholamines, there was increased diastolic SR calcium leak, resulting in premature contractile events generated from the SR and triggered beats.

One feature that we discovered was that the mutated *CASQ2* lines plated in monolayers had a significantly higher spontaneous beating rate than isogenic control even in the absence of isoproterenol. The reason likely stems from increased calcium leak from the SR generating higher frequency of cellular contractions. These results are contradictory to phenotypes observed in patients with CPVT: who present with normal sinus rhythm at rest and sinus bradycardia in some patients (Postma *et al.*, 2005; Faggioni *et al.*, 2013; Miyata *et al.*, 2018). Clinical cases are suggested to have sinoatrial node dysfunction that would not be evident in hiPSC-CM due to the lack of the physiological structures that are present in the heart. Our group has previously discovered that increasing the pacing rates reduced the likelihood of spontaneous calcium release and triggered beats in isolated CPVT mouse cardiomyocytes (Faggioni *et al.*, 2013).

Observations in our *CASQ2*^{-/-} human model showed some similarities to our published data from *CASQ2*^{-/-} mice. In intact hiPSC-CM calcium transients, there was no difference between *CASQ2*^{-/-} and isogenic control in calcium transient amplitude and SR content even in the presence

of β -adrenergic stimulation. This suggests that the functional capacity of the SR to store calcium remains unchanged; a similar result to the observations in mouse cardiomyocytes lacking Casq2 (Knollmann *et al.*, 2006). Also, diastolic calcium ratio, SR calcium leak and fractional SR calcium release were all increased in the knockout lines suggesting an increased propensity towards premature contractions. Clinically, *CASQ2*-linked CPVT presents often as an autosomal recessive inheritance. However, our results indicated a phenotype in the heterozygous *CASQ2*^{+/-} cardiomyocytes indicating that some individuals may have subclinical dysfunction. Recent studies have confirmed the importance of heterozygous *CASQ2* variants. A multicenter study found multiple *CASQ2* heterozygous variants that followed an autosomal dominant inheritance, and patients experienced the same severity of CPVT symptoms as autosomal recessive families (Ng *et al.*, 2020).

Our studies in *CASQ2*^{-/-} hiPSC-CM recapitulate hallmark phenotypes observed in previous work with mice- namely, hyperactive RyR2-mediated calcium release, triggered activity, and changes in Casq2 protein expression. Importantly, our findings in the Casq2 heterozygous model corroborated our previous reports that subtle reductions in Casq2 protein increase calcium leak at the cellular level (Chopra *et al.*, 2007). This result was surprising, given that hiPSC-CM are widely considered to be less mature than primary CM. This may be due to our recent efforts to generate mature hiPSC-CM using T3 and dexamethasone and plating cells on a stiff extracellular Matrigel substrate. To our knowledge, we have generated the first full *CASQ2*^{-/-} hiPSC model and the findings from this project suggest that hiPSC-CM are an excellent human model to extend our understanding of the pathogenesis and treatment of CPVT.

CHAPTER IV

Conclusion, Limitations, and Future Directions

Motivation

Casq is a vital calcium handling protein found within the SR of both skeletal and cardiac muscle cells. The main purpose of the protein is buffer the amount of calcium that is available for release during and in-between EC coupling cycles. Extensive research has been done to understand structure and function of Casq. Due to the 60-70 negatively charged amino acids, Casq has been found to bind 40-50 calcium ions (Yano & Zarain-Herzberg, 1994), making it the perfect protein to handle SR calcium levels (Pape *et al.*, 2007). Structurally, Casq is a monomer in isolation. The addition of calcium promotes the formation of Casq dimers through front-front interactions. As calcium levels increase, the dimers interact with one another, creating a polymer through back-back connections of dimers (Park *et al.*, 2003). With the recent crystallization of the polymer, novel calcium binding sites and intra/inter-dimerization sites have been uncovered (Titus *et al.*, 2020). More work is needed to continue growing our understanding of the key binding sites within Casq as mutations in the protein have been found to cause disease related to the mishandling of calcium.

My work has focused on cardiac Casq (Casq2) and its role in the disease Catecholaminergic Polymorphic Ventricular Tachycardia (CPVT). Casq2-associated CPVT, termed CPVT2, was first discovered in 2001 and 2002 when missense/nonsense variants were discovered in a family with autosomal recessive CPVT (Lahat *et al.*, 2001b; Postma *et al.*, 2002). Autosomal-recessive CPVT2 is a result of a decrease in Casq2 protein levels, altering the ability of the SR to buffer calcium. The decrease in calcium buffering increases how quickly free calcium levels near RyR2 release channels rise in the SR. The absence of Casq2 in mice also leads to hyperactive RyR2 channels,

impaired calcium-release termination, shortened calcium release refractory period, and enhanced spontaneous release of calcium (Knollmann *et al.*, 2006; Chopra *et al.*, 2007; Kryshtal *et al.*, 2015). It is generally accepted that CPVT2 was a result of autosomal recessive mutations in *CASQ2*. In 2016, a novel autosomal-dominant mutation, K180R, was found in *CASQ2* (Gray *et al.*, 2016). The proposed hypothesis was that K180R would still decrease Casq2 levels through a dominant-negative mechanism where mutated protein would bind wild-type protein, and both would be degraded. With the discovery of an autosomal-dominant mutation, the field began to question how common autosomal-dominant mutations in *CASQ2* are, how relevant are they for the development of CPVT, and whether they follow a similar mechanism of action as the autosomal-recessive mutations.

While the mechanism of CPVT is generally agreed upon, the anatomical origin of the disease is still unclear. Within the heart, the three main components that are thought to play a role in the formation of the disease are the sinus node, ventricular myocytes, and Purkinje cells. Sinus node dysfunction is a hallmark of CPVT in both patients and animal models, but it is unclear if the low sinus heart rates contribute to the mechanism of the disease (Faggioni *et al.*, 2014b; Miyata *et al.*, 2018). Given that the arrhythmia results in the formation of ventricular tachycardia, another question that has been asked is if the trigger that causes the arrhythmias is originating in the ventricular cardiomyocytes of the working myocardium or in the specialized cells of the cardiac conduction system, the Purkinje cells. Currently, experimental and modeling studies suggest that the Purkinje cells are responsible for arrhythmia generation in CPVT (Cerrone *et al.*, 2007; Herron *et al.*, 2010; Kang *et al.*, 2010). Cellular data have found that Purkinje cells have differential protein expression (e.g. ion channels) and structural properties (lack of T-tubules) that make them particularly prone to develop spontaneous calcium releases (Vassalle & Lin, 2004; Li & Rudy,

2011). Modeling data have demonstrated that Purkinje cells have increased sodium load and susceptibility to calcium overload, enhanced SR load, and lower action potential threshold. Studies done using ventricular cardiomyocytes carrying CPVT mutations have found that the myocytes exhibit spontaneous calcium release in response to catecholamine challenge and can generate DADs and spontaneous action potentials (Knollmann *et al.*, 2006; Fernandez-Velasco *et al.*, 2009). As a result, current research has been unable to identify the anatomical and cellular origin of CPVT focal activation.

A better understanding of the mechanism of CPVT and the anatomical origin of the disease are important for developing treatments for CPVT patients. While there are currently several therapeutic options recommended by consensus guidelines (Priori *et al.* 2013), many patients still experience symptoms. The current therapies available for patients are beta-adrenergic receptor blockers, combination medical therapy (e.g. the addition of flecainide), or left cardiac sympathetic denervation. On beta-blockers alone, over 30% of patients still experience events even after 8 years of treatment (van der Werf *et al.*, 2012). For those patients, the addition of flecainide is the next step to help prevent the occurrence of CPVT. While the initiation of flecainide reduces symptoms in nearly 80% of patients, additional studies are needed to gain a better understanding of the role of sodium channel versus RyR2 inhibition in flecainide's mechanism of action, and the potential of using the drug as a first-line therapy (van der Werf *et al.*, 2011; Khoury *et al.*, 2013; Watanabe *et al.*, 2013; Behere & Weindling, 2016; Kannankeril *et al.*, 2017; Wangüemert Pérez *et al.*, 2018). Left or bilateral cardiac sympathetic denervation has been effective in reducing symptoms in patients resistant to pharmacological intervention. One study found that major cardiac events reduced from 86% to 21% in patients that had undergone the procedure (De Ferrari *et al.*, 2015). Since some patients still experience symptoms even on optimal therapies, new models and

methods are needed to uncover potential treatments for the disease. One area that has shown promise is human induced pluripotent stem cells (hiPSC). First generated in 2006, hiPSCs overcome some of these limitations found in mouse models and they have proven to be useful in disease modeling (Kim, 2014). Reports have found that cardiomyocytes generated from mutated hiPSCs have abnormal calcium handling and local calcium release events within beats (Novak *et al.*, 2015). One of the most exciting aspects of using hiPSCs is the ability to screen different pharmacological compounds. Studies have shown that various medications, such as flecainide, can prevent arrhythmias in an iPSC-CM model (Preininger *et al.*, 2016). A limitation of most of the iPSC work is that all current lines have been generated directly from families with specific CPVT mutations (Itzhaki *et al.*, 2012). While patient-specific lines contain the CPVT mutation, it is also possible that the genetic background of the patient may contribute to the disease phenotype. An iPSC CPVT model generated from an isogenic control line would target CASQ2 directly, reduce the effects from genetic background, provide data that would continue to advance our understanding of CPVT, and serve as a target for future drug screens.

The next sections will highlight the importance of the research conducted during my time in the program, the limitations of the work, and suggest some future directions that could be pursued.

A novel mechanism for autosomal dominant CPVT2

Until 2016, all reported mutations for CPVT2 were autosomal recessive. When the first autosomal dominant variant in Casq2, K180R, was found the proposed hypothesis was that K180R would decrease Casq2 protein levels and cause CPVT (Gray *et al.*, 2016). This proposed hypothesis had not been confirmed though and how/if K180R could cause CPVT was still

unknown. The use of a K180R mouse model allowed us to link K180R to autosomal dominant CPVT. K180R mice have CPVT and a decreased calcium release refractoriness period. Different from other autosomal-recessive mutations K180R does not decrease Casq2 protein levels, other calcium handling protein levels (e.g. triadin), or affect the steady-state calcium buffering within the SR. We found that K180R alters the dynamic calcium buffering within the SR, resulting in a more rapid rise of free calcium in the SR. This would affect the ability of the SR to buffer calcium ions as they are moving in and out of the SR during the EC coupling cycle. The decrease in dynamic buffering capacity from the K180R mutation could lead to premature calcium release and cause CPVT.

How does K180R impair dynamic SR calcium buffering? The variant itself is a conserved amino acid change from a lysine to an arginine. One recently proposed hypothesis is that K180R may decrease the ability of Casq2 to polymerize (Ng *et al.*, 2020; Titus *et al.*, 2020). As discussed in the introduction, Casq2 monomers can interact with one another to form dimers, and Casq2 dimers can polymerize together to form a large Casq2 polymer. The polymerization process is calcium dependent, plays an important role in calcium binding, and provides a structural component for the SR (Park *et al.*, 2003; Park *et al.*, 2004). K180R was recently studied *in vitro* using the latest crystal structure of the Casq2 polymer (Titus *et al.*, 2020). Results from turbidity assays suggested that K180R decreased the ability of Casq2 to polymerize. Within the crystallized polymer, K180R was found to be in a potential inter-dimerization site of Casq2. The authors hypothesized that the inability of the K180R variant to polymerize will cause a decrease in Casq2 levels. Our western blot analysis would suggest a different mechanism. We found there was no change in Casq2 protein levels, monomers, or polymers, in the K180R mice. The visualization of the polymers in western blotting and electron microscopy experiments also support that K180R is

indeed able to form polymers. Finally, the polymerization of Casq2 is critical for retention and trafficking of the protein to the SR (Milstein *et al.*, 2009; McFarland *et al.*, 2010; Sleiman *et al.*, 2015). Our immunostaining data suggest that K180R Casq2 is trafficking to the SR and being retained there.

Based on the data we have collected, the K180R mutation seems to cause a more subtle defect in Casq2, causing the rate of calcium binding to be reduced. The recent Casq2 polymer crystal structure revealed that there are potentially novel calcium binding sites within the polymer and the structure was found to have a large cavity within the center of the polymer where calcium ions could bind (Titus *et al.*, 2020). K180 was mapped onto the polymer and is proposed to be at an inter-dimer region where two potential calcium binding sites are located (Titus *et al.*, 2020). We suggest that K180R is affecting the ability of the Casq2 polymer to bind calcium, which increases the calcium Kd of the polymer, and results in a decrease in the dynamic buffering capabilities of the SR. The faster refilling would then lead to a decrease in calcium release refractoriness (Figure 15), an increase in the potential for spontaneous calcium release events (Figure 7), and ultimately the possibility of CPVT (Figure 6).

The novel mechanism for how autosomal-dominant Casq2 mutations can cause CPVT is important for the CPVT field. A large multi-center study was recently conducted to find the prevalence of autosomal-dominant *CASQ2* variants within CPVT families (Ng *et al.*, 2020). Twelve of the 36 probands had heterozygous *CASQ2* variants and the heterozygous patients still experienced similar symptoms and severity of arrhythmias as homozygous patients (e.g., aborted cardiac arrest). The experimental work above has uncovered a novel mechanism responsible for autosomal-dominant CPVT2 and provides a template to investigate if other heterozygous variants causing CPVT2 follow a similar pathophysiology.

The Purkinje-myocardial junction is the tissue mechanism of CPVT

By uncovering more about the pathophysiology of CPVT, we have been able to gain a better understanding of arrhythmias that develop in various heart conditions as a result of impaired calcium handling (e.g. heart failure). As discussed before, one of the more commonly debated points regarding CPVT is the cellular origin of the ventricular arrhythmias seen in the disease. The current hypothesis is that the Purkinje cells are the cellular foci in CPVT. To review, there are multiple studies that have generated evidence in support of this hypothesis. First there is a 180° QRS axis shift that characterizes the bidirectional pattern that is seen during ECG recordings, which is consistent with the idea that the ectopic activity is originating alternatively from right and left bundle branches (Cerrone *et al.*, 2007). Other data have found that there are higher rates of spontaneous calcium release in isolated Purkinje cells compared to VM (Kang *et al.*, 2010).

However, there are also data that has been generated to support that the origin of CPVT is outside of the Purkinje cells. Observations in human patients have found anatomical foci that are located outside of Purkinje fibers and can be successfully ablated (Kaneshiro *et al.*, 2012; Kaneshiro *et al.*, 2017). Another study found that there was an inverse correlation between sudden death and arrhythmogenic focal distance from the conduction system (Sumitomo *et al.*, 2003). It is important to note though that both the sudden death cohort and surviving cohort had foci that were found near the conduction system. Cellular studies have found that Purkinje cells have a prolonged refractory period, which means they would be less likely to generate the triggered ectopic beats that are required for CPVT to form.

To answer the question of where the anatomical origin of CPVT is, we generated a mouse model that would allow us to study the expression of *Casq2* with cellular specificity. We had four different genetic models where *Casq2* expression was present everywhere, only in the Purkinje

cells, only in the ventricular myocardium, or knocked out in the whole heart. Due to the leakiness of the cre system, we were also able to generate an accidental mouse model where Casq2 expression occurred in the Purkinje cells and the subendocardial cardiomyocytes that were juxtaposed to the Purkinje system. Data from our work supports three important conclusions regarding the cellular and anatomical origin of CPVT:

1) The cell type responsible for triggering arrhythmogenesis in CPVT is the ventricular cardiomyocyte. Using isoproterenol and caffeine to evaluate arrhythmia burden, we found that VM-Casq2^{-/-} and global Casq2^{-/-} mice had a similar phenotype (Figure 19 and 20), which suggest that the expression of Casq2 only in the Purkinje cells is not enough to protect the mice against catecholamine-induced VT. In silico modeling was also done to confirm our *in vivo* findings. When looking at the Purkinje-myocardial junction, subthreshold DADs from ventricular myocytes caused full Purkinje action potentials that are capable of propagating. In contrast, DADs from the Purkinje cells are unable to excite ventricular myocytes and cause propagation of electrical signal (antegrade excitation).

2) Subendocardial cardiomyocytes juxtaposed to Purkinje cells are the cellular source for arrhythmogenesis. By using immunostaining techniques to visualize Casq2, Purkinje cells, and ventricular myocytes, we found that subendocardial expression of Casq2 near Purkinje cells was sufficient to prevent CPVT. Previous reports had also suggested the anatomical origin of CPVT is somewhere within the endocardial wall and not the epicardium. We confirmed these findings by being able to prevent CPVT formation after ablation of the endocardial surface of the heart using Lugol's solution. In silico modeling further supported our experimental findings by showing that

only DADs near the Purkinje-myocardial junction were able to trigger action potentials in the Purkinje fibers.

3) CPVT foci predominately arise from the right side of the heart. Similar to reports from humans with CPVT (Sumitomo *et al.*, 2003; Sy *et al.*, 2011), when we conducted voltage mapping, we found showed right sided epicardial breakthrough in 70% of all arrhythmogenic ventricular ectopy.

A question that arises from these data is why are the subendocardial ventricular cardiomyocytes juxtaposed to Purkinje cells capable of triggering CPVT foci, but Purkinje cells are not. Previous single cell data have found that both cell types are capable of triggering DADs/spontaneous beats, are susceptible to calcium overload, and have a high rate of DADs (Liu *et al.*, 2006; Cerrone *et al.*, 2007). Our modeling data found that DAD-like activity in Purkinje fibers cannot excite the myocardium, whereas sub-threshold excitation of the ventricular bulk myocardium can initiate retrograde excitation of the Purkinje fibers. Observations in superfused preparations suggest that there is a favorable source-sink mismatch and a restrictive barrier at the Purkinje-myocardial junction which can lead to longer delay times that allow for retrograde conduction to occur (Wiedmann *et al.*, 1996; Huelsing *et al.*, 1998). Other studies that support retrograde conduction found that propagation from high- to low-conductivity tissue (i.e., PF to VM) enjoys a high safety margin, which would help antegrade transmission, but there is a large reduction of the safety factor when the electrical impulse propagates across thin-to-thick tissue expansions (i.e., at the Purkinje-myocardial junction) which favors retrograde transmission overall (Boyle & Vigmond, 2010; Boyle *et al.*, 2019).

Although our simulation studies favor retrograde excitation caused by subthreshold depolarizations in the ventricular myocardium, we should not exclude the possibility that ectopic

foci could also be caused by full ventricular action potentials. Action potentials causing ectopic foci are less likely though because if they are arising from the mid-myocardium or epicardium they would have to compete with a large sink. Juxta-Purkinje ventricular myocytes on the other hand, have less sink to overcome and can more easily conduct into the nearby Purkinje cells. Further support for the Purkinje-myocardial junction as the anatomic origin comes from our immunostaining data. We found that restoration of *Casq2* near *Cntn2*-positive (Purkinje) cells was sufficient to prevent arrhythmias and that cardiomyocytes distal from the Purkinje-myocardial junction do not trigger ventricular ectopy.

Together our data identify the subendocardial cardiomyocytes juxtaposed to Purkinje fibers as the cellular driver and the Purkinje-myocardial junction as the anatomical origin of focal ventricular ectopy. These findings have important implications that go beyond CPVT, specifically in diseases that result from calcium handling. In heart failure and myocardial infarctions, DADs have been found to be caused by spontaneous calcium release (Hoeker *et al.*, 2009; Luo & Anderson, 2013; Dries *et al.*, 2018). Like CPVT, the ectopic beats that occur in heart failure may also be generated at the Purkinje-myocardial junction, where subthreshold membrane depolarizations in the ventricular myocardium can generate action potentials in adjacent Purkinje fibers. Due to the membrane depolarizations being caused by spontaneous calcium release through RyR2, intervention with pharmacological agents that target RyR2 can prevent arrhythmias not only in CPVT but also in heart failure models (Kubalova *et al.*, 2005).

Generation of a Casq2KO CPVT human induced pluripotent stem cell (hiPSC) model

As discussed before, *CASQ2* variants cause CPVT by decreasing levels of *CASQ2*, reducing the ability of the SR to buffer calcium appropriately. The result is a propensity to release

calcium prematurely, cause delayed afterdepolarizations, triggered beats and ultimately CPVT (Cerrone *et al.*, 2005; Knollmann *et al.*, 2006; Rizzi *et al.*, 2008; Uchinoumi *et al.*, 2010). Due to the large amount of research conducted in mouse models, it is important to understand how the ablation of *CASQ2* affects human cardiomyocytes in order to continue expanding our treatment options for CPVT. Previous studies have shown that mouse models are limited when trying to mimic human physiology (Sallam *et al.*, 2014; Sallam *et al.*, 2015; Liang *et al.*, 2016). In order to study CPVT in humans, a model is needed that is accessible, can be genetically altered, and is reproducible. One of the best tools that address these problems are human induced pluripotent stem cells (hiPSC). HiPSCs have proven to be useful in disease modeling (Kim, 2014), and studies have found that cardiomyocytes generated from hiPSCs can be used to investigate cellular triggers of CPVT phenotypes, such as DADs, EADs, and triggered arrhythmias (Novak *et al.*, 2015). When stimulated, the cardiomyocytes were found to have multiple peaks, oscillations, varying amplitude, and local calcium release events (Novak *et al.*, 2015). Another benefit of using human models is the ability to identify and test novel therapeutics. Various medications have been tested on hiPSC cardiomyocytes and it was found that compounds, such as flecainide, were able to prevent arrhythmias, reproducing the effects seen in patients (Preininger *et al.*, 2016).

Recently, multiple hiPSC lines have been created and differentiated from patients with mutations in *CASQ2*, but a major limitation is that the lines are specific and do not address how the ablation of *CASQ2* affects human cardiomyocytes (Novak *et al.*, 2012; Novak *et al.*, 2015; Sasaki *et al.*, 2016; Maizels *et al.*, 2017). Having a *CASQ2*^{-/-} hiPSC line would provide a human model that could be used to both advance our understanding of CPVT and serve as a target for future drug screens. To create the *CASQ2*^{-/-} hiPSC line, CRISPR/Cas9 was used to generate both

a homozygous and a heterozygous *CASQ2* (*CASQ2*^{-/-} and *CASQ2*^{+/-}) model. We found that the *CASQ2*^{-/-} hiPSC cardiomyocytes recapitulated human disease features.

By using RNA-sequencing, western blotting, and immunostaining techniques, we found that the cardiomyocytes generated from the *CASQ2*^{-/-} hiPSCs had a decrease in Casq2 levels, which is similar to what is seen when *CASQ2* is ablated in mice. Even though Casq2 levels were decreased, the cardiomyocytes still had normal contractility parameters and were able to release calcium from the SR. The ability of the *CASQ2* knockout cardiomyocytes to have normal contractility comes from findings that are reported in *CASQ2*^{-/-} mice. *CASQ2*^{-/-} mice have (1) an increase in the SR volume, (2) reductions in SR membrane proteins, such as junctin and triadin, and (3) an increased gain in calcium-induced SR calcium release. Even though the cells had normal baseline contractility, when stimulated using catecholamines, there was increased diastolic SR calcium leak. In single cell and monolayer preparations, the *CASQ2*^{-/-} hiPSC cardiomyocytes were found to have an increase in spontaneous calcium release events, premature contractile episodes, and triggered beats.

An interesting feature that we discovered when analyzing the *CASQ2*^{-/-} lines was they had a significantly higher spontaneous beating rate than the control cells when plated in monolayers, even in the absence of stimulation. The increased spontaneous beating rate is most likely due to an increase in calcium leak from the SR. The increase leak could generate a higher frequency of cellular contractions. The main concern with the results is that patients who present with CPVT have been found to have normal sinus rhythm at rest or even sinus bradycardia in some patients (Postma *et al.*, 2005; Faggioni *et al.*, 2013; Miyata *et al.*, 2018). An explanation for the differences seen between patients and the generated cardiomyocytes would be that the hiPSC cardiomyocytes are lacking the sinoatrial node dysfunction that would be present in patients.

Another question is what are the similarities between the human *CASQ2*^{-/-} model, and the data published on the *CASQ2*^{-/-} mice? One difference that was observed was there was no significant decrease in other calcium handling proteins (e.g. triadin) in the *CASQ2*^{-/-} hiPSC cardiomyocytes. In the mouse model, the absence of Casq2 was found to decrease the levels of junctin and triadin, most likely a result of the proteins interacting with one another (Knollmann *et al.*, 2006). A reason for the differences could be that the hiPSC cardiomyocytes are immature. Even with advancements in cardiomyocytes differentiation (Parikh *et al.*, 2017), the resulting myocytes still lack t-tubule organization and striation. It is possible that Casq2, junctin, and triadin are not interacting with one another yet in the immature myocytes, allowing for the correct trafficking and retention of the calcium handling proteins. It is also possible that the interactions between the calcium handling proteins are not as crucial for the trafficking and retention of the junctin and triadin in human cardiomyocytes compare to the mouse cardiomyocytes (Chopra *et al.*, 2009; Lee *et al.*, 2012). Similar to mouse myocytes lacking Casq2, there was no difference between the knockout and control lines in calcium transient amplitude and SR calcium content even in the presence of β -adrenergic stimulation, suggesting that there is no change in functional capacity of the SR to store calcium. Another similarity is that there was an increase in the diastolic calcium ratio, SR calcium leak and the fractional SR calcium release, suggesting an increased propensity towards premature contractions.

In patients, CPVT2 often presents as an autosomal recessive inheritance, but we were interested to see how human cardiomyocytes were affected by heterozygous *CASQ2* deletion (*CASQ2*^{+/-}). The results indicated that *CASQ2*^{+/-} cardiomyocytes still had abnormal calcium handling and dysfunction, but it was not as severe as the *CASQ2*^{-/-} cells. It is possible then that some individuals may have heterozygous *CASQ2* mutations and thus subclinical dysfunction. A

recent multicenter study confirmed the importance of identifying heterozygous *CASQ2* variants. Multiple *CASQ2* heterozygous variants were found in families that followed an autosomal dominant inheritance and those patients still experienced the same severity of CPVT symptoms as patients with homozygous *CASQ2* mutations (Ng *et al.*, 2020).

Overall, the work on *CASQ2*^{-/-} hiPSC cardiomyocytes recapitulate hallmark phenotypes observed in previous work with mice including, a decrease in Casq2 protein levels, hyperactive RyR2-mediated calcium release, and triggered activity. Importantly, our findings in heterozygous Casq2 human cardiomyocytes also corroborated previous reports that found subtle reductions in Casq2 protein could increase calcium leak at the cellular level (Chopra *et al.*, 2007). These findings suggest that the *CASQ2*^{-/-} hiPSCs can serve as an excellent human model to extend our understanding of the pathogenesis CPVT and serve as a future platform for identifying potential treatments for patients suffering from the disease.

Limitations

With every project there are limitations that should be discussed to help future research be conducted and acknowledge the pitfalls of the experiments that were conducted. Here I will highlight some the techniques used in the different chapters that limit our ability to interpret the data and provide potentials techniques or experiments that could be done to address the limitations. One of the experiments done while investigating the mechanism of the K180R mutation was immunostaining of isolated cardiomyocytes for Casq2, RyR2, and triadin. The goal of the experiment was address localization and protein interaction between the calcium handling proteins within the SR. The immunostaining provides an initial test to look at both properties as previous papers have found significant differences in Casq2 localization when using triadin knockout mice (Chopra *et al.*, 2009). One issue is that the resolution does not confirm that there is indeed protein

interaction occurring. We can infer that it is based on the localization pattern, but there are more techniques though that could be used to confirm that Casq2 is interacting with other SR membrane proteins. For example, co-immunoprecipitation or biomolecular fluorescence complementation (BiFC) is an alternative approach. Both approaches would provide a more robust readout of protein interaction but are technical and require optimization. BiFC allows for visualization of protein interactions in live myocytes but has drawbacks due to the attachment of large fluorescent receptor proteins on the proteins of interest.

Another limitation is trying to assess Casq2 polymerization and calcium binding *in vitro*. The *in vitro* environment lacks the complexity of myocytes and more importantly the SR, losing the potential interactions or modifications that would increase/decrease the function of Casq2 *in vivo*. The differences that are seen in these experiments could be due to number of things including, the absence of other calcium handling proteins, the lack of post-translational modifications (PTM) on Casq2, or absence of various ions and molecules that make up the SR environment. To address some of the *in vitro* limitations, calcium handling proteins can be overexpressed and added to the mixtures used to assess polymerization and calcium handling. The addition of PTMs could be achieved by combing Casq2 with various kinases to achieve the phosphorylation that has been found to occur in cardiomyocytes (Lewis *et al.*, 2016).

A limitation of the tissue mechanism project is that generation of the mice expressing Casq2 in the subendocardial cells near Purkinje fibers was an accidental finding due to the leakiness of cre. While we were able to obtain a large data set that provided the evidence we needed to make our conclusions, further characterization of subsequent mice have not had similar Casq2 expression patterns. One way to investigate the Purkinje-myocardial junction further would be the analysis and characterization of transitional cells. Transitional cells have been shown to be the cell

type that is located at these junctions and has various morphological and electrophysiological characteristics that allow it be differentiated from myocytes or Purkinje fibers (Garcia-Bustos *et al.*, 2017; Goodyer *et al.*, 2019). We attempted to investigate the transitional cells within the sections of our mouse myocardium using immunostaining techniques but did not find an antibody that worked well for identifying the transitional cells. It is possible that they are involved in the Purkinje-myocardial junction and could be the target of future studies for rescuing Casq2 expression and localizing the anatomical origin of CPVT even further.

A limitation of the *CASQ2*^{-/-} hiPSC project is that cardiomyocytes that are generated from hiPSCs are immature and lack t-tubule organization. Even with the advancements in maturation of hiPSC cardiomyocytes, more work is needed to continue improving maturity of the differentiated cardiomyocytes. The lack of t-tubule organization could decrease the severity of the phenotype that we were seeing in both the *CASQ2*^{-/-} and *CASQ2*^{+/-} cell lines. While spark frequency was able to be successfully measured, wave frequency proved to be impossible to obtain. Without proper organization of the SR, cells were unable to form full waves and instead generated broken waves or a large frequency of sparks. Recent efforts have been made to further improve the maturation of cardiomyocytes but more research is needed. Some efforts include the generation of tissue rings that utilize contraction and 3D organization to help the stem cells differentiate. One medium that has helped increase the expression of Casq2 is IMDM (Iscoe's Modified Dulbecco's Medium). Culturing the cells in the IMDM media during maturation helped to increase the expression of Casq2. More work is still needed to continue improving the organization and maturation of t-tubules in hiPSC cardiomyocytes, but our results show promise for using the *CASQ2*^{-/-} hiPSC as a human model for CPVT.

Future directions

The results from each of the projects has helped generate some important future experiments that would continue improving our understanding of CPVT and ways to treat it.

One of the important findings we uncovered while investigating the mechanism of autosomal dominant CPVT2 was an alteration in intra-SR calcium buffering. Even though it is proposed that intra-SR calcium kinetics are also altered in mice that have *CASQ2* ablated, these experiments have not been conducted yet. Given we were able to successfully measure and visualize both the cytosolic and intra-SR calcium levels, a similar approach could be used to confirm that *CASQ2*^{-/-} mouse myocytes also have decrease intra-SR calcium buffering capabilities. To take the experiments further, it would be important to investigate if other types of CPVT have a similar effect on calcium buffering. Other mouse models that have mutations in RyR2, triadin, or calmodulin could also be included in these studies to see if the pathophysiology of CPVT changes depending on the calcium handling protein that is mutated.

With the advancements in genetic editing, we were able to generate a hiPSC line that had *CASQ2* ablated. Given that we were to test the calcium handling capabilities in the *CASQ2*^{-/-} hiPSC cardiomyocytes, it would be interesting to include hiPSC lines that have both the heterozygous and homozygous K180R mutation present. If the phenotype is still present in the mutated lines, CRISPR/Cas9 could be used again to correct the mutation in hiPSC lines that have been generated from the patient and see if the phenotype remains. An hiPSC patient line has already been generated from the lab that discovered the K180R variant so that line could undergo genetic correction and testing to confirm that the variant is indeed casual (Ross *et al.*, 2019).

After the discovery of K180R, a large multicenter study was conducted to investigate the prevalence of heterozygous *Casq2* mutations (Ng *et al.*, 2020). The authors found that heterozygous variants were more common than previously thought and had the same severity of

CPVT as patients with homozygous variants. Within that study they identified some other novel variants that could undergo further testing (e.g. Y55C, S173I, R251H). Both mouse models or human iPSC models could be generated with these variants and similar experiments could be conducted to see if those variants are able to produce CPVT. If they are, it would be interesting to find out if they follow the same pathophysiology as the K180R variant and confirm that our novel mechanism of autosomal dominant CPVT2 is conserved across other mutations.

After K180R was discovered, one of the first manuscripts that was published focused on the crystal structure of the Casq2 polymer and how these autosomal dominant mutations affect the ability of the protein to polymerize (Titus *et al.*, 2020). One of the main techniques used to assess polymerization was a turbidity assay. The turbidity assay looks at absorbance at a certain wavelength as a direct correlation to the amount of protein that is polymerized. One of the interesting findings from these assays was that K180R only had an effect on polymerization when there was magnesium present in the solution. Without it, there was no difference in absorbance over time. The amount of magnesium that was added was 2 mM, which is physiologic, so that might suggest the findings were not initially seen due to the conditions not being physiologic. I was still interested in testing if the magnesium concentration would have an effect on the calcium handling properties of the K180R cardiomyocytes, so I did some initial tests on spark and wave frequency to see if there was a difference. Even though the results are preliminary, there was a significant effect on the spark and wave frequency at various levels of magnesium (Figure 37 and 38). Studies have shown that magnesium can be used as an antiarrhythmic (Fazekas *et al.*, 1993) so it would be worth investigating further if magnesium could have an effect on the pathophysiology and possibly the prevention of CPVT.

I discussed some of the limitations of the work that investigated the anatomical origin of the CPVT, but I also think those limitations could serve as future directions for the project as well. Given that we found the Purkinje-myocardial junction to be the anatomical origin of CPVT, it is important to investigate the cell types that have been found there. As mentioned in the limitations, the transitional cell has been found at this junction and has distinct characteristics compared to the myocyte and Purkinje cell (Garcia-Bustos *et al.*, 2017; Goodyer *et al.*, 2019). A recent paper had identified genetic markers that could be used to isolate and target the transitional cells within the mouse heart (Goodyer *et al.*, 2019). The transitional cells could be targeted to help confirm that they are not involved in the generation of the ectopic beats that occur at the junction by deleting or rescuing *Casq2* specifically in the transitional cells. We had attempted staining the cells but were unable to find an antibody that was specific enough to identify them. If transitional cells are important to the generation of ectopic beats, being able to locate and isolate them could be beneficial for our understanding of CPVT.

Discovering that the Purkinje-myocardial junction is the anatomical origin of CPVT also helps our understanding of other arrhythmias that occur due to calcium mishandling. It is known that DADs that are caused by increases in spontaneous calcium release are part of the pathophysiology for arrhythmias that develop after myocardial infarction or in patients suffering from heart failure (Hoeker *et al.*, 2009; Luo & Anderson, 2013; Dries *et al.*, 2018). Our data suggest that the ectopic beats seen in these diseases could also be generated at the Purkinje-myocardial junction where spontaneous RyR2 calcium release in the subendocardial cells generate full action potentials that activate the adjacent Purkinje fibers. Future experiments could investigate the effectiveness of pharmacological agents that are known to target RyR2 activity in

preventing the ability of these ventricular arrhythmias to form in CPVT, heart failure, and myocardial infarctions.

Another limitation that was discussed before but could serve as a future direction is the maturity of hiPSC cardiomyocytes. Currently, differentiated cardiomyocytes lack t-tubule organization which could affect the calcium handling properties and protein interactions within the SR. Future studies are needed to continue advancing the maturation process. There are multiple approaches that have been taken to help the hiPSCs mature. They are usually either the addition of small molecules or drugs (Parikh *et al.*, 2017), or the use of scaffolds and structures to promote 3D environments (Li *et al.*, 2020). Both approaches have shown that they can help the maturation process of hiPSCs and using them together could prove to have an even greater effect. Within the lab there is a focus on the generation of tissue rings that have been cultured in various small molecules. Future studies should include the hiPSC lines with ablated CASQ2 to see how the maturity of the differentiated cardiomyocytes affect the t-tubule organization and the expression of various calcium handling proteins.

A difference that we found between the *CASQ2*^{-/-} mouse and human models was how the absence of Casq2 affects the levels of other calcium handling proteins. Previous work has showed that in mouse models, alterations in calcium handling proteins within the SR usually decrease levels of the other proteins located within the calcium release unit (Knollmann *et al.*, 2006; Chopra *et al.*, 2009). We found that the *CASQ2*^{-/-} hiPSC cardiomyocytes only had a reduction in Casq2 protein levels and no differences in RyR2, triadin, or junctin. It would be important to continue to conduct experiments that investigate these findings more thoroughly. Other techniques, such as immunostaining or co-immunoprecipitation, could be used to confirm that the other calcium handling proteins are present and are interacting with one another even when Casq2 is absent. One

other difference that was found was the increase in spontaneous beating rate that was seen in the hiPSC lines that had mutations in Casq2. Seeing as patients normally present with either a normal sinus rate or bradycardia (Postma *et al.*, 2005; Faggioni *et al.*, 2013; Miyata *et al.*, 2018), it is important to understand why these differences occur or if it is a result of the maturity of the differentiated cardiomyocytes.

Final Thoughts

The original goal of my thesis project was to help advance the field of CPVT by focusing my efforts into understanding more about Casq2 and its function within the heart. While on that journey and with the help of my lab mates and collaborators, I have been able to uncover a novel mechanism for autosomal dominant CPVT2 and locate the anatomic origin of CPVT.

We found that unlike traditional autosomal recessive CPVT2, the K180R variant causes CPVT without affecting the levels of Casq2 protein. Instead, the mutation most likely decreases the ability of the protein to bind calcium during diastole which results in a decrease in the buffering capabilities of the SR. The faster rise of free levels of calcium decreases the calcium release refractory period and increase the amount of spontaneous calcium release events that occur. The methods that were used to investigate the K180R mechanism can serve as a template for future studies into autosomal dominant CPVT2.

By specifically deleting or rescuing Casq2 expression in various parts of the heart we were able to conclude that the ectopic beats that generate CPVT are originating in the subendocardial cardiomyocytes that are located in the Purkinje-myocardial junction. These findings are important for multiple disease states in the heart where calcium dysfunction is the major pathogenesis for the

development of arrhythmias and suggest that investigations into blocking RyR2 activity might provide a therapeutic benefit for patients.

Even on first line therapies there are still patients that are experiencing CPVT symptoms. In order to continue advancing the treatment options that exist, human models that are faithful to the disease, easy to manipulate, can produce large amounts of data, and are cost effective are necessary. Human iPSCs provide these benefits and have become widely used for disease modeling. Here we were able to create a hiPSC model that had *CASQ2* expression ablated. The absence of *Casq2* caused dysfunction in calcium handling and made differentiated cardiomyocytes more prone to spontaneous calcium release events. The *CASQ2*^{-/-} hiPSC line can serve as a model for continuing our understanding of CPVT in human cardiomyocytes and be used as a way to screen novel therapeutics to treat CPVT and other disorders that are caused by a disruption in calcium handling.

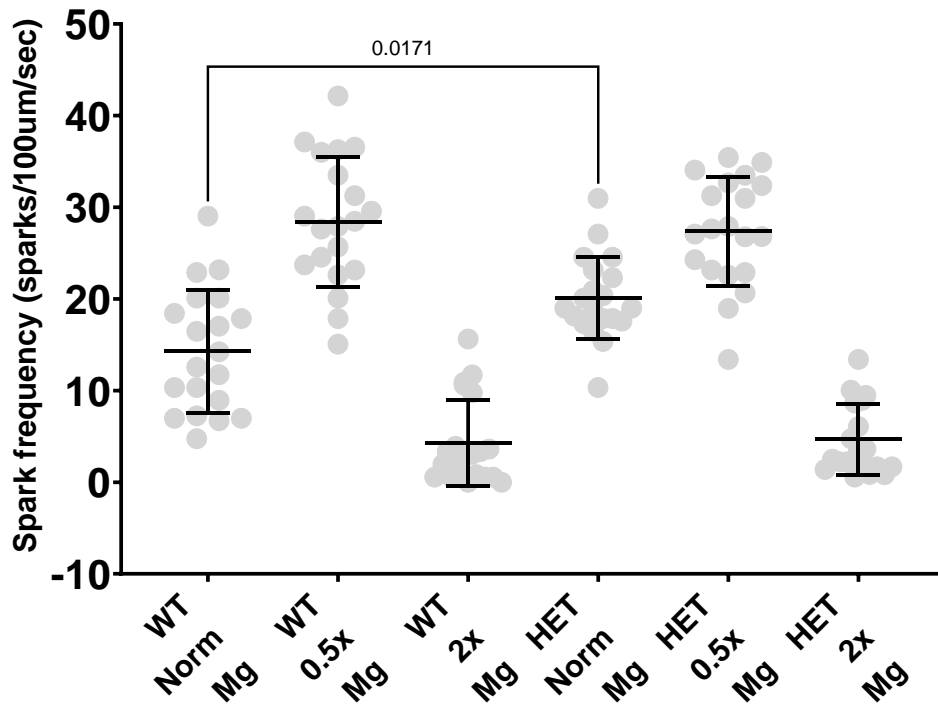


Figure 37. The effect of magnesium concentration on spark frequency in K180R isolated cardiomyocytes. Cardiomyocytes isolated from mouse hearts underwent calcium handling analysis by measuring sparks in permeabilized cardiomyocytes. Briefly, isolated cardiomyocytes underwent permeabilization and were incubated in an internal solution with varying levels of magnesium and a calcium indicator (Fluo-4). Cells were imaged using an inverted confocal microscope in line-scan mode and analyzed using ImageJ. Data represented as mean with error bars as SD. Data analyzed with one-way ANOVA plus Tukey's post-hoc test.

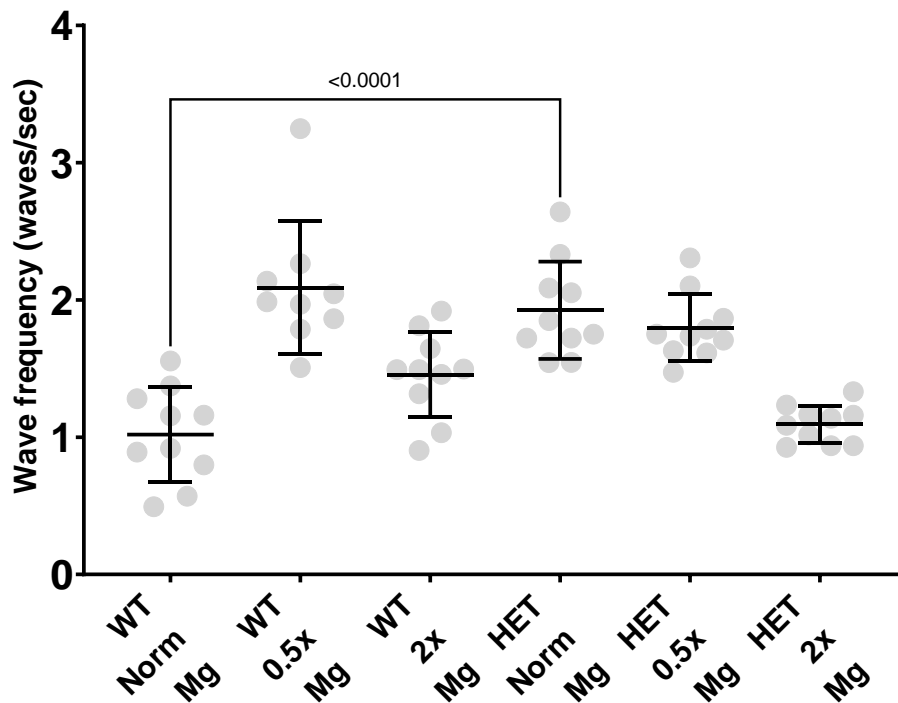


Figure 38. The effect of magnesium concentration on wave frequency in K180R isolated cardiomyocytes. Cardiomyocytes isolated from mouse hearts underwent calcium handling analysis by measuring waves in permeabilized cardiomyocytes. Briefly, isolated cardiomyocytes underwent permeabilization and were incubated in an internal solution with varying levels of magnesium and a calcium indicator (Fluo-4). Cells were imaged using an inverted confocal microscope in line-scan mode and analyzed using ImageJ. Data represented as mean with error bars as SD. Data analyzed with one-way ANOVA plus Tukey's post-hoc test.

REFERENCES

- Al-Khatib SM, Stevenson WG, Ackerman MJ, Bryant WJ, Callans DJ, Curtis AB, Deal BJ, Dickfeld T, Field ME, Fonarow GC, Gillis AM, Granger CB, Hammill SC, Hlatky MA, Joglar JA, Kay GN, Matlock DD, Myerburg RJ & Page RL. (2018). 2017 AHA/ACC/HRS Guideline for Management of Patients With Ventricular Arrhythmias and the Prevention of Sudden Cardiac Death: Executive Summary. *Circulation* **138**, e210-e271.
- Alcalai R, Wakimoto H, Arad M, Planer D, Konno T, Wang L, Seidman JG, Seidman CE & Berul CI. (2011). Prevention of ventricular arrhythmia and calcium dysregulation in a catecholaminergic polymorphic ventricular tachycardia mouse model carrying calsequestrin-2 mutation. *J Cardiovasc Electrophysiol* **22**, 316-324.
- Altmann HM, Tester DJ, Will ML, Middha S, Evans JM, Eckloff BW & Ackerman MJ. (2015). Homozygous/Compound Heterozygous Triadin Mutations Associated With Autosomal-Recessive Long-QT Syndrome and Pediatric Sudden Cardiac Arrest: Elucidation of the Triadin Knockout Syndrome. *Circulation* **131**, 2051-2060.
- Baher AA, Uy M, Xie F, Garfinkel A, Qu Z & Weiss JN. (2011). Bidirectional ventricular tachycardia: ping pong in the His-Purkinje system. *Heart Rhythm* **8**, 599-605.
- Batiste SM, Blackwell DJ, Kim K, Kryshtal DO, Gomez-Hurtado N, Rebbeck RT, Cornea RL, Johnston JN & Knollmann BC. (2019). Unnatural verticilide enantiomer inhibits type 2 ryanodine receptor-mediated calcium leak and is antiarrhythmic. *Proc Natl Acad Sci U S A* **116**, 4810-4815.
- Behere SP & Weindling SN. (2016). Catecholaminergic polymorphic ventricular tachycardia: An exciting new era. *Ann Pediatr Cardiol* **9**, 137-146.
- Ben-Ari Fuchs S, Lieder I, Stelzer G, Mazor Y, Buzhor E, Kaplan S, Bogoch Y, Plaschkes I, Shitrit A, Rappaport N, Kohn A, Edgar R, Shenhav L, Safran M, Lancet D, Guan-Golan Y, Warshawsky D & Shtrichman R. (2016). GeneAnalytics: An Integrative Gene Set Analysis Tool for Next Generation Sequencing, RNAseq and Microarray Data. *OMICS* **20**, 139-151.
- Bers DM. (2001). *Excitation-contraction coupling and cardiac contractile force*. Kluwer Academic Publishers, Dordrecht; Boston.
- Bers DM. (2002). Cardiac excitation-contraction coupling. *Nature* **415**, 198-205.
- Bezzerrides VJ, Caballero A, Wang S, Ai Y, Hyland RJ, Lu F, Heims-Waldron DA, Chambers KD, Zhang D, Abrams DJ & Pu WT. (2019). Gene Therapy for Catecholaminergic Polymorphic Ventricular Tachycardia by Inhibition of Ca. *Circulation* **140**, 405-419.

- Blackwell DJ, Faggioni M, Wleklinski MJ, Gomez-Hurtado N, Venkataraman R, Gibbs CE, Baudenbacher FJ, Gong S, Fishman GI, Boyle PM, Pfeifer K & Knollmann BC. (2022). The Purkinje-myocardial junction is the anatomic origin of ventricular arrhythmia in CPVT. *JCI Insight* **7**.
- Borlak J & Thum T. (2003). Hallmarks of ion channel gene expression in end-stage heart failure. *FASEB J* **17**, 1592-1608.
- Boyle PM, Franceschi WH, Constantin M, Hawks C, Desplantez T, Trayanova NA & Vigmond EJ. (2019). New insights on the cardiac safety factor: Unraveling the relationship between conduction velocity and robustness of propagation. *J Mol Cell Cardiol* **128**, 117-128.
- Boyle PM & Vigmond EJ. (2010). An intuitive safety factor for cardiac propagation. *Biophys J* **98**, L57-59.
- BurrIDGE PW, Matsa E, Shukla P, Lin ZC, Churko JM, Ebert AD, Lan F, Diecke S, Huber B, Mordwinkin NM, Plews JR, Abilez OJ, Cui B, Gold JD & Wu JC. (2014). Chemically defined generation of human cardiomyocytes. *Nat Methods* **11**, 855-860.
- Cacheux M, Fauconnier J, Thireau J, Osseni A, Brocard J, Roux-Buisson N, Fauré J, Lacampagne A & Marty I. (2019). Interplay between Triadin and Calsequestrin in the Pathogenesis of CPVT in the Mouse. *Mol Ther*.
- Cerrone M, Colombi B, Santoro M, di Barletta MR, Scelsi M, Villani L, Napolitano C & Priori SG. (2005). Bidirectional ventricular tachycardia and fibrillation elicited in a knock-in mouse model carrier of a mutation in the cardiac ryanodine receptor. *Circ Res* **96**, e77-82.
- Cerrone M, Napolitano C & Priori SG. (2009). Catecholaminergic polymorphic ventricular tachycardia: A paradigm to understand mechanisms of arrhythmias associated to impaired Ca(2+) regulation. *Heart Rhythm* **6**, 1652-1659.
- Cerrone M, Noujaim SF, Tolkacheva EG, Talkachou A, O'Connell R, Berenfeld O, Anumonwo J, Pandit SV, Vikstrom K, Napolitano C, Priori SG & Jalife J. (2007). Arrhythmogenic mechanisms in a mouse model of catecholaminergic polymorphic ventricular tachycardia. *Circ Res* **101**, 1039-1048.
- Chavali NV, Kryshnal DO, Parikh SS, Wang L, Glazer AM, Blackwell DJ, Kroncke BM, Shoemaker MB & Knollmann BC. (2019). Patient-independent human induced pluripotent stem cell model: A new tool for rapid determination of genetic variant pathogenicity in long QT syndrome. *Heart Rhythm* **16**, 1686-1695.
- Chopra N, Kannankeril PJ, Yang T, Hlaing T, Holinstat I, Etensohn K, Pfeifer K, Akin B, Jones LR, Franzini-Armstrong C & Knollmann BC. (2007). Modest reductions of cardiac calsequestrin increase sarcoplasmic reticulum Ca²⁺ leak independent of luminal Ca²⁺ and trigger ventricular arrhythmias in mice. *Circ Res* **101**, 617-626.

- Chopra N, Yang T, Asghari P, Moore ED, Huke S, Akin B, Cattolica RA, Perez CF, Hlaing T, Knollmann-Ritschel BE, Jones LR, Pessah IN, Allen PD, Franzini-Armstrong C & Knollmann BC. (2009). Ablation of triadin causes loss of cardiac Ca²⁺ release units, impaired excitation-contraction coupling, and cardiac arrhythmias. *Proc Natl Acad Sci U S A* **106**, 7636-7641.
- Concordet JP & Haeussler M. (2018). CRISPOR: intuitive guide selection for CRISPR/Cas9 genome editing experiments and screens. *Nucleic Acids Res* **46**, W242-W245.
- Costello B, Chadwick C, Saito A, Chu A, Maurer A & Fleischer S. (1986). Characterization of the junctional face membrane from terminal cisternae of sarcoplasmic reticulum. *J Cell Biol* **103**, 741-753.
- De Almeida MC, Stephenson RS, Anderson RH, Benvenuti LA, Loukas M & Aiello VD. (2020). Human subpulmonary infundibulum has an endocardial network of specialized conducting cardiomyocytes. *Heart Rhythm* **17**, 123-130.
- De Ferrari GM, Dusi V, Spazzolini C, Bos JM, Abrams DJ, Berul CI, Crotti L, Davis AM, Eldar M, Kharlap M, Khoury A, Krahn AD, Leenhardt A, Moir CR, Otero A, Olde Nordkamp L, Paul T, Rosés I, Nogueira F, Shkolnikova M, Till J, Wilde AA, Ackerman MJ & Schwartz PJ. (2015). Clinical Management of Catecholaminergic Polymorphic Ventricular Tachycardia: The Role of Left Cardiac Sympathetic Denervation. *Circulation* **131**, 2185-2193.
- de la Fuente S, Van Langen IM, Postma AV, Bikker H & Meijer A. (2008). A case of catecholaminergic polymorphic ventricular tachycardia caused by two calsequestrin 2 mutations. *Pacing Clin Electrophysiol* **31**, 916-919.
- Denegri M, Bongianino R, Lodola F, Boncompagni S, De Giusti VC, Avelino-Cruz JE, Liu N, Persampieri S, Curcio A, Esposito F, Pietrangelo L, Marty I, Villani L, Moyaho A, Baiardi P, Auricchio A, Protasi F, Napolitano C & Priori SG. (2014). Single delivery of an adeno-associated viral construct to transfer the CASQ2 gene to knock-in mice affected by catecholaminergic polymorphic ventricular tachycardia is able to cure the disease from birth to advanced age. *Circulation* **129**, 2673-2681.
- Desai KH, Sato R, Schauble E, Barsh GS, Kobilka BK & Bernstein D. (1997). Cardiovascular indexes in the mouse at rest and with exercise: new tools to study models of cardiac disease. *Am J Physiol* **272**, H1053-1061.
- Dries E, Santiago DJ, Gilbert G, Lenaerts I, Vandenberg B, Nagaraju CK, Johnson DM, Holemans P, Roderick HL, Macquaide N, Claus P & Sipido KR. (2018). Hyperactive ryanodine receptors in human heart failure and ischaemic cardiomyopathy reside outside of couplons. *Cardiovasc Res* **114**, 1512-1524.

- Fabiato A. (1985). Time and calcium dependence of activation and inactivation of calcium-induced release of calcium from the sarcoplasmic reticulum of a skinned canine cardiac Purkinje cell. *J Gen Physiol* **85**, 247-289.
- Faggioni M, Hwang HS, van der Werf C, Nederend I, Kannankeril PJ, Wilde AA & Knollmann BC. (2013). Accelerated sinus rhythm prevents catecholaminergic polymorphic ventricular tachycardia in mice and in patients. *Circ Res* **112**, 689-697.
- Faggioni M, Savio-Galimberti E, Venkataraman R, Hwang HS, Kannankeril PJ, Darbar D & Knollmann BC. (2014a). Suppression of spontaneous ca elevations prevents atrial fibrillation in calsequestrin 2-null hearts. *Circ Arrhythm Electrophysiol* **7**, 313-320.
- Faggioni M, van der Werf C & Knollmann BC. (2014b). Sinus node dysfunction in catecholaminergic polymorphic ventricular tachycardia: risk factor and potential therapeutic target? *Trends Cardiovasc Med* **24**, 273-278.
- Fazekas T, Scherlag BJ, Vos M, Wellens HJ & Lazzara R. (1993). Magnesium and the heart: antiarrhythmic therapy with magnesium. *Clin Cardiol* **16**, 768-774.
- Feaster TK, Cadar AG, Wang L, Williams CH, Chun YW, Hempel JE, Bloodworth N, Merryman WD, Lim CC, Wu JC, Knollmann BC & Hong CC. (2015). Matrigel Mattress: A Method for the Generation of Single Contracting Human-Induced Pluripotent Stem Cell-Derived Cardiomyocytes. *Circ Res* **117**, 995-1000.
- Fernandez-Velasco M, Rueda A, Rizzi N, Benitah JP, Colombi B, Napolitano C, Priori SG, Richard S & Gomez AM. (2009). Increased Ca²⁺ sensitivity of the ryanodine receptor mutant RyR2R4496C underlies catecholaminergic polymorphic ventricular tachycardia. *Circ Res* **104**, 201-209, 212p following 209.
- Flores DJ, Duong T, Brandenberger LO, Mitra A, Shirali A, Johnson JC, Springer D, Noguchi A, Yu ZX, Ebert SN, Ludwig A, Knollmann BC, Levin MD & Pfeifer K. (2018). Conditional ablation and conditional rescue models for Casq2 elucidate the role of development and of cell-type specific expression of Casq2 in the CPVT2 phenotype. *Hum Mol Genet* **27**, 1533-1544.
- Franciosi S, Roston TM, Perry FKG, Knollmann BC, Kannankeril PJ & Sanatani S. (2019). Chronotropic incompetence as a risk predictor in children and young adults with catecholaminergic polymorphic ventricular tachycardia. *J Cardiovasc Electrophysiol* **30**, 1923-1929.
- Franzini-Armstrong C, Kenney LJ & Varriano-Marston E. (1987). The structure of calsequestrin in triads of vertebrate skeletal muscle: a deep-etch study. *J Cell Biol* **105**, 49-56.
- Galimberti ES & Knollmann BC. (2011). Efficacy and potency of class I antiarrhythmic drugs for suppression of Ca²⁺ waves in permeabilized myocytes lacking calsequestrin. *J Mol Cell Cardiol* **51**, 760-768.

- Garcia-Bustos V, Sebastian R, Izquierdo M, Molina P, Chorro FJ & Ruiz-Sauri A. (2017). A quantitative structural and morphometric analysis of the Purkinje network and the Purkinje-myocardial junctions in pig hearts. *J Anat* **230**, 664-678.
- George CH, Jundi H, Walters N, Thomas NL, West RR & Lai FA. (2006). Arrhythmogenic mutation-linked defects in ryanodine receptor autoregulation reveal a novel mechanism of Ca²⁺ release channel dysfunction. *Circ Res* **98**, 88-97.
- Glukhov AV, Kalyanasundaram A, Lou Q, Hage LT, Hansen BJ, Belevych AE, Mohler PJ, Knollmann BC, Periasamy M, Györke S & Fedorov VV. (2015). Calsequestrin 2 deletion causes sinoatrial node dysfunction and atrial arrhythmias associated with altered sarcoplasmic reticulum calcium cycling and degenerative fibrosis within the mouse atrial pacemaker complex1. *Eur Heart J* **36**, 686-697.
- Gomez-Hurtado N, Boczek NJ, Kryshstal DO, Johnson CN, Sun J, Nitu FR, Cornea RL, Chazin WJ, Calvert ML, Tester DJ, Ackerman MJ & Knollmann BC. (2016). Novel CPVT-Associated Calmodulin Mutation in CALM3 (CALM3-A103V) Activates Arrhythmogenic Ca Waves and Sparks. *Circ Arrhythm Electrophysiol* **9**.
- Gonano LA & Jones PP. (2017). FK506-binding proteins 12 and 12.6 (FKBPs) as regulators of cardiac Ryanodine Receptors: Insights from new functional and structural knowledge. *Channels (Austin)* **11**, 415-425.
- Gong S, Zheng C, Doughty ML, Losos K, Didkovsky N, Schambra UB, Nowak NJ, Joyner A, Leblanc G, Hatten ME & Heintz N. (2003). A gene expression atlas of the central nervous system based on bacterial artificial chromosomes. *Nature* **425**, 917-925.
- Goodyer WR, Beyersdorf BM, Paik DT, Tian L, Li G, Buikema JW, Chirikian O, Choi S, Venkatraman S, Adams EL, Tessier-Lavigne M, Wu JC & Wu SM. (2019). Transcriptomic Profiling of the Developing Cardiac Conduction System at Single-Cell Resolution. *Circ Res* **125**, 379-397.
- Gray B, Bagnall RD, Lam L, Ingles J, Turner C, Haan E, Davis A, Yang PC, Clancy CE, Sy RW & Semsarian C. (2016). A novel heterozygous mutation in cardiac calsequestrin causes autosomal dominant catecholaminergic polymorphic ventricular tachycardia. *Heart Rhythm* **13**, 1652-1660.
- Guo W, Jorgensen AO, Jones LR & Campbell KP. (1996). Biochemical characterization and molecular cloning of cardiac triadin. *J Biol Chem* **271**, 458-465.
- Györke I, Hester N, Jones LR & Györke S. (2004). The role of calsequestrin, triadin, and junctin in conferring cardiac ryanodine receptor responsiveness to luminal calcium. *Biophys J* **86**, 2121-2128.

- Györke S, Stevens SC & Terentyev D. (2009). Cardiac calsequestrin: quest inside the SR. *J Physiol* **587**, 3091-3094.
- Hayakawa K, Swenson L, Baksh S, Wei Y, Michalak M & Derewenda ZS. (1994). Crystallization of canine cardiac calsequestrin. *J Mol Biol* **235**, 357-360.
- Hayashi M, Denjoy I, Extramiana F, Maltret A, Buisson NR, Lupoglazoff JM, Klug D, Takatsuki S, Villain E, Kamblock J, Messali A, Guicheney P, Lunardi J & Leenhardt A. (2009). Incidence and risk factors of arrhythmic events in catecholaminergic polymorphic ventricular tachycardia. *Circulation* **119**, 2426-2434.
- Hernandez OM, Szczesna-Cordary D, Knollmann BC, Miller T, Bell M, Zhao J, Sirenko SG, Diaz Z, Guzman G, Xu Y, Wang Y, Kerrick WG & Potter JD. (2005). F110I and R278C troponin T mutations that cause familial hypertrophic cardiomyopathy affect muscle contraction in transgenic mice and reconstituted human cardiac fibers. *J Biol Chem* **280**, 37183-37194.
- Herron TJ, Milstein ML, Anumonwo J, Priori SG & Jalife J. (2010). Purkinje cell calcium dysregulation is the cellular mechanism that underlies catecholaminergic polymorphic ventricular tachycardia. *Heart Rhythm* **7**, 1122-1128.
- Hoeker GS, Katra RP, Wilson LD, Plummer BN & Laurita KR. (2009). Spontaneous calcium release in tissue from the failing canine heart. *Am J Physiol Heart Circ Physiol* **297**, H1235-1242.
- Hoesl E, Stieber J, Herrmann S, Feil S, Tybl E, Hofmann F, Feil R & Ludwig A. (2008). Tamoxifen-inducible gene deletion in the cardiac conduction system. *J Mol Cell Cardiol* **45**, 62-69.
- Huelsing DJ, Spitzer KW, Cordeiro JM & Pollard AE. (1998). Conduction between isolated rabbit Purkinje and ventricular myocytes coupled by a variable resistance. *Am J Physiol* **274**, H1163-1173.
- Huke S & Knollmann BC. (2011). Oxidized CaMKII: a "heart stopper" for the sinus node? *J Clin Invest* **121**, 2975-2977.
- Hwang HS, Hasdemir C, Laver D, Mehra D, Turhan K, Faggioni M, Yin H & Knollmann BC. (2011). Inhibition of cardiac Ca²⁺ release channels (RyR2) determines efficacy of class I antiarrhythmic drugs in catecholaminergic polymorphic ventricular tachycardia. *Circ Arrhythm Electrophysiol* **4**, 128-135.
- Hwang HS, Nitu FR, Yang Y, Walweel K, Pereira L, Johnson CN, Faggioni M, Chazin WJ, Laver D, George AL, Cornea RL, Bers DM & Knollmann BC. (2014). Divergent regulation of ryanodine receptor 2 calcium release channels by arrhythmogenic human calmodulin missense mutants. *Circ Res* **114**, 1114-1124.

- Ikemoto N & Yamamoto T. (2002). Regulation of calcium release by interdomain interaction within ryanodine receptors. *Front Biosci* **7**, d671-683.
- Imberti JF, Underwood K, Mazzanti A & Priori SG. (2016). Clinical Challenges in Catecholaminergic Polymorphic Ventricular Tachycardia. *Heart Lung Circ* **25**, 777-783.
- Itzhaki I, Maizels L, Huber I, Gepstein A, Arbel G, Caspi O, Miller L, Belhassen B, Nof E, Glikson M & Gepstein L. (2012). Modeling of catecholaminergic polymorphic ventricular tachycardia with patient-specific human-induced pluripotent stem cells. *J Am Coll Cardiol* **60**, 990-1000.
- Jabbari J, Jabbari R, Nielsen MW, Holst AG, Nielsen JB, Haunsø S, Tfelt-Hansen J, Svendsen JH & Olesen MS. (2013). New exome data question the pathogenicity of genetic variants previously associated with catecholaminergic polymorphic ventricular tachycardia. *Circ Cardiovasc Genet* **6**, 481-489.
- Jayaraman T, Brillantes AM, Timerman AP, Fleischer S, Erdjument-Bromage H, Tempst P & Marks AR. (1992). FK506 binding protein associated with the calcium release channel (ryanodine receptor). *J Biol Chem* **267**, 9474-9477.
- Jiang D, Xiao B, Yang D, Wang R, Choi P, Zhang L, Cheng H & Chen SR. (2004). RyR2 mutations linked to ventricular tachycardia and sudden death reduce the threshold for store-overload-induced Ca²⁺ release (SOICR). *Proc Natl Acad Sci U S A* **101**, 13062-13067.
- Jiménez-Jáimez J, Palomino Doza J, Ortega Á, Macías-Ruiz R, Perin F, Rodríguez-Vázquez del Rey MM, Ortiz-Genga M, Monserrat L, Barriales-Villa R, Blanca E, Álvarez M & Tercedor L. (2016). Calmodulin 2 Mutation N98S Is Associated with Unexplained Cardiac Arrest in Infants Due to Low Clinical Penetrance Electrical Disorders. *PLoS One* **11**, e0153851.
- Jones LR, Zhang L, Sanborn K, Jorgensen AO & Kelley J. (1995). Purification, primary structure, and immunological characterization of the 26-kDa calsequestrin binding protein (junctin) from cardiac junctional sarcoplasmic reticulum. *J Biol Chem* **270**, 30787-30796.
- Kaneshiro T, Naruse Y, Nogami A, Tada H, Yoshida K, Sekiguchi Y, Murakoshi N, Kato Y, Horigome H, Kawamura M, Horie M & Aonuma K. (2012). Successful catheter ablation of bidirectional ventricular premature contractions triggering ventricular fibrillation in catecholaminergic polymorphic ventricular tachycardia with RyR2 mutation. *Circ Arrhythm Electrophysiol* **5**, e14-17.
- Kaneshiro T, Nogami A, Kato Y, Kuroki K, Komatsu Y, Tada H, Sekiguchi Y, Horigome H & Aonuma K. (2017). Effects of Catheter Ablation Targeting the Trigger Beats in Inherited Catecholaminergic Polymorphic Ventricular Tachycardia. *JACC Clin Electrophysiol* **3**, 1062-1063.

- Kang G, Giovannone SF, Liu N, Liu FY, Zhang J, Priori SG & Fishman GI. (2010). Purkinje cells from RyR2 mutant mice are highly arrhythmogenic but responsive to targeted therapy. *Circ Res* **107**, 512-519.
- Kannankeril PJ, Moore JP, Cerrone M, Priori SG, Kertesz NJ, Ro PS, Batra AS, Kaufman ES, Fairbrother DL, Saarel EV, Etheridge SP, Kanter RJ, Carboni MP, Dzurik MV, Fountain D, Chen H, Ely EW, Roden DM & Knollmann BC. (2017). Efficacy of Flecainide in the Treatment of Catecholaminergic Polymorphic Ventricular Tachycardia: A Randomized Clinical Trial. *JAMA Cardiol* **2**, 759-766.
- Kannankeril PJ, Shoemaker MB, Gayle KA, Fountain D, Roden DM & Knollmann BC. (2020). Atropine-induced sinus tachycardia protects against exercise-induced ventricular arrhythmias in patients with catecholaminergic polymorphic ventricular tachycardia. *Europace* **22**, 643-648.
- Katz G, Arad M & Eldar M. (2009). Catecholaminergic polymorphic ventricular tachycardia from bedside to bench and beyond. *Curr Probl Cardiol* **34**, 9-43.
- Katz G, Khoury A, Kurtzwald E, Hochhauser E, Porat E, Shainberg A, Seidman JG, Seidman CE, Lorber A, Eldar M & Arad M. (2010). Optimizing catecholaminergic polymorphic ventricular tachycardia therapy in calsequestrin-mutant mice. *Heart Rhythm* **7**, 1676-1682.
- Khoury A, Marai I, Suleiman M, Blich M, Lorber A, Gepstein L & Boulos M. (2013). Flecainide therapy suppresses exercise-induced ventricular arrhythmias in patients with CASQ2-associated catecholaminergic polymorphic ventricular tachycardia. *Heart Rhythm* **10**, 1671-1675.
- Kim C. (2014). Disease modeling and cell based therapy with iPSC: future therapeutic option with fast and safe application. *Blood Res* **49**, 7-14.
- Kirchhefer U, Wehrmeister D, Postma AV, Pohlentz G, Mormann M, Kucerova D, Muller FU, Schmitz W, Schulze-Bahr E, Wilde AA & Neumann J. (2010a). The human CASQ2 mutation K206N is associated with hyperglycosylation and altered cellular calcium handling. *J Mol Cell Cardiol* **49**, 95-105.
- Kirchhefer U, Wehrmeister D, Postma AV, Pohlentz G, Mormann M, Kucerova D, Müller FU, Schmitz W, Schulze-Bahr E, Wilde AA & Neumann J. (2010b). The human CASQ2 mutation K206N is associated with hyperglycosylation and altered cellular calcium handling. *J Mol Cell Cardiol* **49**, 95-105.
- Knollmann BC. (2011). Carvedilol tweaks calcium release to ease arrhythmias. *Nat Med* **17**, 923-924.

- Knollmann BC, Chopra N, Hlaing T, Akin B, Yang T, Etensohn K, Knollmann BE, Horton KD, Weissman NJ, Holinstat I, Zhang W, Roden DM, Jones LR, Franzini-Armstrong C & Pfeifer K. (2006). Casq2 deletion causes sarcoplasmic reticulum volume increase, premature Ca²⁺ release, and catecholaminergic polymorphic ventricular tachycardia. *J Clin Invest* **116**, 2510-2520.
- Knollmann BC & Roden DM. (2008). A genetic framework for improving arrhythmia therapy. *Nature* **451**, 929-936.
- Knudson CM, Stang KK, Moomaw CR, Slaughter CA & Campbell KP. (1993). Primary structure and topological analysis of a skeletal muscle-specific junctional sarcoplasmic reticulum glycoprotein (triadin). *J Biol Chem* **268**, 12646-12654.
- Kobayashi YM & Jones LR. (1999). Identification of triadin 1 as the predominant triadin isoform expressed in mammalian myocardium. *J Biol Chem* **274**, 28660-28668.
- Korneyev D, Petrosky AD, Zepeda B, Ferreiro M, Knollmann B & Escobar AL. (2012). Calsequestrin 2 deletion shortens the refractoriness of Ca²⁺ release and reduces rate-dependent Ca²⁺-alternans in intact mouse hearts. *J Mol Cell Cardiol* **52**, 21-31.
- Kryshtal DO, Gryshchenko O, Gomez-Hurtado N & Knollmann BC. (2015). Impaired calcium-calmodulin-dependent inactivation of Cav1.2 contributes to loss of sarcoplasmic reticulum calcium release refractoriness in mice lacking calsequestrin 2. *J Mol Cell Cardiol* **82**, 75-83.
- Kubalova Z, Terentyev D, Viatchenko-Karpinski S, Nishijima Y, Györke I, Terentyeva R, da Cunha DN, Sridhar A, Feldman DS, Hamlin RL, Carnes CA & Györke S. (2005). Abnormal intrastore calcium signaling in chronic heart failure. *Proc Natl Acad Sci U S A* **102**, 14104-14109.
- Kurtzwald-Josefson E, Yadin D, Harun-Khun S, Waldman M, Aravot D, Shainberg A, Eldar M, Hochhauser E & Arad M. (2017). Viral delivered gene therapy to treat catecholaminergic polymorphic ventricular tachycardia (CPVT2) in mouse models. *Heart Rhythm* **14**, 1053-1060.
- Lahat H, Eldar M, Levy-Nissenbaum E, Bahan T, Friedman E, Khoury A, Lorber A, Kastner DL, Goldman B & Pras E. (2001a). Autosomal recessive catecholamine- or exercise-induced polymorphic ventricular tachycardia: clinical features and assignment of the disease gene to chromosome 1p13-21. *Circulation* **103**, 2822-2827.
- Lahat H, Pras E, Olender T, Avidan N, Ben-Asher E, Man O, Levy-Nissenbaum E, Khoury A, Lorber A, Goldman B, Lancet D & Eldar M. (2001b). A missense mutation in a highly conserved region of CASQ2 is associated with autosomal recessive catecholamine-induced polymorphic ventricular tachycardia in Bedouin families from Israel. *Am J Hum Genet* **69**, 1378-1384.

- Lee KW, Maeng JS, Choi JY, Lee YR, Hwang CY, Park SS, Park HK, Chung BH, Lee SG, Kim YS, Jeon H, Eom SH, Kang C, Kim DH & Kwon KS. (2012). Role of Junctin protein interactions in cellular dynamics of calsequestrin polymer upon calcium perturbation. *J Biol Chem* **287**, 1679-1687.
- Leenhardt A, Lucet V, Denjoy I, Grau F, Ngoc DD & Coumel P. (1995). Catecholaminergic polymorphic ventricular tachycardia in children. A 7-year follow-up of 21 patients. *Circulation* **91**, 1512-1519.
- Leren IS, Saberniak J, Majid E, Haland TF, Edvardsen T & Haugaa KH. (2016). Nadolol decreases the incidence and severity of ventricular arrhythmias during exercise stress testing compared with β 1-selective β -blockers in patients with catecholaminergic polymorphic ventricular tachycardia. *Heart Rhythm* **13**, 433-440.
- Lewis KM, Munske GR, Byrd SS, Kang J, Cho HJ, Ríos E & Kang C. (2016). Characterization of Post-Translational Modifications to Calsequestrins of Cardiac and Skeletal Muscle. *Int J Mol Sci* **17**.
- Li J, Zhang L, Yu L, Minami I, Miyagawa S, Hörning M, Dong J, Qiao J, Qu X, Hua Y, Fujimoto N, Shiba Y, Zhao Y, Tang F, Chen Y, Sawa Y, Tang C & Liu L. (2020). Circulating re-entrant waves promote maturation of hiPSC-derived cardiomyocytes in self-organized tissue ring. *Commun Biol* **3**, 122.
- Li P & Rudy Y. (2011). A model of canine purkinje cell electrophysiology and Ca(2+) cycling: rate dependence, triggered activity, and comparison to ventricular myocytes. *Circ Res* **109**, 71-79.
- Liang P, Sallam K, Wu H, Li Y, Itzhaki I, Garg P, Zhang Y, Vermglinchan V, Lan F, Gu M, Gong T, Zhuge Y, He C, Ebert AD, Sanchez-Freire V, Churko J, Hu S, Sharma A, Lam CK, Scheinman MM, Bers DM & Wu JC. (2016). Patient-Specific and Genome-Edited Induced Pluripotent Stem Cell-Derived Cardiomyocytes Elucidate Single-Cell Phenotype of Brugada Syndrome. *J Am Coll Cardiol* **68**, 2086-2096.
- Limpitikul WB, Dick IE, Joshi-Mukherjee R, Overgaard MT, George AL & Yue DT. (2014). Calmodulin mutations associated with long QT syndrome prevent inactivation of cardiac L-type Ca(2+) currents and promote proarrhythmic behavior in ventricular myocytes. *J Mol Cell Cardiol* **74**, 115-124.
- Linse S, Helmersson A & Forsén S. (1991). Calcium binding to calmodulin and its globular domains. *J Biol Chem* **266**, 8050-8054.
- Liu B, Ho HT, Brunello L, Unudurthi SD, Lou Q, Belevych AE, Qian L, Kim DH, Cho C, Janssen PM, Hund TJ, Knollmann BC, Kranias EG & Györke S. (2015). Ablation of HRC alleviates cardiac arrhythmia and improves abnormal Ca handling in CASQ2 knockout mice prone to CPVT. *Cardiovasc Res* **108**, 299-311.

- Liu B, Walton SD, Ho HT, Belevych AE, Tikunova SB, Bonilla I, Shettigar V, Knollmann BC, Priori SG, Volpe P, Radwański PB, Davis JP & Györke S. (2018). Gene Transfer of Engineered Calmodulin Alleviates Ventricular Arrhythmias in a Calsequestrin-Associated Mouse Model of Catecholaminergic Polymorphic Ventricular Tachycardia. *J Am Heart Assoc* **7**.
- Liu N, Colombi B, Memmi M, Zissimopoulos S, Rizzi N, Negri S, Imbriani M, Napolitano C, Lai FA & Priori SG. (2006). Arrhythmogenesis in catecholaminergic polymorphic ventricular tachycardia: insights from a RyR2 R4496C knock-in mouse model. *Circ Res* **99**, 292-298.
- Liu N, Rizzi N, Boveri L & Priori SG. (2009). Ryanodine receptor and calsequestrin in arrhythmogenesis: what we have learnt from genetic diseases and transgenic mice. *J Mol Cell Cardiol* **46**, 149-159.
- Liu N, Ruan Y, Denegri M, Bachetti T, Li Y, Colombi B, Napolitano C, Coetzee WA & Priori SG. (2011). Calmodulin kinase II inhibition prevents arrhythmias in RyR2(R4496C+/-) mice with catecholaminergic polymorphic ventricular tachycardia. *J Mol Cell Cardiol* **50**, 214-222.
- Love MI, Huber W & Anders S. (2014). Moderated estimation of fold change and dispersion for RNA-seq data with DESeq2. *Genome Biol* **15**, 550.
- Luo M & Anderson ME. (2013). Mechanisms of altered Ca²⁺ handling in heart failure. *Circ Res* **113**, 690-708.
- MacLennan DH & Wong PT. (1971). Isolation of a calcium-sequestering protein from sarcoplasmic reticulum. *Proc Natl Acad Sci U S A* **68**, 1231-1235.
- Maguire PB, Briggs FN, Lennon NJ & Ohlendieck K. (1997). Oligomerization is an intrinsic property of calsequestrin in normal and transformed skeletal muscle. *Biochem Biophys Res Commun* **240**, 721-727.
- Maguire PB, Lennon NJ & Ohlendieck K. (1998). Oligomerisation of calsequestrin from rabbit skeletal muscle. *Biochem Soc Trans* **26**, S292.
- Maizels L, Huber I, Arbel G, Tijssen AJ, Gepstein A, Khoury A & Gepstein L. (2017). Patient-Specific Drug Screening Using a Human Induced Pluripotent Stem Cell Model of Catecholaminergic Polymorphic Ventricular Tachycardia Type 2. *Circ Arrhythm Electrophysiol* **10**.
- Manno C, Figueroa LC, Gillespie D, Fitts R, Kang C, Franzini-Armstrong C & Rios E. (2017). Calsequestrin depolymerizes when calcium is depleted in the sarcoplasmic reticulum of working muscle. *Proc Natl Acad Sci U S A* **114**, E638-E647.

- Marsman RF, Barc J, Beekman L, Alders M, Dooijes D, van den Wijngaard A, Ratbi I, Sefiani A, Bhuiyan ZA, Wilde AA & Bezzina CR. (2014). A mutation in CALM1 encoding calmodulin in familial idiopathic ventricular fibrillation in childhood and adolescence. *J Am Coll Cardiol* **63**, 259-266.
- Marx A, Lange B, Nalenz C, Hoffmann B, Rostock T & Konrad T. (2019). A 35-year effective treatment of catecholaminergic polymorphic ventricular tachycardia with propafenone. *HeartRhythm Case Rep* **5**, 74-77.
- McFarland TP, Milstein ML & Cala SE. (2010). Rough endoplasmic reticulum to junctional sarcoplasmic reticulum trafficking of calsequestrin in adult cardiomyocytes. *J Mol Cell Cardiol* **49**, 556-564.
- Milstein ML, Houle TD & Cala SE. (2009). Calsequestrin isoforms localize to different ER subcompartments: evidence for polymer and heteropolymer-dependent localization. *Exp Cell Res* **315**, 523-534.
- Miyata K, Ohno S, Itoh H & Horie M. (2018). Bradycardia Is a Specific Phenotype of Catecholaminergic Polymorphic Ventricular Tachycardia Induced by RYR2 Mutations. *Intern Med* **57**, 1813-1817.
- Modell SM, Bradley DJ & Lehmann MH. (2012). Genetic testing for long QT syndrome and the category of cardiac ion channelopathies. *PLoS Curr*, e4f9995f9969e9996c9997.
- Murphy RM, Mollica JP, Beard NA, Knollmann BC & Lamb GD. (2011). Quantification of calsequestrin 2 (CSQ2) in sheep cardiac muscle and Ca²⁺-binding protein changes in CSQ2 knockout mice. *Am J Physiol Heart Circ Physiol* **300**, H595-604.
- Ng K, Titus EW, Lieve KV, Roston TM, Mazzanti A, Deiter FH, Denjoy I, Ingles J, Till J, Robyns T, Connors SP, Steinberg C, Abrams DJ, Pang B, Scheinman MM, Bos JM, Duffett SA, van der Werf C, Maltret A, Green MS, Rutberg J, Balaji S, Cadrin-Tourigny J, Orland KM, Knight LM, Brateng C, Wu J, Tang AS, Skanes AC, Manlucu J, Healey JS, January CT, Krahn AD, Collins KK, Maginot KR, Fischbach P, Etheridge SP, Eckhardt LL, Hamilton RM, Ackerman MJ, Nogueira FRI, Semsarian C, Jura N, Leenhardt A, Gollob MH, Priori SG, Sanatani S, Wilde AAM, Deo RC & Roberts JD. (2020). An International Multicenter Evaluation of Inheritance Patterns, Arrhythmic Risks, and Underlying Mechanisms of. *Circulation* **142**, 932-947.
- Novak A, Barad L, Lorber A, Gherghiceanu M, Reiter I, Eisen B, Eldor L, Itskovitz-Eldor J, Eldar M, Arad M & Binah O. (2015). Functional abnormalities in iPSC-derived cardiomyocytes generated from CPVT1 and CPVT2 patients carrying ryanodine or calsequestrin mutations. *J Cell Mol Med* **19**, 2006-2018.
- Novak A, Barad L, Zeevi-Levin N, Shick R, Shtrichman R, Lorber A, Itskovitz-Eldor J & Binah O. (2012). Cardiomyocytes generated from CPVT307H patients are arrhythmogenic in response to β -adrenergic stimulation. *J Cell Mol Med* **16**, 468-482.

- Nyegaard M, Overgaard MT, Søndergaard MT, Vranas M, Behr ER, Hildebrandt LL, Lund J, Hedley PL, Camm AJ, Wettrell G, Fosdal I, Christiansen M & Børghlum AD. (2012). Mutations in calmodulin cause ventricular tachycardia and sudden cardiac death. *Am J Hum Genet* **91**, 703-712.
- Pallante BA, Giovannone S, Fang-Yu L, Zhang J, Liu N, Kang G, Dun W, Boyden PA & Fishman GI. (2010). Contactin-2 expression in the cardiac Purkinje fiber network. *Circ Arrhythm Electrophysiol* **3**, 186-194.
- Pan X, Philippen L, Lahiri SK, Lee C, Park SH, Word TA, Li N, Jarrett KE, Gupta R, Reynolds JO, Lin J, Bao G, Lagor WR & Wehrens XHT. (2018). In Vivo Ryr2 Editing Corrects Catecholaminergic Polymorphic Ventricular Tachycardia. *Circ Res* **123**, 953-963.
- Pape PC, Fénelon K, Lamboley CR & Stachura D. (2007). Role of calsequestrin evaluated from changes in free and total calcium concentrations in the sarcoplasmic reticulum of frog cut skeletal muscle fibres. *J Physiol* **581**, 319-367.
- Parikh SS, Blackwell DJ, Gomez-Hurtado N, Frisk M, Wang L, Kim K, Dahl CP, Fiane A, Tønnessen T, Kryshal DO, Louch WE & Knollmann BC. (2017). Thyroid and Glucocorticoid Hormones Promote Functional T-Tubule Development in Human-Induced Pluripotent Stem Cell-Derived Cardiomyocytes. *Circ Res* **121**, 1323-1330.
- Park H, Park IY, Kim E, Youn B, Fields K, Dunker AK & Kang C. (2004). Comparing skeletal and cardiac calsequestrin structures and their calcium binding: a proposed mechanism for coupled calcium binding and protein polymerization. *J Biol Chem* **279**, 18026-18033.
- Park H, Wu S, Dunker AK & Kang C. (2003). Polymerization of calsequestrin. Implications for Ca²⁺ regulation. *J Biol Chem* **278**, 16176-16182.
- Patro R, Duggal G, Love MI, Irizarry RA & Kingsford C. (2017). Salmon provides fast and bias-aware quantification of transcript expression. *Nat Methods* **14**, 417-419.
- Penttinen K, Swan H, Vanninen S, Paavola J, Lahtinen AM, Kontula K & Aalto-Setälä K. (2015). Correction: Antiarrhythmic Effects of Dantrolene in Patients with Catecholaminergic Polymorphic Ventricular Tachycardia and Replication of the Responses Using iPSC Models. *PLoS One* **10**, e0134746.
- Peterson BZ, DeMaria CD, Adelman JP & Yue DT. (1999). Calmodulin is the Ca²⁺ sensor for Ca²⁺ -dependent inactivation of L-type calcium channels. *Neuron* **22**, 549-558.
- Picht E, Zima AV, Blatter LA & Bers DM. (2007). SparkMaster: automated calcium spark analysis with ImageJ. *Am J Physiol Cell Physiol* **293**, C1073-1081.
- Plank G, Loewe A, Neic A, Augustin C, Huang YL, Gsell MAF, Karabelas E, Nothstein M, Prassl AJ, Sanchez J, Seemann G & Vigmond EJ. (2021). The openCARP simulation

- environment for cardiac electrophysiology. *Comput Methods Programs Biomed* **208**, 106223.
- Postma AV, Denjoy I, Hoorntje TM, Lupoglazoff JM, Da Costa A, Sebillon P, Mannens MM, Wilde AA & Guicheney P. (2002). Absence of caldesmon 2 causes severe forms of catecholaminergic polymorphic ventricular tachycardia. *Circ Res* **91**, e21-26.
- Postma AV, Denjoy I, Kamblock J, Alders M, Lupoglazoff JM, Vaksman G, Dubosq-Bidot L, Sebillon P, Mannens MM, Guicheney P & Wilde AA. (2005). Catecholaminergic polymorphic ventricular tachycardia: RYR2 mutations, bradycardia, and follow up of the patients. *J Med Genet* **42**, 863-870.
- Preininger MK, Jha R, Maxwell JT, Wu Q, Singh M, Wang B, Dalal A, Mceachin ZT, Rossoll W, Hales CM, Fischbach PS, Wagner MB & Xu C. (2016). A human pluripotent stem cell model of catecholaminergic polymorphic ventricular tachycardia recapitulates patient-specific drug responses. *Dis Model Mech* **9**, 927-939.
- Priori SG & Corr PB. (1990). Mechanisms underlying early and delayed afterdepolarizations induced by catecholamines. *Am J Physiol* **258**, H1796-1805.
- Priori SG, Napolitano C, Memmi M, Colombi B, Drago F, Gasparini M, DeSimone L, Coltorti F, Bloise R, Keegan R, Cruz Filho FE, Vignati G, Benatar A & DeLogu A. (2002). Clinical and molecular characterization of patients with catecholaminergic polymorphic ventricular tachycardia. *Circulation* **106**, 69-74.
- Priori SG, Napolitano C, Tiso N, Memmi M, Vignati G, Bloise R, Sorrentino V & Danieli GA. (2001). Mutations in the cardiac ryanodine receptor gene (hRyR2) underlie catecholaminergic polymorphic ventricular tachycardia. *Circulation* **103**, 196-200.
- Pérez-Riera AR, Barbosa-Barros R, de Rezende Barbosa MPC, Daminello-Raimundo R, de Lucca AA & de Abreu LC. (2018). Catecholaminergic polymorphic ventricular tachycardia, an update. *Ann Noninvasive Electrocardiol* **23**, e12512.
- Ran FA, Hsu PD, Wright J, Agarwala V, Scott DA & Zhang F. (2013). Genome engineering using the CRISPR-Cas9 system. *Nat Protoc* **8**, 2281-2308.
- Reyes-Juárez JL, Juárez-Rubí R, Rodríguez G & Zarain-Herzberg A. (2007). Transcriptional analysis of the human cardiac caldesmon gene in cardiac and skeletal myocytes. *J Biol Chem* **282**, 35554-35563.
- Rizzi N, Liu N, Napolitano C, Nori A, Turcato F, Colombi B, Bicciato S, Arcelli D, Spedito A, Scelsi M, Villani L, Esposito G, Boncompagni S, Protasi F, Volpe P & Priori SG. (2008). Unexpected structural and functional consequences of the R33Q homozygous mutation in cardiac caldesmon: a complex arrhythmogenic cascade in a knock in mouse model. *Circ Res* **103**, 298-306.

- Rooryck C, Kyndt F, Bozon D, Roux-Buisson N, Sacher F, Probst V & Thambo JB. (2015). New Family With Catecholaminergic Polymorphic Ventricular Tachycardia Linked to the Triadin Gene. *J Cardiovasc Electrophysiol* **26**, 1146-1150.
- Ross S, Holliday M, Lim S & Semsarian C. (2019). Characterization of the first induced pluripotent stem cell line generated from a patient with autosomal dominant catecholaminergic polymorphic ventricular tachycardia due to a heterozygous mutation in cardiac calsequestrin-2. *Stem Cell Res* **37**, 101450.
- Rossi D, Gamberucci A, Pierantozzi E, Amato C, Migliore L & Sorrentino V. (2021). Calsequestrin, a key protein in striated muscle health and disease. *J Muscle Res Cell Motil* **42**, 267-279.
- Rosso R, Kalman JM, Rogowski O, Diamant S, Birger A, Biner S, Belhassen B & Viskin S. (2007). Calcium channel blockers and beta-blockers versus beta-blockers alone for preventing exercise-induced arrhythmias in catecholaminergic polymorphic ventricular tachycardia. *Heart Rhythm* **4**, 1149-1154.
- Roston TM, Jones K, Hawkins NM, Bos JM, Schwartz PJ, Perry F, Ackerman MJ, Laksman ZWM, Kaul P, Lieve KVV, Atallah J, Krahn AD & Sanatani S. (2018a). Implantable cardioverter-defibrillator use in catecholaminergic polymorphic ventricular tachycardia: A systematic review. *Heart Rhythm* **15**, 1791-1799.
- Roston TM, Sanatani S & Chen SR. (2017). Suppression-of-function mutations in the cardiac ryanodine receptor: Emerging evidence for a novel arrhythmia syndrome? *Heart Rhythm* **14**, 108-109.
- Roston TM, Yuchi Z, Kannankeril PJ, Hathaway J, Vinocur JM, Etheridge SP, Potts JE, Maginot KR, Salerno JC, Cohen MI, Hamilton RM, Pflaumer A, Mohammed S, Kimlicka L, Kanter RJ, LaPage MJ, Collins KK, Gebauer RA, Temple JD, Batra AS, Erickson C, Mischczak-Knecht M, Kubuš P, Bar-Cohen Y, Kantoch M, Thomas VC, Hessling G, Anderson C, Young ML, Choi SHJ, Cabrera Ortega M, Lau YR, Johnsrude CL, Fournier A, Van Petegem F & Sanatani S. (2018b). The clinical and genetic spectrum of catecholaminergic polymorphic ventricular tachycardia: findings from an international multicentre registry. *Europace* **20**, 541-547.
- Roux-Buisson N, Cacheux M, Fourest-Lieuvain A, Fauconnier J, Brocard J, Denjoy I, Durand P, Guicheney P, Kyndt F, Leenhardt A, Le Marec H, Lucet V, Mabo P, Probst V, Monnier N, Ray PF, Santoni E, Trémeaux P, Lacampagne A, Fauré J, Lunardi J & Marty I. (2012). Absence of triadin, a protein of the calcium release complex, is responsible for cardiac arrhythmia with sudden death in human. *Hum Mol Genet* **21**, 2759-2767.
- Sallam K, Kodo K & Wu JC. (2014). Modeling inherited cardiac disorders. *Circ J* **78**, 784-794.

- Sallam K, Li Y, Sager PT, Houser SR & Wu JC. (2015). Finding the rhythm of sudden cardiac death: new opportunities using induced pluripotent stem cell-derived cardiomyocytes. *Circ Res* **116**, 1989-2004.
- Sasaki K, Makiyama T, Yoshida Y, Wuriyanghai Y, Kamakura T, Nishiuchi S, Hayano M, Harita T, Yamamoto Y, Kohjitani H, Hirose S, Chen J, Kawamura M, Ohno S, Itoh H, Takeuchi A, Matsuoka S, Miura M, Sumitomo N, Horie M, Yamanaka S & Kimura T. (2016). Patient-Specific Human Induced Pluripotent Stem Cell Model Assessed with Electrical Pacing Validates S107 as a Potential Therapeutic Agent for Catecholaminergic Polymorphic Ventricular Tachycardia. *PLoS One* **11**, e0164795.
- Satoh H, Blatter LA & Bers DM. (1997). Effects of $[Ca^{2+}]_i$, SR Ca^{2+} load, and rest on Ca^{2+} spark frequency in ventricular myocytes. *Am J Physiol* **272**, H657-668.
- Savio-Galimberti E & Knollmann BC. (2015). Channel Activity of Cardiac Ryanodine Receptors (RyR2) Determines Potency and Efficacy of Flecainide and R-Propafenone against Arrhythmogenic Calcium Waves in Ventricular Cardiomyocytes. *PLoS One* **10**, e0131179.
- Seidel M, Lai FA & Zissimopoulos S. (2015). Structural and functional interactions within ryanodine receptor. *Biochem Soc Trans* **43**, 377-383.
- Shimizu W. (2009). Arrhythmias originating from the right ventricular outflow tract: how to distinguish "malignant" from "benign"? *Heart Rhythm* **6**, 1507-1511.
- Sikkel MB, Francis DP, Howard J, Gordon F, Rowlands C, Peters NS, Lyon AR, Harding SE & MacLeod KT. (2017). Hierarchical statistical techniques are necessary to draw reliable conclusions from analysis of isolated cardiomyocyte studies. *Cardiovasc Res* **113**, 1743-1752.
- Sleiman NH, McFarland TP, Jones LR & Cala SE. (2015). Transitions of protein traffic from cardiac ER to junctional SR. *J Mol Cell Cardiol* **81**, 34-45.
- Sommer JR & Johnson EA. (1968). Cardiac muscle. A comparative study of Purkinje fibers and ventricular fibers. *J Cell Biol* **36**, 497-526.
- Stuyvers BD, Dun W, Matkovich S, Sorrentino V, Boyden PA & ter Keurs HE. (2005). Ca^{2+} sparks and waves in canine purkinje cells: a triple layered system of Ca^{2+} activation. *Circ Res* **97**, 35-43.
- Sumitomo N. (2016). Current topics in catecholaminergic polymorphic ventricular tachycardia. *J Arrhythm* **32**, 344-351.
- Sumitomo N, Harada K, Nagashima M, Yasuda T, Nakamura Y, Aragaki Y, Saito A, Kurosaki K, Jouo K, Koujiro M, Konishi S, Matsuoka S, Oono T, Hayakawa S, Miura M, Ushinohama H, Shibata T & Niimura I. (2003). Catecholaminergic polymorphic

- ventricular tachycardia: electrocardiographic characteristics and optimal therapeutic strategies to prevent sudden death. *Heart* **89**, 66-70.
- Sumitomo N, Sakurada H, Taniguchi K, Matsumura M, Abe O, Miyashita M, Kanamaru H, Karasawa K, Ayusawa M, Fukamizu S, Nagaoka I, Horie M, Harada K & Hiraoka M. (2007). Association of atrial arrhythmia and sinus node dysfunction in patients with catecholaminergic polymorphic ventricular tachycardia. *Circ J* **71**, 1606-1609.
- Swaminathan PD, Purohit A, Soni S, Voigt N, Singh MV, Glukhov AV, Gao Z, He BJ, Luczak ED, Joiner ML, Kutschke W, Yang J, Donahue JK, Weiss RM, Grumbach IM, Ogawa M, Chen PS, Efimov I, Dobrev D, Mohler PJ, Hund TJ & Anderson ME. (2011). Oxidized CaMKII causes cardiac sinus node dysfunction in mice. *J Clin Invest* **121**, 3277-3288.
- Swan H, Laitinen P, Kontula K & Toivonen L. (2005). Calcium channel antagonism reduces exercise-induced ventricular arrhythmias in catecholaminergic polymorphic ventricular tachycardia patients with RyR2 mutations. *J Cardiovasc Electrophysiol* **16**, 162-166.
- Swan H, Piippo K, Viitasalo M, Heikkilä P, Paavonen T, Kainulainen K, Kere J, Keto P, Kontula K & Toivonen L. (1999a). Arrhythmic disorder mapped to chromosome 1q42-q43 causes malignant polymorphic ventricular tachycardia in structurally normal hearts. *J Am Coll Cardiol* **34**, 2035-2042.
- Swan H, Piippo K, Viitasalo M, Heikkilä P, Paavonen T, Kainulainen K, Kere J, Keto P, Kontula K & Toivonen L. (1999b). Arrhythmic disorder mapped to chromosome 1q42-q43 causes malignant polymorphic ventricular tachycardia in structurally normal hearts. *J Am Coll Cardiol* **34**, 2035-2042.
- Sy RW, Gollob MH, Klein GJ, Yee R, Skanes AC, Gula LJ, Leong-Sit P, Gow RM, Green MS, Birnie DH & Krahn AD. (2011). Arrhythmia characterization and long-term outcomes in catecholaminergic polymorphic ventricular tachycardia. *Heart Rhythm* **8**, 864-871.
- Tanaka M, Ozawa T, Maurer A, Cortese JD & Fleischer S. (1986). Apparent cooperativity of Ca²⁺ binding associated with crystallization of Ca²⁺-binding protein from sarcoplasmic reticulum. *Arch Biochem Biophys* **251**, 369-378.
- ten Tusscher KH & Panfilov AV. (2006). Alternans and spiral breakup in a human ventricular tissue model. *Am J Physiol Heart Circ Physiol* **291**, H1088-1100.
- Terentyev D, Cala SE, Houle TD, Viatchenko-Karpinski S, Gyorke I, Terentyeva R, Williams SC & Gyorke S. (2005). Triadin overexpression stimulates excitation-contraction coupling and increases predisposition to cellular arrhythmia in cardiac myocytes. *Circ Res* **96**, 651-658.
- Terentyev D, Nori A, Santoro M, Viatchenko-Karpinski S, Kubalova Z, Gyorke I, Terentyeva R, Vedamoorthyrao S, Blom NA, Valle G, Napolitano C, Williams SC, Volpe P, Priori SG & Gyorke S. (2006). Abnormal interactions of calsequestrin with the ryanodine receptor

- calcium release channel complex linked to exercise-induced sudden cardiac death. *Circ Res* **98**, 1151-1158.
- Titus EW, Deiter FH, Shi C, Wojciak J, Scheinman M, Jura N & Deo RC. (2020). The structure of a calsequestrin filament reveals mechanisms of familial arrhythmia. *Nat Struct Mol Biol* **27**, 1142-1151.
- Tranum-Jensen J, Wilde AA, Vermeulen JT & Janse MJ. (1991). Morphology of electrophysiologically identified junctions between Purkinje fibers and ventricular muscle in rabbit and pig hearts. *Circ Res* **69**, 429-437.
- Uchinoumi H, Yano M, Suetomi T, Ono M, Xu X, Tateishi H, Oda T, Okuda S, Doi M, Kobayashi S, Yamamoto T, Ikeda Y, Ohkusa T, Ikemoto N & Matsuzaki M. (2010). Catecholaminergic polymorphic ventricular tachycardia is caused by mutation-linked defective conformational regulation of the ryanodine receptor. *Circ Res* **106**, 1413-1424.
- van der Werf C, Kannankeril PJ, Sacher F, Krahn AD, Viskin S, Leenhardt A, Shimizu W, Sumitomo N, Fish FA, Bhuiyan ZA, Willems AR, van der Veen MJ, Watanabe H, Laborderie J, Haïssaguerre M, Knollmann BC & Wilde AA. (2011). Flecainide therapy reduces exercise-induced ventricular arrhythmias in patients with catecholaminergic polymorphic ventricular tachycardia. *J Am Coll Cardiol* **57**, 2244-2254.
- van der Werf C, Lieve KV, Bos JM, Lane CM, Denjoy I, Roses-Noguer F, Aiba T, Wada Y, Ingles J, Leren IS, Rudic B, Schwartz PJ, Maltret A, Sacher F, Skinner JR, Krahn AD, Roston TM, Tfelt-Hansen J, Swan H, Robyns T, Ohno S, Roberts JD, van den Berg MP, Kammeraad JA, Probst V, Kannankeril PJ, Blom NA, Behr ER, Borggrefe M, Haugaa KH, Semsarian C, Horie M, Shimizu W, Till JA, Leenhardt A, Ackerman MJ & Wilde AA. (2019). Implantable cardioverter-defibrillators in previously undiagnosed patients with catecholaminergic polymorphic ventricular tachycardia resuscitated from sudden cardiac arrest. *Eur Heart J* **40**, 2953-2961.
- van der Werf C, Zwinderman AH & Wilde AA. (2012). Therapeutic approach for patients with catecholaminergic polymorphic ventricular tachycardia: state of the art and future developments. *Europace* **14**, 175-183.
- VanScyoc WS, Sorensen BR, Rusinova E, Laws WR, Ross JB & Shea MA. (2002). Calcium binding to calmodulin mutants monitored by domain-specific intrinsic phenylalanine and tyrosine fluorescence. *Biophys J* **83**, 2767-2780.
- Vassalle M & Lin CI. (2004). Calcium overload and cardiac function. *J Biomed Sci* **11**, 542-565.
- Volpe P & Simon BJ. (1991). The bulk of Ca²⁺ released to the myoplasm is free in the sarcoplasmic reticulum and does not unbind from calsequestrin. *FEBS Lett* **278**, 274-278.
- Wang L, Kim K, Parikh S, Cadar AG, Bersell KR, He H, Pinto JR, Kryshtal DO & Knollmann BC. (2018). Hypertrophic cardiomyopathy-linked mutation in troponin T causes

- myofibrillar disarray and pro-arrhythmic action potential changes in human iPSC cardiomyocytes. *J Mol Cell Cardiol* **114**, 320-327.
- Wang L, Wada Y, Ballan N, Schmeckpeper J, Huang J, Rau CD, Wang Y, Gepstein L & Knollmann BC. (2021). Triiodothyronine and dexamethasone alter potassium channel expression and promote electrophysiological maturation of human-induced pluripotent stem cell-derived cardiomyocytes. *J Mol Cell Cardiol* **161**, 130-138.
- Wang S, Trumble WR, Liao H, Wesson CR, Dunker AK & Kang CH. (1998). Crystal structure of calsequestrin from rabbit skeletal muscle sarcoplasmic reticulum. *Nat Struct Biol* **5**, 476-483.
- Wang YY, Mesirca P, Marqués-Sulé E, Zahradnikova A, Villejoubert O, D'Ocon P, Ruiz C, Domingo D, Zorio E, Mangoni ME, Benitah JP & Gómez AM. (2017). RyR2R420Q catecholaminergic polymorphic ventricular tachycardia mutation induces bradycardia by disturbing the coupled clock pacemaker mechanism. *JCI Insight* **2**.
- Wangüemert Pérez F, Hernández Afonso JS, Groba Marco MDV, Caballero Dorta E, Álvarez Acosta L, Campuzano Larrea O, Pérez G, Brugada Terradellas J & Brugada Terradellas R. (2018). Flecainide Reduces Ventricular Arrhythmias in Patients With Genotype RyR2-positive Catecholaminergic Polymorphic Ventricular Tachycardia. *Rev Esp Cardiol (Engl Ed)* **71**, 185-191.
- Watanabe H, Chopra N, Laver D, Hwang HS, Davies SS, Roach DE, Duff HJ, Roden DM, Wilde AA & Knollmann BC. (2009). Flecainide prevents catecholaminergic polymorphic ventricular tachycardia in mice and humans. *Nat Med* **15**, 380-383.
- Watanabe H, van der Werf C, Roses-Noguer F, Adler A, Sumitomo N, Veltmann C, Rosso R, Bhuiyan ZA, Bikker H, Kannankeril PJ, Horie M, Minamino T, Viskin S, Knollmann BC, Till J & Wilde AA. (2013). Effects of flecainide on exercise-induced ventricular arrhythmias and recurrences in genotype-negative patients with catecholaminergic polymorphic ventricular tachycardia. *Heart Rhythm* **10**, 542-547.
- Wehrens XH, Lehnart SE, Huang F, Vest JA, Reiken SR, Mohler PJ, Sun J, Guatimosim S, Song LS, Rosemblyt N, D'Armiento JM, Napolitano C, Memmi M, Priori SG, Lederer WJ & Marks AR. (2003). FKBP12.6 deficiency and defective calcium release channel (ryanodine receptor) function linked to exercise-induced sudden cardiac death. *Cell* **113**, 829-840.
- Wiedmann RT, Tan RC & Joyner RW. (1996). Discontinuous conduction at Purkinje-ventricular muscle junction. *Am J Physiol* **271**, H1507-1516.
- Wilde AA, Bhuiyan ZA, Crotti L, Facchini M, De Ferrari GM, Paul T, Ferrandi C, Koolbergen DR, Odero A & Schwartz PJ. (2008). Left cardiac sympathetic denervation for catecholaminergic polymorphic ventricular tachycardia. *N Engl J Med* **358**, 2024-2029.

- Wleklinski MJ, Kannankeril PJ & Knollmann BC. (2020). Molecular and tissue mechanisms of catecholaminergic polymorphic ventricular tachycardia. *J Physiol* **598**, 2817-2834.
- Xiao J, Tian X, Jones PP, Bolstad J, Kong H, Wang R, Zhang L, Duff HJ, Gillis AM, Fleischer S, Kotlikoff M, Copello JA & Chen SR. (2007). Removal of FKBP12.6 does not alter the conductance and activation of the cardiac ryanodine receptor or the susceptibility to stress-induced ventricular arrhythmias. *J Biol Chem* **282**, 34828-34838.
- Xie Y, Sato D, Garfinkel A, Qu Z & Weiss JN. (2010). So little source, so much sink: requirements for afterdepolarizations to propagate in tissue. *Biophys J* **99**, 1408-1415.
- Yamaguchi N, Takahashi N, Xu L, Smithies O & Meissner G. (2007). Early cardiac hypertrophy in mice with impaired calmodulin regulation of cardiac muscle Ca release channel. *J Clin Invest* **117**, 1344-1353.
- Yamaguchi N, Xu L, Pasek DA, Evans KE & Meissner G. (2003). Molecular basis of calmodulin binding to cardiac muscle Ca(2+) release channel (ryanodine receptor). *J Biol Chem* **278**, 23480-23486.
- Yamniuk AP & Vogel HJ. (2004). Calmodulin's flexibility allows for promiscuity in its interactions with target proteins and peptides. *Mol Biotechnol* **27**, 33-57.
- Yano K & Zarain-Herzberg A. (1994). Sarcoplasmic reticulum calsequestrins: structural and functional properties. *Mol Cell Biochem* **135**, 61-70.
- Yano M, Yamamoto T, Kobayashi S & Matsuzaki M. (2009). Role of ryanodine receptor as a Ca²⁺ regulatory center in normal and failing hearts. *J Cardiol* **53**, 1-7.
- Yin G, Hassan F, Haroun AR, Murphy LL, Crotti L, Schwartz PJ, George AL & Satin J. (2014). Arrhythmogenic calmodulin mutations disrupt intracellular cardiomyocyte Ca²⁺ regulation by distinct mechanisms. *J Am Heart Assoc* **3**, e000996.
- Zhang JZ, Waddell HM, Wu E, Dholakia J, Okolo CA, McLay JC & Jones PP. (2016). FKBP_s facilitate the termination of spontaneous Ca²⁺ release in wild-type RyR2 but not CPVT mutant RyR2. *Biochem J* **473**, 2049-2060.
- Zhang L, Kelley J, Schmeisser G, Kobayashi YM & Jones LR. (1997). Complex formation between junctin, triadin, calsequestrin, and the ryanodine receptor. Proteins of the cardiac junctional sarcoplasmic reticulum membrane. *J Biol Chem* **272**, 23389-23397.
- Zühlke RD, Pitt GS, Deisseroth K, Tsien RW & Reuter H. (1999). Calmodulin supports both inactivation and facilitation of L-type calcium channels. *Nature* **399**, 159-162.